UNIVERSITÀ DEGLI STUDI DI MILANO

Scuola di Dottorato in Scienze Biologiche e Molecolari

XXVIII Ciclo

CHARACTERIZATION OF DISEASE GENES IN NEURODEGENERATION WITH BRAIN IRON ACCUMULATION

Sabrina Dusi

PhD Thesis

Scientific tutor: Valeria Tiranti, PhD

Academic year: 2014-2015

SSD: [BIO/11]

Thesis performed at Unit of Molecular Neurogenetics, IRCCS Foundation - Neurological Institute “Carlo Besta”, Milan, Italy

to my friend Paolina

Index

Summary

Neurodegeneration with brain iron accumulation (NBIA) comprises a heterogeneous group of genetically defined disorders clinically characterized by progressive extrapyramidal deterioration and by iron accumulation in the basal ganglia. The clinical spectrum of NBIA is extremely wide and includes early-onset neurodegeneration and adult-onset parkinsonisms-dystonia. Recessive NBIA syndromes may be due to mutations in the PANK2, PLA2G6, FA2H, and C19orf12 genes, but still in a large proportion of patients, no genetic alteration can be found. Using Whole Exome Sequencing (WES) strategy we identified, in a NBIA patient, a homozygous missense mutation in the gene codifying for coenzyme A synthase (COASY). By performing traditional Sanger sequencing in a cohort of NBIA subjects, we found another mutant patient. COASY is a bifunctional mitochondrial enzyme involved in the two last steps of coenzyme A (CoA) biosynthesis, a molecule of primary importance for several metabolic pathways. The missense mutation found affects a highly conserved aminoacid residue in the catalytic site of COASY. Western-blot analysis showed that the protein is absent in patient-derived skin fibroblasts. We synthesized human wild-type and mutated catalytic domain and full-length COASY to analyze, by HPLC, in-vitro protein activity. Additional experiments were performed on yeast cells and on patient-derived skin fibroblasts. Together with mutations in *PANK2*, coding for the first enzyme involved in CoA biosynthesis, mutations in *COASY* impinge on the same biosynthetic pathway causing NBIA. For this reason further analysis were performed also on PKAN patient-derived skin fibroblasts and on *Pank2* knockout mouse model, to better understand the link between CoA synthesis defect and neurodegeneration.

Section I

State of the Art

NEURODEGENERATION WITH BRAIN IRON ACCUMULATION

Neurodegeneration with brain iron accumulation (NBIA) is a group of neurodegenerative disorders clinically characterized by iron overload in discrete brain regions, specifically in the basal ganglia. Prevalence data regarding this disorder remains incomplete, however it is estimated that anywhere between 1 in 1,000,000 to 3 in 1,000,000 individuals will be afflicted with this disorder [Gregory and Hayflick, 2013]. The basal ganglia consist of four interconnected nuclei: striatum, globus pallidus, substantia nigra and subthalamic nucleus. A family of basal ganglia circuits are involved in skeletomotor, oculomotor and limbic functions. Other basal ganglia circuits are involved in regulation of eye movements, mood, reward and executive functions. Diseases in the basal ganglia are associated with movement disorders and neuropsychiatric diseases [Kandel et al., 2013].

In NBIA, excess iron accumulates in the globus pallidus and in the substantia nigra and can be visualized with magnetic resonance imaging (MRI). The substantia nigra and the globus pallidus naturally contain high iron concentrations (up to 450 μg per g wet weight of brain) and also have a high metabolic requirement, potentially predisposing these areas to iron-related damage. The accumulation of iron has neither been proven to be cause nor symptom in NBIA. Iron is indispensable in mammalian metabolism because it is integral to the formation of haem and iron–sulphur clusters and functions as a cofactor in numerous metabolic reactions [Roualt, 2013]. Abnormalities in brain iron metabolism are involved in the pathogenesis of several degenerative brain diseases. It is often not known whether iron accumulation contributes to disease progression or whether accumulation of iron occurs only after widespread neuronal death. In general, when iron accumulation is detected by MRI, it is often assumed to have a causal role in disease by enhancing free radical formation and contributing to oxidative stress and neuronal death in iron-overloaded cells [Sian-Hulsmann et al., 2011; Weinreb et al., 2010].

As well as iron accumulation, patients with NBIA, exhibit dystonia, parkinsonism and spasticity. Genetically confirmed pathological studies have identified protein aggregates and axonal swellings that are reminiscent of other common neurodegenerative disorders.

Most NBIA disorders are inherited in an autosomal recessive mode and generally begin in childhood or adolescence. NBIA diseases are associated with mutations in identified genes. Genetic screening over the last decade has identified 10 disease-associated genes, which lead to NBIA;

however, around 20% of NBIA cases remain genetically undefined [Arber et al., 2015]. At first glance, these 10 genes appear to be unrelated and are involved in diverse cellular pathways. Only two genes related to NBIA, encode proteins that are specifically involved in iron metabolism: ceruloplasmin (CP) and ferritin light chain (FTL). The other NBIA disease genes encode proteins with other functions, some of which are related to coenzyme A biosynthesis (PANK2 and COASY), fatty acid metabolism (C19orf12, PLA2G6, FA2H), DNA damage response (DCAF17), autophagy (WDR45) or lysosomal activity (ATP13A2) [Table 1]**.**

DISEASE	DISEASE GENE	INHERITANCE	SYMPTOMS
Neuroferritinopathy	*FTL* (19q13.3)	Autosomal dominant	Extrapyramidal signs, dystonia, orofacial dystonia, cognitive decline
Acaeruloplasminaemia	*CP* (3q23.25)	Autosomal recessive	Iron in the basal ganglia, liver, pancreas and myocardium; cognitive impairment, diabetes mellitus, retinal degeneration, blepharospasm, facial and neck dystonia, chorea, dysarthria, ataxia
PANK2-associated neurodegeneration (PKAN)	*PANK2* (20p12.3)	Autosomal recessive	Dystonia, spasticity, cognitive decline, pigmentary retinopathy
PLA2G6-associated neurodegeneration (PLAN)	*PLA2G6* (22q12.13)	Autosomal recessive	Infantile neuroaxonal dystrophy, progressive motor and mental retardation, cerebellar ataxia, pyramidal signs
Mitochondrial membrane protein-associated neurodegeneration (MPAN)	*C19orf12* (19q12)	Autosomal recessive	Iron-containing deposits, dystonia, parkinsonism, psychiatric symptoms, spastic paraparesis
FA2H-ssociated neurodegeneration (FAHN)	*FA2H* (16q23)	Autosomal recessive	Spastic quadriparesis, severe ataxia, dystonia

Kufor–Rakeb disease	*ATP13A2* (1p36)	Autosomal recessive	Early-onset levodopa-responsive parkinsonism with pyramidal tract involvement, dementia
Woodhouse–Sakati syndrome	*DCAF17* (2q31.1)	Autosomal recessive	Hypogonadism, alopecia, diabetes mellitus, mental retardation, deafness, electrocardiographic abnormalities
β-Propeller protein-associated neurodegeneration (BPAN)	*WDR45* (Xp11.23)	X-linked	Cognitive impairment, progressive dystonia-parkinsonism, corticospinal signs
COASY-associated neurodegeneration (CoPAN)	*COASY* (17q12.21)	Autosomal recessive	Oro-mandibular dystonia, dysarthria, spastic dystonic paraparesis, obsessive-compulsive behaviour

Table 1. **NBIA and associated genes.** The table summarizes the currently known genes involved in NBIA. *FTL*, ferritin light chain polypeptide; *CP*, ceruloplasmin; *PANK2*, pantothenate kinase 2; *PLA2G6*, phospholipase A2, group VI; *C19orf12*, chromosome 19 open reading frame 12; *FA2H*, fatty acid 2 hydroxylase; *ATP13A2*, ATPase type 13A2; *DCAF17*, DDB1- and CUL4-associated factor 17; *WDR45*, WD40 repeat domain 45; *COASY*, CoA synthase.

1. NBIA caused by defective lipid metabolism

1.1 NBIA caused by defective coenzyme A biosynthesis

Coenzyme A

Coenzyme A (CoA) is an indispensable cofactor in all living organisms. CoA is utilized in about 100 biosynthetic and degrading reactions. Over 4% of cellular reactions utilize CoA. As a high-energy carrier of acetyl and acyl groups, CoA is central to diverse cellular metabolic processes including citric acid cycle, fatty acid biosynthesis, β-oxidation, cholesterol and sphingolipid synthesis. In addition, CoA is a crucial factor in regulating a variety of enzymatic reactions and cellular metabolic processes. De novo synthesis of CoA is a highly conserved pathway that includes five enzymatic steps: pantothenic acid (vitamin B5) phosphorylation, cysteine conjugation, decarboxylation, conjugation to an adenosyl group and phosphorylation. In mammals, the first step

is catalysed by PANK, whereas the last two steps are catalysed by COASY, a mitochondrial bifunctional enzyme having a PPAT (4-phosphopantetheine-adenylyl transferase) and a DPCK (dephospho-CoA kinase) activities [Figure 1].

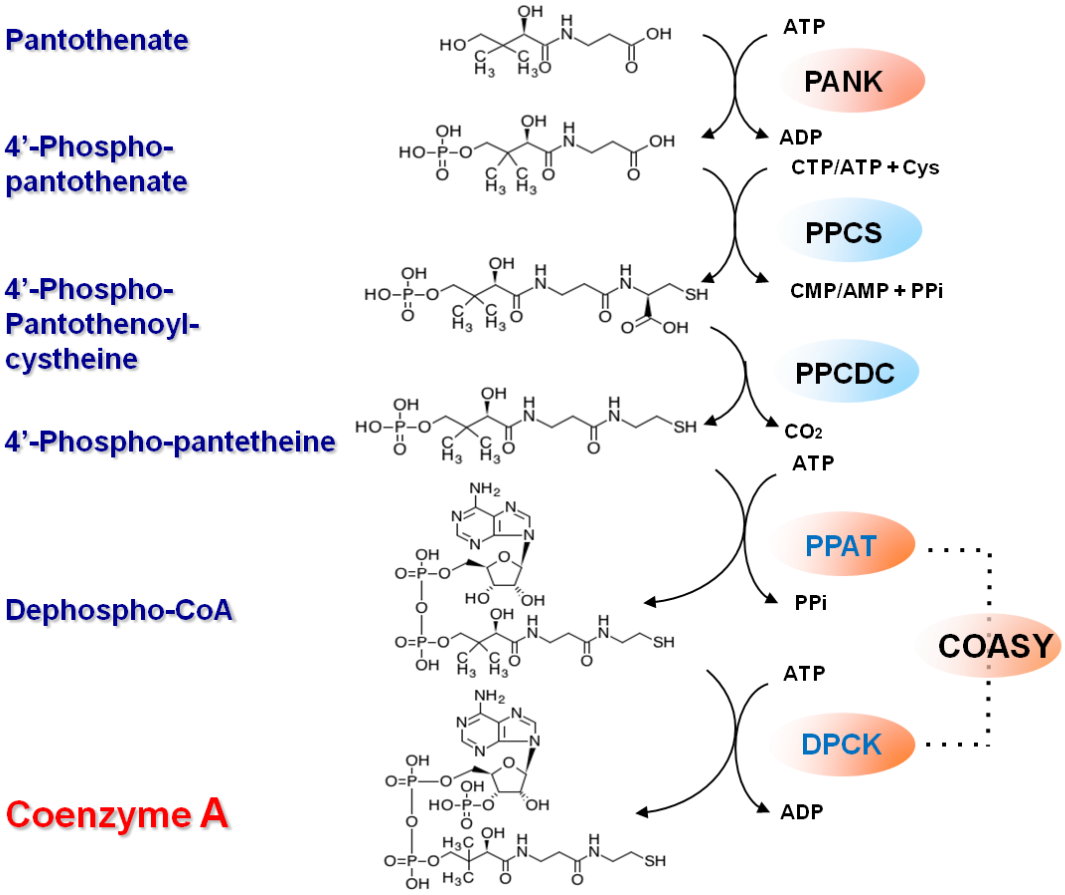

Figure 1. **Coenzyme A biosynthetic pathway in human**

In other organisms, such as bacteria and yeast, PPAT and DPCK activities reside in two different enzymes: Cab4 and Cab5 in yeast, CoAD and CoAE in bacteria.

The reaction catalysed by PANK is the primary rate-limiting step in CoA biosynthesis and it is controlled by CoA and CoA thioesters, the end-products of the pathway. In bacteria, a second level of regulation is evident at PPAT (or CoAD). CoA consists of 3'-phosphoadenosine linked through the 5' position of the ribose, to pantothenic acid via pyrophosphate linkage. The carboxyl end of pantothenic acid is linked through a peptidic bond to 2-mercaptoethanol amine. The thiol group at the end is essential to the chemical reactions where CoA is involved in, for this reason the enzymes involved in CoA biosynthesis are highly specific in incorporating cysteine, but not other amino acids [Strauss and Begley, 2005].

Tissue levels can vary widely depending on the organ in question, diet and fed/fasting state. The ratio of free CoA to acyl-CoA is important for regulating many key metabolic enzymes, such as acyl-CoA synthetase, PDH (pyruvate dehydrogenase) and 2-OG (2-oxoglutarate) dehydrogenase. The level of CoA is regulated by numerous extracellular stimuli, including hormones, glucocorticoids, nutrients and cellular metabolites [Tahiliani and Beinlich, 1991] and a link between the complex signaling mTOR pathway, which is implicated in numerous metabolic and signalling processes, and CoA biosynthesis has been proposed [Nemazanyy et al., 2004].

CoA is required in mitochondria for the citric acid cycle, in chloroplasts for fatty acid synthesis, and in peroxisomes for β-oxidation. CoA must be imported into these organelles from the cytosol. Yeast and mammalian mitochondria and peroxisomes have to import CoA because they cannot make it [Agrimi et al., 2012]. Mitochondrial CoA transporters belong to the mitochondrial carrier family (MCF) and have been identified in yeast [Prohl et al., 2001] and human [Fiermonte et al., 2009]. The compartmentalization of CoA in all eukaryotes appears to be highly regulated: cytosol and organelles maintaining separate CoA pools whose levels can modulate fluxes through CoA-dependent reactions. Mammalian cytosolic concentrations are estimated to be in the range 0.02–0.14 mM in animal tissues, whereas mitochondrial concentrations are much higher: from 2 to over 5 mM [Leonardi et al., 2005].

Mutations in *PANK2* and *COASY* have been identified as responsible for some forms of NBIA, namely PKAN and CoPAN. It is interesting to notice that PANK2 and COASY are both localized into mitochondria. Mitochondria are the main sites of iron utilisation in the cell [Levi and Rovida, 2009]. This organelle employs iron for the biosynthesis of the iron sulphur cluster and heme cofactors, which are prosthetic groups of many proteins involved in key biological processes, such as electron transfer, DNA synthesis and repair, metabolic and regulatory processes [Stehling et al., 2014].

Pantothenate kinase-associated neurodegeneration (PKAN)

Mutations in the pantothenate kinase 2 gene (*PANK2*) lead to pantothenate kinase-associated neurodegeneration (PKAN) that represents the most common genetic cause of NBIA and occurs in around two-thirds of NBIA patients [Hayflick et al., 2003; Zhou et al., 2001].

PKAN, previously known as Hallervorden-Spatz syndrome is the best-known example of neuronal brain iron accumulation associated with neurological impairments, including childhood-onset dystonia and spasticity [Kruer et al., 2012]. The gene associated with the disease was identified in 2001 as the gene that encodes pantothenate kinase 2 (PANK2), an enzyme that occupies the mitochondrial inter-membrane space [Leonardi et al., 2007; Brunetti et al., 2012] and is important

for biosynthesis of coenzyme A from pantothenate. *PANK2* is a gene with seven exons, which is alternatively spliced to form two transcript variants. There is a strong correlation between loss of enzymatic activity and disease onset. Despite the fact that PANK2 proteins form homodimers, it is unlikely that mutant PANK2 has a dominant negative effect, as co-expression of mutant PANK2 and wild-type PANK2 shows similar activity to wild-type PANK2 alone [Zhang et al., 2006]. PANK2 is one of four human pantothenate kinase proteins and is specifically located in the mitochondria [Hortnagel, 2003; Kotzbauer, 2005]. PANK4 is proposed to be nonfunctional while PANK1 and PANK3 are active in the cytosol. PANK2 dysfunction is compatible with life, and the two functional homologues, *PANK1* and *PANK3*, may compensate for the loss of PANK2. The PANK2 polypeptide contains a mitochondrial localization signal. There is a catalytic ATP binding domain located at the N-terminus of the protein and a domain of unknown function at the C-terminus of the protein. PANK2 homodimers are located in the mitochondrial intermembrane space. Mutations in PANK2 result in enzyme deficiency, leading to insufficiency of the final product and accumulation of upstream substrates, such as N-pantothenoil-cysteine and pantetheine, which are potentially toxic [Leoni et al., 2012]. In particular, cysteine is a potent iron chelator, and it has been proposed that high local levels of cysteine are the basis of the subsequent accumulation of iron, resulting in increased oxidative stress. The other hypothesis to explain the observed iron accumulation suggests that alterations in phospholipid metabolism due to CoA-deficiency may injure the membranes, with consequent oxidative stress that leads to iron accumulation [Leonardi et al., 2005].

Different animal models have been developed using *Drosophila melanogaster* and *Mus musculus*. Mice lacking *Pank2* (*Pank2-/-* mice) did not develop brain iron accumulation or apparent neurological difficulties as expected, but they developed retinal problems and had a lack of viable sperm [Kuo et al., 2005]. A subsequent study showed that neurological symptoms occurred only when *Pank2-/-* mice were deprived of dietary pantothenic acid [Kuo et al., 2007]. *D. melanogaster PANK2* homologue (*fumble*) hypomorphs did not show CNS iron overload, although they developed neurodegeneration and had diminished CoA levels [Bosveld et al., 2008; Wu et al., 2009]. Both effects could be prevented by providing pantethine in the diet, which may allow bypass of the mutant enzyme and may be a possible approach for the treatment of human subjects [Rana et al., 2010]. A very recent study has demonstrated that there are alternative mechanisms, which allow cells and organisms to adjust intracellular CoA levels by using exogenous CoA. CoA was hydrolyzed extracellularly by the enzyme ectonucleotide pyrophosphatases to 4′-phosphopantetheine, a biologically stable molecule able to translocate through membranes via

passive diffusion. Inside the cell, 4′-phosphopantetheine was enzymatically converted back to CoA [Srinivasan et al., 2015].

Patients with PKAN have increased serum levels of lactic acid and pantothenate, and an analysis of fibroblasts from these patients suggested that cholesterol levels and fatty acid synthesis were decreased [Leoni et al., 2012]. Moreover, mitochondria from *Pank2-/-* mice have a reduction in mitochondrial potential, oxygen consumption and ATP generation, and that numerous mitochondria are swollen and contain disrupted cristae [Brunetti et al., 2012]. It is unknown the reason why PANK2 deficiency is associated with iron overload specifically in the globus pallidus. Abnormal ferroportin expression has been described in PANK2-deficient cell lines [Poli et al., 2010].

PKAN fibroblasts, maintained in chronic iron supplementation, showed disturbed iron sensor protein iron regulatory protein 1 (IRP1) activity, resulting in deregulation of ferritin and transferrin receptor1 (TfR1), as well as a larger intracellular bioactive labile iron pool (LIP). This effect results in higher ROS development and leads to increased cellular oxidative status [Campanella et al., 2012].

Perhaps the globus pallidus is particularly affected in PKAN because the expression levels of PANK1 and/or PANK3 are too low to compensate for the loss of PANK2. In the globus pallidus area, iron was increased in the cytoplasm of degenerating neurons, implying that neurons manifest iron overload before their death and that iron overload may contribute to neuronal loss in PKAN. Astrocytes showed marked iron overload in the globus pallidus of patients with PKAN, but there was no substantial iron accumulation in microglia or oligodendrocytes. These findings provided an explanation for the characteristic MRI finding in PKAN patients, known as the ‘eye of the tiger’ [Kruer et al., 2011], that is a region of hyperintensity surrounded by an area of hypointensity (characteristic of iron accumulation) [Figure 2**]**.

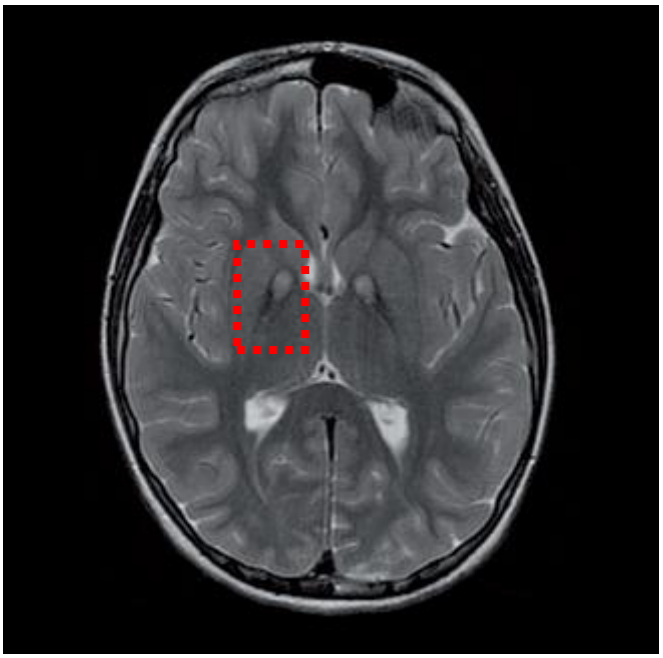

Figure 2. **MRI of a PKAN patient.** It is shown the classical 'eye of the tiger' sign. Hyperintense (white) signals indicative of tissue rarefaction are seen (centre of red rectangle) surrounded by areas of hypointensity (black areas) attributable to iron accumulation.

In PKAN patients, cortical and subcortical brain regions show axonal swellings and spheroid bodies. These represent degenerating neurones and dystrophic axons. A loss of myelin and vacuolization has been described in the pallidum [Li et al., 2012], potentially linking PKAN to other demyelinating conditions.

Coenzyme A synthase protein-associated neurodegeneration (CoPAN)

Mutations in the Coenzyme A synthase (*COASY*) gene were recently shown to lead to NBIA. COASY protein-associated neurodegeneration (CoPAN) patients display similar clinical features to PKAN patients [Dusi et al., 2014].

COASY is a bifunctional enzyme that contains a mitochondrial localization signal, a regulatory region and a domain for each of the two catalytic domains: adenyl-transferase and dephospho-CoA kinase. COASY is localized to the mitochondrial matrix [Dusi et al., 2014; Daugherty et al., 2002]. There are two COASY isoforms, α and β produced from alternate splicing. The longer β isoform is brain specific and has an additional proline-rich protein interaction domain but has identical enzymatic activity to the ubiquitous α isoform [Nemazanyy et al., 2006]. The mutation identified in two NBIA patients, affects a conserved residue involved in ATP binding and dephospho-CoA kinase activity (R499C). This mutation is proposed to completely abrogate the protein functionality in a homozygous condition [Dusi et al., 2014]. Yeast knockout model for the two COASY

orthologue lead to a lethal phenotype. Human wild-type COASY can rescue this lethality, while mutant COASY containing the R499C change, are able to rescue knockout cells but lead to a higher requirement for pantothenate in the growth media [Dusi et al., 2014]. COASY belongs to the same metabolic pathway as PANK2 and catalyzes the final two steps of CoA synthesis [Nemazanyy et al., 2006; Aghajanian and Worral, 2002]. Mutant dephospho-CoA kinase domain appears to have no activity *in vitro*, whereas CoA levels in patient and control fibroblasts appear normal [Dusi et al., 2014]. This suggests CoA levels are maintained by a residual activity of the COASY, or via an alternative, as yet unknown, pathway for CoA synthesis. The fact that COASY acts in the same pathway as PANK2 suggests common mechanisms may be shared between PKAN and COPAN, such as reduced acyl-CoA and lipid synthesis leading to mitochondrial insufficiencies. *COASY* shows a putative iron response element (IRE). The sequence is a putative 3' IRE and could lead to mRNA stabilization in the presence of iron. This could potentially link *COASY* expression to iron availability in the cell.

1.2 NBIA caused by defective fatty acid metabolism

Phospholipase A2, group VI-associated neurodegeneration (PLAN)

The first disease to be recognized as a distinctive non-PKAN type of NBIA disease was PLAN. Mutations in the gene encoding phospholipase A2 group VI calcium-independent (*PLA2G6*, also known as *iPLA2β*) have been associated with two diseases: phospholipase-associated neurodegeneration (PLAN) and dystonia-parkinsonism. PLA2G6-associated disease may have previously represented infantile neuroaxonal dystrophy (INAD) before NBIA reclassification. There are four groups of PLA2 enzymes containing more than 20 proteins: secreted PLA2s, calcium-dependent cytosolic PLA2s, platelet-activating acetylhydrolases and calcium-independent PLA2s (iPLA2). PLA2G6 is responsible for 70% of total PLA2 activity in the brain. The *PLA2G6* gene encodes an 806 amino acid protein with predicted size of 88 kDa. The mature protein is tetrameric and composed of an ankyrin repeat domain that is involved in protein interaction, a GXSXG lipase motif, an ATP binding pocket and a Calmodulin binding domain [Balsinde and Balboa, 2005]. There are at least five splice variants, three of which contain the lipase motif GXSXG, whereas two contain only the ankyrin repeats and most likely act as competitive inhibitors within the tetramer [Larsson et al., 1998]. PLA2G6 has been shown to be expressed in the mitochondria [Liou et al., 2005] and be important for mitochondrial health [Seleznev et al., 2006]. PLA2G6 is ubiquitously expressed [Song et al., 2010]. Autosomal recessive mutations are found throughout *PLA2G6* and lead to reduced enzyme activity. Some adult patients with PLAN develop dystonia and spasticity.

The major pathological hallmark of PLAN is the presence of axonal swellings throughout the cortex, globus pallidus, striatum, cerebellum, brain stem and spinal cord [Morgan et al., 2006].

PLA2G6 hydrolyses glycerophospholipids at the sn-2 position of acyl chains to produce lysophospholipids and free fatty acids, such as arachidonic acid. The downstream metabolites of free fatty acids, such as leukotrienes and prostaglandin, perform essential cellular functions and contribute to a variety of signalling events including membrane remodelling, fatty acid oxidation, cell signalling and growth, and apoptosis [Balsinde and Balboa, 2005]. The 2-lysophophospholipid may also play a role in signalling such as in the production of platelet activating factor. Phospholipase activity is crucial for membrane integrity via phospholipid recycling and homeostasis. PLA2G6-mediated neurodegeneration may occur via the inability to remodel oxidized and damaged phospholipids. Polyunsaturated inner-membrane mitochondrial components, such as cardiolipin, are extremely sensitive to ROS. Mice that lack PLA2G6 (*Pla2g6*$^{-/-}$) have disorganized mitochondrial inner membranes, which are distinctive because they contain large amounts of cardiolipin. It is a flexible molecule in which two fatty acid-bearing glycerol molecules are bridged by a single glycerol. The structure of cardiolipin envelopes respiratory chain complexes, tether these complexes to the inner mitochondrial membrane and protect proteins from free radical damage by donating electrons from the unsaturated fatty acid side-chains of cardiolipin. The role of PLA2G6 may be to remove saturated fatty acid side-chains from newly synthesized cardiolipins so that they can be replaced with unsaturated linoleic fatty acids (which are characteristic of cardiolipins) and also to remove fatty acids damaged by oxidative stress. A study in mice revealed that one of the first pathological signs of PLA2G6 deficiency is disorganization of the mitochondrial inner membrane cristae, followed by mitochondrial rupture, release of cytochrome C and formation of swollen axons as the disease progresses. Presynaptic membranes were also abnormal in PLA2G6-deficient mice, perhaps because mitochondria at these sites require PLA2G6-mediated phospholipid remodelling to maintain integrity [Beck et al., 2011].

PKAN and PLAN have common features maybe because PANK2 and PLA2G6, converge on cardiolipin metabolism in the mitochondrial inner membrane, either by synthesizing coenzyme A to activate fatty acids required for its remodelling and repair (this is the case for PKAN), or by supplying an enzyme that facilitates deacylation and remodelling of mature cardiolipin (this is the case for PLAN) [Figure 3**]**. A study in mouse model of PKAN, showed that mitochondrial inner membranes are highly disorganized in *Pank2*$^{-/-}$ mice [Brunetti et al., 2012], similar to the mitochondrial inner membrane abnormalities observed in mouse models of PLAN [Beck et al., 2011]. Studies in *Saccharomyces cerevisiae* demonstrated that loss of cardiolipin synthase results in diminished synthesis of iron–sulphur clusters and mitochondrial iron overload [Paisán-Ruiz et al.,

2012], a complication that is frequently observed in human diseases caused by dysfunctional assembly of iron–sulphur clusters.

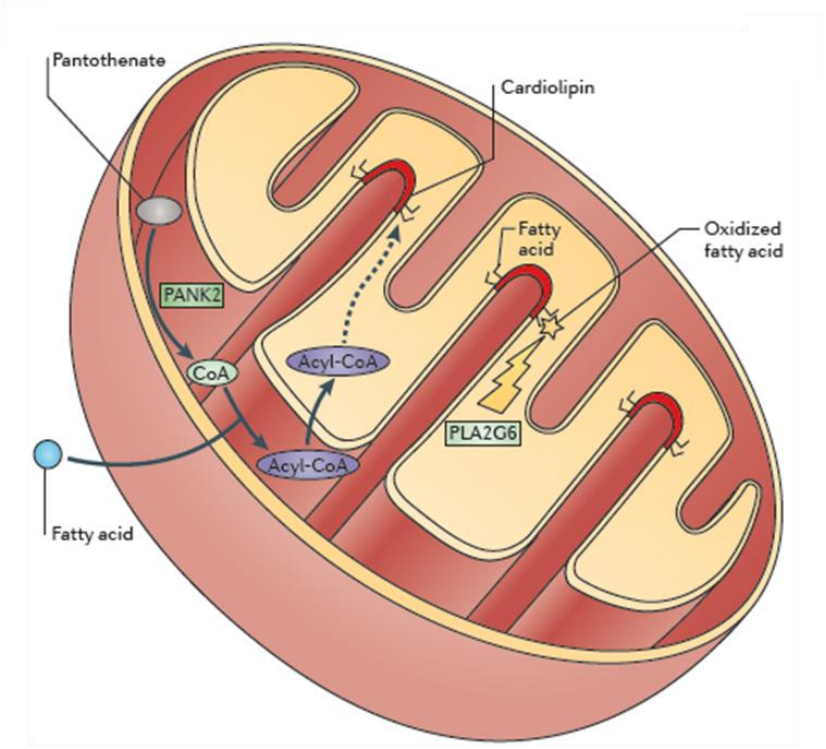

Figure 3. **PANK2 and PLA2G6 in mitochondria.** Mutations in *PANK2* and in *PLA2G6* may interfere with synthesis and remodelling of cardiolipin. PANK2 is needed for the formation of CoA from pantothenate. CoA condenses with fatty acids to form acyl-CoA, which crosses into the mitochondrial matrix using the carnitine carrier system. Acyl-CoA in the mitochondrial matrix either delivers fatty acids for incorporation into complex intra-mitochondrial lipids, such as cardiolipin, or may alternatively undergo oxidation by the mitochondrial respiratory chain to generate ATP. The matrix membrane contains cardiolipin that enables the inner membrane to bend and turn. PLA2G6 may remove damaged fatty acids to allow incorporation of flexible unsaturated fatty acids, such as linoleic acid, from the acyl-CoA pool in the matrix [Rouault, 2013].

Cells that aberrantly produce ROS sequester PLA2G6 to the mitochondria, and this is protective against apoptosis [Seleznev et al., 2006]. Patient cells were shown to display faulty mitochondrial at the ultrastructural level [Itoh et al., 1993; Mahadevan et al., 2000]. Uncoupling of the mitochondrial respiratory chain and associated depolarization can lead to activation of PLA2G6 within the mitochondria and therefore free fatty acid accumulation [Broekemeier et al., 2002]. This can initiate apoptosis through stimulating the permeability transition pore and cytochrome C release leading to further lipid damage and apoptotic signals [Gadd et al., 2006]. Reduced PLA2G6 activity may lead to deregulation of this process. Related to this, ER stress can increase the expression and activity of PLA2G6, bringing about the loss of mitochondrial membrane potential and increasing the likelihood of apoptosis [Lei et al., 2012]. Altered axonal and/or organelle membrane integrity may

lead to improper axonal transport and accumulation of cellular components at distal axon locations, subsequently leading to axonal blockage and degeneration [Roy et al., 2005]. Both products of PLA2G6 catalysis, lysophospholipids and free fatty acids, may be able to increase membrane fusion via increased fluidity in the local environment [Balsinde and Balboa, 2005]. This could have important roles in autophagy, mitophagy and other vesicle-based processes that have been shown to be involved in neurodegeneration. Docosahexaenoic acid (DHA) is an essential fatty acid that cannot be synthesized in neurons. Astrocytes have been shown to produce and release DHA due to PLA2G6 action [Green et al., 2008]. Knockdown of the enzyme in astrocytes leads to a reduction of arachidonic acid and DHA in neurons and increased prostaglandin production [Strokin et al., 2007], which could lead to increased apoptosis [Kondo et al., 2002]. *PLA2G6* is also mutated in cases of Parkinson disease and, for this reason, it is classified as a PD gene (PARK14) [Lu et al., 2012]. Iron accumulation is found in macrophages and in aggregates in the globus pallidus of patients with the parkinsonian presentation [Paisán-Ruiz et al., 2012]. In addition, a reduction of PLA2G6 protein levels has been shown in the brains of patients affected by Alzheimer's disease [Ross et al., 2002].

Mitochondrial membrane protein-associated neurodegeneration (MPAN)

Mutations in chromosome 19 open reading frame 12 (C19orf12) lead to mitochondrial membrane protein-associated neurodegeneration (MPAN). MPAN accounts for around 30% of NBIA cases [Hogarth et al., 2013]. Chromosome 19 open reading frame 12 (C19orf12) protein is a 17 kDa mitochondrial membrane-associated protein whose function is still unknown but it is co-expressed with genes involved in fatty acid metabolism and branched chain amino acid degradation. C19orf12 is a two-pass transmembrane protein with two alternative start codons. Missense mutations have been described to add charged amino acids to putative hairpin domains, potentially disrupting the 3D structure [Hartig et al., 2011]. MPAN has been successfully modelled in *Drosophila melanogaster* [Iuso et al., 2014]. Post-mortem examination of two MPAN cases showed iron accumulation mainly confined to the globus pallidus. Iron accumulation was accompanied by neuronal atrophy, and depositions were present in neurons, macrophages and, to a lesser extent, astrocytes. Lewy bodies and Lewy neurites were a characteristic feature of MPAN [Hogarth et al., 2013]. Lewy neurites in the globus pallidus were adjacent to the atrophied region and Lewy pathology extended to the SN where they were associated with near complete neuronal loss. Lewy bodies were also present in the cortex, striatum and hippocampus. Axonal swellings and hyperphosphorylated tau were also present in the cortex, globus pallidus, caudate/putamen, substantia nigra and brain stem. Demyelination was evident in the spinal pyramidal tracts and optic nerve.

C19orf12 codes for a transmembrane glycine zipper containing mitochondrial protein and a recent study have demonstrated that wild-type C19orf12 was not exclusively present in mitochondria, but also in the endoplasmic reticulum (ER) and MAM (Mitochondria Associated Membrane), while missense mutant C19orf12 variants presented a different localization. After induction of oxidative stress, a GFP-tagged C19orf12 wild-type protein was able to relocate to the cytosol. On the contrary, mutant isoforms were not able to respond to oxidative stress [Venco et al., 2015].

Fatty acid hydroxylase-associated neurodegeneration (FAHN)

Fatty acid hydroxylase-associated neurodegeneration (FAHN) is caused by mutations in the gene encoding fatty acid-2-hydroxylase (FA2H). FAHN is characterized initially by spasticity, a mixed movement disorder, ataxia, dystonia, optic atrophy and oculomotor abnormalities, and later by progressive intellectual impairment and seizures [Kruer et al., 2010]. FA2H is a 43 kDa membrane-bound protein, residing in the ER [Eckhardt et al., 2005]. The protein has a C-terminal sterol desaturase domain, which contains an iron binding histidine motif and is responsible for catalytic activity, and an N-terminal cytochrome b5 haem-binding domain, involved in redox activity and electron donation. [Alderson et al., 2004; Hama, 2010]. FA2H produces the 2-hydroxylated fatty acids that are incorporated into sphingolipids [Dan et al.,2011]. 2-hydroxylated fatty acids are precursors for the synthesis of ceramide, a critical component of myelin sheaths [Eckhardt et al., 2005]. Inactivating mutations in *FA2H* are likely to affect normal myelin production due to loss of the hydroxylase activity of the enzyme. The late onset and slow progression are consistent with this idea, analogous to demyelinating diseases such as multiple sclerosis. Altered ceramide signalling may have roles in Lewy body formation, and the role of ceramide in apoptosis and neurodegeneration has been implicated [Bras et al., 2008; Jana et al., 2009]. FA2H also has a role in lipid signalling pathways that can affect cell cycle and apoptotic pathways [Hama, 2010].

Moreover, axonal function is compromised in mice lacking FA2H. In mouse models of FAHN, regions of pronounced white matter degeneration showed accumulation of microglia-like cells. These cells may accumulate iron-loaded ferritin [Potter et al., 2011]. MRI studies in patients with FAHN have detected iron accumulation not only in the globus pallidus but also in the substantia nigra and subcortical and periventricular regions [Gregory and Hayflick, 2011].

2. NBIA caused by defective iron homeostasis

Neuroferritinopathy

Neuroferritinopathy is an autosomal dominant neurodegenerative disease caused by mutations in the ferritin light chain (FTL). Seven distinct disease-causing mutations have been reported in this disease, but it is most commonly caused by the insertion of an extra nucleotide in the fourth exon of the gene encoding the FTL, which causes a frame-shift and synthesis of an abnormal C-terminus [McNeill and Chinnery, 2011]. When FTL with this abnormal C-terminus (that may constitute an important part of the iron entry pore [Burn and Chinnery, 2011] is incorporated into the ferritin heteropolymer, the spherical ferritin no longer has an intact proteinaceous shell to protect sequestered iron, and as a result, it is likely that iron 'leaks' out of ferritin [Friedman et al., 2011]. This could cause iron-dependent oxidation, particularly in cells that normally express high amounts of FTL. The presence of one abnormal allele that encodes a truncated form of ferritin is sufficient to cause neuroferritinopathy associated with cognitive and behavioural impairments, which generally manifest between the third and sixth decades of life [Baraibar et al., 2010]. Pathological investigations have shown ferritin inclusions in glia and neurons, as well as iron deposition. Mitochondrial abnormalities have been observed, and an increased oxidative stress of the cells, possibly due to iron, was shown via peroxidation and nitrosylation [Curtis et al., 2001; Vidal et al., 2004; Mancuso et al., 2005]. A mouse model of neuroferritinopathy recapitulates many aspects of the disease [Vidal et al., 2008]. Crystal structures of ferritin containing the mutant light chain, have revealed that the initial iron sequestration is impaired and that iron-induced ferritin precipitation is enhanced [Baraibar et al., 2010].

Aceruloplasminaemia

Aceruloplasminaemia is caused by mutations in ceruloplasmin (CP), which result in loss of the functional protein. CP is a glycoprotein containing many copper atoms (and potentially iron atoms) that acts as a ferroxidase to facilitate ferroportin mediated cellular iron export. Oxidation of ferrous iron (Fe^{2+}) to ferric iron (Fe^{3+}) enables binding to transferrin for iron transport in the extracellular environment. In aceruloplasminaemia, iron entering the CNS as ferrous iron might not undergo oxidation. Consequently, cells exposed to the resulting excess ferrous iron could readily become iron-loaded through an unregulated pathway of non-transferrin-bound iron uptake [Brissot et al., 2012]. The unregulated uptake of ferrous iron, coupled with an inability to export iron, could produce the astrocytic iron overload that has been observed in this disease. Marked astrocytic iron overload, in conjunction with neuronal loss, was observed not only in the basal ganglia but also in

the cerebrum in a human case report [Kaneko et al., 2012]. Some mutant forms of ceruloplasmin may also accumulate in aggresomes and cause cell death through a non-iron related mechanism [Kono and Miyajima 2006; Kono et al., 2006].

Symptoms of aceruloplasminaemia include a triad of adult-onset neurological disease, diabetes mellitus and retinal degeneration. This pathology has been characterized in human autopsy samples [Gonzalez-Cuyar et al., 2008] and in mice lacking *Cp*, which develop ataxia [Jeong and David, 2006]. Iron overload has been observed in astrocytes in the affected brain regions of patients with aceruloplasminaemia, particularly in the basal ganglia [Jeong and David, 2003]. There is evidence for increased levels of oxidative stress, as indicated by increased lipid peroxidation and protein carbonylation [Kono and Miyajima 2006].

3. NBIA caused by defects in autophagy

β-propeller protein-associated neurodegeneration (BPAN)

Mutations in the WD repeat domain 45 gene (*WDR45*) are linked to β-propeller protein-associated neurodegeneration (BPAN). Despite *WDR45* being on the X chromosome, BPAN does not follow normal X-linked dominant inheritance. Both genders have similar clinical features, and the disease is always sporadic. Disease-associated mutations are predicted to lead to inactive proteins, and are presumed to be lethal for male embryos. Male BPAN sufferers are presumed to have de novo mutations and were shown to have somatic or germline mosaicism [Haack et al., 2012].

WDR45 is a β-propeller scaffold protein that has been predicted to have a role in autophagy. WDR45 is a member of the WD40 protein family, which is involved in protein–protein interactions and perform cellular functions such as autophagy, cell cycle progression and transcriptional control. WDR45 binds to phospholipids and autophagy-related proteins [Lu et al., 2011].

Yeast has over 30 autophagy-related genes (*atg*). Many mammalian *atg*-homologues have been found. WDR45 is one of 4 *atg18* homologues, crucial for autophagosome formation. *atg18* binds the ER membrane via a phosphotidylinositide-3-phosphate binding motif and facilitates downstream protein complex formation. Phosphatidylinositol-3-phosphate (PI3P) is a critical factor in autophagy and is a major component of autophagosome membranes. Upstream signalling (e.g. mTOR) controls PI3P and autophagic flux. PI3P may be involved in early membrane curvature and autophagosome size, for this reason WDR45 could regulate autophagosome size and maturation [Dall'Armi et al., 2013]. Lymphoid cells from five patients with truncated or mutated WDR45, show a blockage in autophagic flux when exposed to inhibitors or activators of autophagy [Saitsu et al., 2013].

In BPAN, iron deposition was strongest in the substantia nigra but also evident in the globus pallidus. Axonal spheroids were present in the basal ganglia and gliosis was prominent [Hayflick et al., 2013].

Recently, a central nervous system-specific Wdr45 knockout mouse model was generated. It shows poor motor coordination, greatly impaired learning and memory, and extensive axon swelling with numerous axon spheroids. Also its autophagic flux is defective and ubiquitin-positive protein aggregates accumulate in neurons and swollen axons [Zhao et al., 2015].

4. NBIA caused by defects in lysosomal metabolism

Kufor-Rakeb disease

Mutations in ATPase type13A2 (ATP13A2, also known as PARK9) lead to Kufor-Rakeb disease, a pathology characterized by juvenile onset parkinsonism and dementia [Di Fonzo et al., 2007], neuronal ceroid-lipofuscinosis [Bras et al., 2012] and NBIA [Schneider et al., 2010].

The protein is a lysosomal P-type ATPase that functions as divalent cation transporter. This superfamily of ATPases comprises transporters like calcium pumps, proton pumps and phospholipid flipases, and consists of highly conserved, 10-pass transmembrane proteins, which utilize the energy stored in ATP to transport ions across membranes [Kühlbrandt, 2004].

Fibroblasts from patients with *ATP13A2* mutations show lysosomal deficiencies that lead to cytotoxic effects in the presence of α-synuclein [Usenovic et al., 2012] and zinc [Tsunemi and Krainc, 2014]. Intracellular manganese levels were shown to be higher in cells with mutant *ATP13A2* compared with wild type, hinting to reduced secretion ability [Tan et al., 2011]. This may directly lead to cytochrome C release from mitochondria and apoptosis. Patient-derived fibroblasts have shown an impaired respiratory chain function and reduced ATP production. A quantification of mitochondrial DNA (mtDNA) levels resulted in a significantly increase of mtDNA to nuclear DNA in patient-derived fibroblasts. However, patient-derived fibroblast showed more mtDNA lesions (nicks, breaks, base modifications or bulky DNA adducts) than controls [Grünewald et al., 2012].

Mitochondria are very dynamic organelles that continuously shift between fusion to each other and division, to form a mitochondrial network in the cell. The proteins that mediate mitochondrial dynamics are highly regulated and loss of either fusion or division activity results in dysfunctional mitochondria. Mitochondrial fusion may buffer partially defects and transient stresses in the cell. For this reason a high fragmented mitochondrial network could be related to a cell-suffering state

[Nunnari and Suomalainen, 2012]. Mitochondrial network in fibroblast from patients with *ATP13A2* mutations, resulted more fragmented than controls [Grünewald et al., 2012].

5. NBIA caused by defects in DNA damage response

Woodhouse-Sakati syndrome

DDB1 and CUL4 associated factor 17 (DCAF17) is a protein of unknown function that is expressed in the nucleolus. Mutations in this gene lead to Woodhouse-Sakati syndrome. A subset of patients with Woodhouse-Sakati syndrome displays brain iron accumulation [Alazami et al., 2008]. DCAF17 is a multipass transmembrane protein that is named due to protein–protein interactions, Ddb1 and Cul4-associated factor (damaged DNA binding protein 1 and cullin 4 ubiquitin ligase complex) [Jin et al., 2006]. This association links DCAF17 to protein ubiquitination involved in DNA damage and cell cycle control. The nucleolar localization leads to intriguing questions about specific function and any links to other NBIA-linked mutations.

6. Current treatment of NBIA

Understanding the pathogenesis of NBIA is necessary for the development of successfully treatments. To date the therapeutic options for NBIA disorders remain largely symptomatic. Pharmacotherapy, such as dopaminergic drugs, anticholinergics, tetrabenazine, and other drugs may bring some relief. Deep brain stimulation can produce some benefit. However, these approaches are rarely fully satisfactory and do not slow disease progression.

With the assumption that iron plays a causative role, chelators, which reduce the amount of free iron have moved into the centre of attention. In a clinical trial on PKAN patients, the oral iron-chelator deferiprone produced significant (median 30%) reduction in globus pallidus iron content, ranging from 15 to 61%, but there was no clinical benefit [Cossu et al., 2014].

Aim of the Project

The specific aims of my PhD project were:

1. Identification and characterization of new disease genes involved in NBIA pathology.

We have performed Whole Exome Sequencing (WES) analysis in one subject with clinical presentation and neuroimaging suggestive of NBIA but without any mutations in previously associated genes. We have identified a homozygous missense mutation in coenzyme A synthase gene (*COASY*), the enzyme involved in the last two steps of CoA biosynthesis. After that, we have performed traditional Sanger sequence analysis on a larger cohort of idiopathic NBIA cases and we found a second subject carrying mutations in the same gene. We have performed several studies to characterize COASY to better understand the role of CoA in NBIA pathology.

2. Further studies on pantothenate kinase 2 (PANK2).

We have performed several studies to better characterize PANK2, the enzyme involved in the first step of CoA biosynthesis, to search for a correlation between defects in lipid metabolism, mitochondrial functionality and NBIA.

Main Results

1. Identification and characterization of new disease genes involved in NBIA pathology.

Molecular and biochemical results

WES analysis of one subject affected by idiopathic NBIA resulted in the identification of a homozygous mutation in coenzyme A synthase (*COASY*), the gene coding for a bifunctional enzyme converting 4-phosphopantetheine into dephospho-CoA and then to coenzyme A, and we have considered this mutation as potentially relevant for the disease. This subject has shown a homozygous missense mutation, a c.1495C>T transition causing an amino acid change p.Arg499Cys (subject 1).

Consequently, we have analyzed *COASY* in a cohort of 280 NBIA-affected individuals by using polymerase chain reaction and direct Sanger sequencing. By this analysis we identified a second Italian subject carrying *COASY* mutations. This subject turned out to be a compound heterozygote for the same mutation c.1495C>T (p.Arg499Cys) and for a c.175C>T transition, resulting in a premature p.Gln59* stop codon in the N-terminal regulatory region of the protein (subject 2). Segregation analysis in the parents demonstrated that the two mutations were localized on different alleles.

The missense mutation p.Arg499Cys, affected the amino acid residue Arg499, which is highly conserved in all available animal, plant, and yeast species, and is localized in the nucleotide-binding site of the DPCK domain.

Quantitative real-time PCR, performed on skin fibroblasts derived from the two patients, shown that in subject 1 the amount of mutant COASY transcript was similar to that of the control sample but it was reduced to 50% in subject 2, suggesting RNA decay. Immunoblot analysis revealed a significant reduction of the protein amount in the fibroblasts of the two patients. This suggests that the p.Arg499Cys change is associated with instability or accelerated degradation of COASY.

To determine if COASY forms potential complexes with other proteins belonging to the CoA biosynthetic pathway, we performed co-immunoprecipitation (Co-IP) assay with PANK2 and PPCS and 2D-Blue Native gel analysis on HeLa cells. We observed that COASY did not co-immunoprecipitate with PPCS and PANK2. A similar result was observed in the 2D-Blue Native gel: COASY did not seem to form a protein complex with the other enzymes involved in CoA biosynthesis (see **Supplementary data**- Figure S3).

Cellular localization studies

COASY is a mitochondrial protein. To better determine the sub-mitochondrial localization of COASY, we have carried out immunoblot analysis of mitochondria and sub-mitochondrial fractions derived from HeLa cells, using a commercially available antibody. Immunoblotting revealed the presence of a band of the expected molecular weight in total lysate and intact mitochondria. We treated mitochondria with proteinase K (PK) and demonstrated COASY resistance to degradation. The protein was also found in mitoplasts and was resistant to PK digestion. Further fractionation of mitoplasts demonstrated that the protein was mainly present in the matrix, probably anchored to the inner mitochondrial membrane.

Effect of p. Arg499Cys substitution

To study the effect of the p.Arg499Cys substitution on the DPCK domain activity, we expressed mRNA corresponding to the wild-type and mutant DPCK in bacteria as His-tag fusion proteins. HPLC analysis was used to evaluate dephospho-CoA conversion into CoA after incubation of wild-type and mutant DPCK domains with ATP and dephospho-CoA. The wild-type enzyme was able to completely convert dephospho-CoA into CoA, on the contrary, the DPCK-Arg499Cys mutant did not have this enzymatic activity and the peak corresponding to CoA was not observed. The same experiment was performed using the entire wild-type and mutant COASY proteins expressed in bacteria as His-tag fusion proteins. Wild-type COASY was able to synthesizes CoA, whereas mutant enzymes had an about 40-50% reduced activity compared to wild-type enzyme. The gain of functionality of the mutant COASY compared to the mutant DPCK domain, is not ascribable to the PPAT domain because wild-type PPAT is not able to synthesize CoA starting from 4-phospho-pantetheine, the typical substrate of COASY (see **Supplementary data**- Figure S1, Figure S2). This finding suggests that CoA biosynthesis might be compromised in the presence of p.Arg499Cys change.

Consequently, we analyzed CoA levels in fibroblasts derived from healthy and affected subjects by HPLC. We observed a general reduction of acetyl-CoA and total CoA in both affected individuals as compared to control.

To examine whether skin fibroblasts from patients were able to synthesize CoA, we evaluated CoA biosynthesis in cell homogenates with 4-PP (4-phosphopantetheine) as substrate. HPLC analysis showed that dephospho-CoA and CoA were efficiently produced de-novo from 4-PP in control fibroblasts. We also observed residual de novo production of dephospho-CoA and CoA in skin fibroblasts from patients, but the level of CoA was approximately 20% of that produced by control

fibroblasts. These findings suggest the existence of an alternative pathway for CoA biosynthesis, or the possibility that the remaining COASY aberrant protein may still retain some catalytic activity.

Studies in Saccharomyces cerevisiae

Biosynthesis of CoA in *Saccharomyces cerevisiae* follows the same pathway described for mammalian cells: pantothenate is converted in CoA in five reactions catalyzed by enzymes encoded by *CAB1* through *CAB5*. The only difference with human is that in yeast, the PPAT and DPCK activities reside on different proteins encoded by *CAB4* and *CAB5* genes, respectively. Sequence analysis indicated that Arg499 is highly conserved from yeast to human and corresponds to Arg146 in the yeast Cab5.

By using the plasmid shuffling method, we generated deletion strains expressing either the mutant alleles *cab5*^{Arg146Cys} and *COASY*^{Arg499Cys} or the *CAB5* and *COASY* wild-type genes. The Δ*cab5* lethal phenotype was rescued by the re-expression of either human *COASY* wild-type or human *COASY*^{Arg499Cys} and yeast *cab5*^{Arg146Cys}. We observed that the mutant strains *cab5*^{Arg146Cys} and *COASY*^{Arg499Cys} became auxotrophic for pantothenate and showed growth reduction: in the absence of pantothenate both strains failed to form colonies at the restrictive temperature of 37°C and a significant impairment of growth was observed at both 23°C and 28°C when compared with that of the strain expressing the wild-type alleles. This result supports the pathogenicity of the substitution p.Arg499Cys and suggests that the mutant enzyme requires a higher concentration of pantothenate to produce enough CoA to sustain yeast growth.

We have also measured CoA level in mitochondria isolated from wild-type, *COASY*^{Arg499Cys}, and *cab5*^{Arg146Cys} and we observed that the level of CoA was reduced to 40% in yeast transformed with the two mutant strains as compared to wild-type. Starting from this result, we searched if a defective CoA biosynthesis could lead to mitochondrial dysfunction. Serial dilutions of the strains *cab5Δ*/*COASY*^{Arg499Cys} and *cab5Δ*/*COASY*, were spotted on medium without pantothenate supplemented with either ethanol or glycerol, at 28°C. The oxidative growth of the *cab5Δ*/*COASY*^{Arg499Cys} mutant was partially affected compared to *cab5Δ*/*COASY* strain.

To further analyze the respiratory deficiency, we measured oxygen consumption and activity of respiratory complexes. The oxygen consumption rate of the *cab5Δ*/*COASY*^{Arg499Cys} strain was 25% less than that of *cab5*Δ/*COASY*. The respiratory complex III and complex IV activities were reduced in the mutant strain respectively to 26% and 42% as compared to wild type. Altogether these results indicate a mitochondrial dysfunction associated to reduced CoA level.

We have also studied the effect of a high iron content in yeast. We added $FeSO_4$ to the medium and we demonstrated a clear growth defect in the mutant strain. We then performed a quantitative

determination of cellular iron level by a colorimetric assay and we obtained a two-fold increase in iron content in the *cab5Δ*/*COASY*^{Arg499Cys} mutant respect to the parental strain.

Fe-S cluster is a marker of mitochondrial functionality linked to iron metabolism, we investigated whether the biosynthesis of the Fe-S cluster, was affected by COASY deficiency. We determined the activity of succinate dehydrogenase, a mitochondrial Fe-S cluster enzyme. SDH activity was decreased by about 50% in the mutant strain.

Since an excess of iron causes an altered oxidative status, we exposed the mutant and the control strain to H_2O_2: wild type cells showed a viability of 10%, while mutant cells showed a viability of 2% demonstrating that a COASY defect leads to oxidative stress susceptibility.

Finally, since CoA is involved in biosynthesis of fatty acid and acetyl-CoA is necessary for the production of neutral lipids, important as a power reserve for the cell, we have evaluated lipid droplets content in the two strains. We have observed that the content of lipid droplets is decreased in the mutant strain *cab5Δ*/*COASY*^{Arg499Cys}.

2. Further studies on pantothenate kinase 2 (PANK2).

Studies on PKAN patient-derived skin fibroblasts

We have analysed skin fibroblasts from three PKAN patients: the first patient carried a homozygous c.569insA mutation in PANK2 that resulted in a premature stop codon at amino acid position 190 (p.Y190X); the second and third patients are brothers and carried a homozygous c.1259delG mutation, resulting in a frame shift mutation with a creation of a stop codon (F419fsX472). In immunoblot analysis we have shown that PANK2 is virtually absent in all the three patients.

We then have determined cellular oxidative status and its relationship with iron content in fibroblasts by treating control and PKAN fibroblasts with an iron chelator and by analyzing carbonylated proteins content. The content of carbonylated proteins in PKAN fibroblasts, not treated with the iron chelator, was incremented compared to control fibroblasts. Interestingly, treatment with the iron chelator, ameliorated the level of carbonylated proteins in PKAN fibroblasts, but it was completely ineffective in control fibroblasts. Then, we measured both total and reduced glutathione in fibroblasts and we observed a significant reduction in patient fibroblasts compared to controls.

To verify whether the defect in PANK2 activity affected mitochondrial iron homeostasis, we have searched for the presence of potentially toxic free iron (LIP) in the mitochondrial compartment. After treatment with the iron chelator, the size of the mitochondrial LIP was statistically higher in PKAN fibroblasts than control cells in both basal growth conditions and with iron supplementation.

As labile iron can promote ROS formation, we have also measured their generation in basal growth conditions and after iron supplementation. We have observed that ROS production was significantly higher in PKAN fibroblast than in control in both conditions. To evaluate biosynthesis of heme, that represents an important iron-containing product in mitochondria, we have measured its content in fibroblasts and we have observed a significant reduction in heme content of PKAN fibroblasts.
We further investigated the ability of mitochondria to maintain the cellular energy requirement. The mitochondrial membrane potential was evaluated on fibroblasts in the presence of an ATPase inhibitor. PKAN fibroblasts have shown lower membrane hyperpolarisation. Also mitochondrial network was compromised in patient-derived fibroblasts: it was more fragmented in PKAN patients. In line with this observation, we have observed a reduction in ATP levels in PKAN fibroblasts compared to control cells.

Studies on induced neurons (iNs) from PKAN patient-derived skin fibroblasts
Human neurons were generated from patient and control fibroblasts by direct neuronal reprogramming.
We have analysed the amount of ROS specifically present in iNs and we have observed that PKAN iNs contained higher ROS levels than control iNs. We have also evaluated reduced glutathione content and we have seen that PKAN iNs contained significant lower reduced glutathione levels compared to control iNs. A similar approach was used to evaluate mitochondrial functionality in neuronal cells. We have measured mitochondrial membrane potential and we have observed that PKAN iNs had significantly lower membrane potentials compared to control iNs.

Studies on Pank2 knockout (Pank2$^{-/-}$) mouse model
Pank2 knockout *(Pank2$^{-/-}$)* mice show reduced growth, retinal degeneration, male infertility and mitochondrial dysfunctions under standard diet conditions.
Based on the role of CoA in several crucial cellular metabolic pathways, we have tested the hypothesis to stress the *Pank2$^{-/-}$* mouse model with a high-fat ketogenic diet. Ketone bodies produced by the ketogenic diet bypass glycolysis and enter the citric acid cycle to produce oxidative phosphorylation (OXPHOS) substrate. Mice on a ketogenic diet use mainly fatty acid oxidation and OXPHOS for ATP production as compared to mice on a standard diet. We have observed that only ketogenic diet-fed *Pank2$^{-/-}$* mice presented typical signs of neurological and motor impairment and neuropathological findings, like the phenotype observed in PKAN patients. In particular, *Pank2$^{-/-}$* mice under ketogenic treatment have shown progressive weight loss, kyphosis, feet clasping and dystonic limb positioning compared to control mice.

Since a PANK2 knockout *Drosophila melanogaster* model has shown that the compound panthethine can bypass the block due to severe impairment of PANK2 and it is able to rescue brain degeneration, we have asked whether these signs could have been prevented by pantethine administration. We have observed that, with pantethine administration to mice fed a ketogenic diet, the weight of *Pank2*$^{-/-}$ mice was similar to that of control mice and no signs of kyphosis or feet clasping were present. Moreover, *Pank2*$^{-/-}$ mice fed a ketogenic diet died after 2 months whereas the administration of pantethine prolonged their survival for up to 5 months.

Pank2$^{-/-}$ mice fed with ketogenic diet were lethargic and showed a significant reduction of spontaneous movements as compared with control mice fed with ketogenic diet, whereas no differences were observed when fed with standard diet. All of these abnormalities were recovered by pantethine treatment.

We have performed a histological and immunohistochemical analysis of the whole brains and we have noticed the presence of small, scattered groups of neurons with round cytoplasmic inclusions positive for ubiquitin, in *Pank2*$^{-/-}$ mice fed a ketogenic diet. Pantethine treatment led to the disappearance of these neuronal inclusions.

Ultrastructural analysis was performed on basal ganglia and peripheral nerve of *Pank2*$^{-/-}$ and control mice. In the basal ganglia, *Pank2*$^{-/-}$ mice on standard diet have shown the presence of numerous mitochondria with abnormal and swollen cristae. These features were worsened by a ketogenic diet. *Pank2*$^{-/-}$ animals fed a ketogenic diet also showed cytoplasmic deposits of lipofuscin. Pantethine administration completely rescued the mitochondrial morphology of *Pank2*$^{-/-}$ animals on standard diet and ameliorated the morphology of ketogenic diet-fed *Pank2*$^{-/-}$ mice. The analysis of peripheral nerve of *Pank2*$^{-/-}$ mice on ketogenic diet has shown the presence of swollen mitochondria, characterized by cristae degeneration and by the presence of amorphous material in the matrix. Pantethine administration was able to completely rescue the mitochondrial morphology.

We have also evaluated mitochondrial membrane potential in neurons derived from mice; neurons from *Pank2*$^{-/-}$ mice treated with standard or ketogenic diet showed defective mitochondrial membrane potential. The same neurons, after addition of pantethine, showed instead preserved mitochondrial membrane potential.

We have evaluated respiration with microscale oxygraphy on mitochondria isolated from brains of *Pank2*$^{-/-}$ and control mice treated with pantethine and we have compared the results with untreated mice. We have measured basal oxygen consumption rate, and oxygen consumption rate after ADP addition, and after oligomycin addition. We have observed that pantethine was able to significantly increase oxygen consumption rate under all conditions tested in both *Pank2*$^{-/-}$ and control

mitochondria. In particular, pantethine determines a doubling in oxygen consumption rate after ADP stimulation suggesting that respiration was tightly coupled with ATP production.

We have performed cytochrome C oxidase (COX or complex IV of the respiratory chain) histochemical reaction on *Pank2*$^{-/-}$ mice and on muscle biopsy derived from a PKAN patient carrying the PANK2 mutations N500I + IVS2-1G>A. We have found a very peculiar COX staining pattern suggestive of the presence of abnormal mitochondria. To further characterize these mitochondria we performed electron microscopy, which highlighted the presence of giant mitochondria spanning the sarcomere between two neighbouring Z-lines and showing irregularly shaped cristae. The histological alterations of the *Pank2*$^{-/-}$ muscle were absent in pantethine-treated mice.

Finally we have analyzed plasma derived from mice. Plasma analysis has shown an increase of cholesterol and triglycerides in mice on a ketogenic diet. Pantethine treatment was able to reduce the levels of both.

Conclusions and Future Perspectives

We reported the second inborn error of CoA biosynthesis leading to a neurodegenerative disorder. The first defect discovered was due to *PANK2* mutations, causing the most prevalent NBIA subtype, PKAN. We have identified mutations in the *COASY* gene in two subjects with clinical and MRI features typical of NBIA. We have proposed CoPAN, standing for COASY protein-associated neurodegeneration, as the acronym for NBIA caused by CoA synthase mutations to conform with the current nomenclature in use to classify these disorders.

Both CoPAN patients identified, had a severe neurological disorder but they have survived up to the third decade of life, suggesting the presence of residual amount of CoA. The complete absence of CoA would be probably incompatible with life, and organisms have developed alternative strategies to counteract deleterious effects of mutations in CoA enzymatic pathway. Considering the ubiquitous presence of the enzymatic COASY activity, it remains unexplained why only the brain is affected and other organs are preserved. It is possible that a more severe impairment of CoA levels occurs in this organ. Moreover, it is relevant to notice that the mutations afflicting genes coding for pantothenate kinase and PPAT activity of CoA synthase are the two rate limiting steps in CoA biosynthesis. All together these factors could contribute to modulate the clinical presentation of individuals carrying *COASY* mutations.

A yeast model for CoPAN disease was generated to better study CoA biosynthesis defects. In *Saccharomyces cerevisiae* the last two steps of CoA biosynthesis are catalyzed by two separate enzymes, namely the product of *CAB4* and *CAB5* genes. Since we have demonstrated that the lethality associated to deletion in *CAB5* could be complemented by human *COASY*, we have further studied the human Arg499Cys substitution in yeast to support the pathogenic role of this mutation. The evaluation of the metabolic consequences of coenzyme A deficiency in yeast, revealed mitochondrial dysfunctions and a reduction of the activity of respiratory chain complexes. We also demonstrated that the growth of the mutant strain is not only strongly inhibited in the presence of iron but that the mutant strain showed iron accumulation. This result is consistent with the patient phenotype, with iron overload being a typical sign of PKAN and CoPAN. Since acetyl-CoA, one of the most important derivatives of CoA, is also required for the synthesis of fatty acids, we have analyzed the lipid droplets content in mutant yeast strain and observed it was 25% reduced. These results are in agreement with the hypothesis that low CoA perturbs lipid homeostasis. The

transcriptional analysis of key genes involved in lipid metabolism would help in elucidating the role of lipid metabolism in the pathology.

Identification of mutations in *COASY* strongly reinforces the essential role of CoA biosynthetic pathway for the development and functioning of the nervous system. This also underlines the importance of further investigations on different subcellular pools of CoA available, because a specific mitochondrial pathway could exist considering that both PANK2 and COASY are mitochondrial enzymes.

The reason why iron accumulates in human brain in CoPAN and PKAN disease is still unknown. A previous study demonstrated that PANK2 deficient fibroblasts showed an alteration of oxidative status in response to treatment with iron [Campanella et al., 2012]. As mitochondrial iron homeostasis and cytosolic iron homeostasis are strictly correlated, we hypothesize that iron mishandling could also occur in the mitochondria, thereby affecting organelle functionality. We have detected a larger mitochondrial labile iron pool (LIP) also under basal conditions, whereas the increase in the size of the cytosolic LIP was appreciable only after chronic iron supplementation. Nevertheless, the availability of high levels of mitochondrial iron did not appear to be properly utilized in iron sulphur cluster (ISC) and heme biosynthesis, thus they resulted defective in PKAN fibroblasts. A recent study on isolated mammalian mitochondria demonstrated that ISC biosynthesis requires, other than iron and sulphur, also GTP, NADH and ATP [Pandey et al., 2015]. A hypothesis could be that the impairment of the Krebs cycle due to CoA deficiency might result in lower production of GTP and NADH, with the consequent partial iron utilization in ISC biosynthesis. Moreover, other mitochondrial features appeared defective in PKAN cells, such as the mitochondrial membrane potential and mitochondrial morphology, suggesting a global organelle impairment, which can lead to energetic failure. We cannot exclude the possibility that the energetic impairment detected in PKAN fibroblasts, could also derive from membrane alterations due to CoA deficiency-induced defects in phospholipid synthesis; more detailed studies are needed to clarify this point. In fact, the partial mitochondrial swelling and depolarisation detected in PKAN fibroblasts suggest mitochondrial membrane damage. However, studies on isolated rat liver mitochondria reported that iron may catalyze lipids peroxidation in the mitochondrial inner membrane, which can result in a limited depolarisation [Gall et al., 2012].

Even if iron deregulation in PKAN may play a secondary role, its accumulation is harmful. Certain brain regions, such as the globus pallidus and the substantia nigra, have high iron content, which is necessary for the synthesis of neurotransmitters. These regions are particularly prone to the process of abnormal intracellular iron distribution, which may also contribute to the age-dependent iron accumulation. We approached this question obtaining human neurons starting from fibroblasts, and

we confirmed the presence of an altered oxidative status and mitochondrial function impairment in PKAN induced neurons.

An altered mitochondrial membrane potential was also detected in neurons derived from a *Pank2*$^{-/-}$ mouse model [Brunetti et al., 2012]. Based on the role of CoA in several metabolic pathways and considering the data obtained by a metabolomics approach in patients with PKAN, indicating the presence of impairment in lipid metabolism [Leoni et al., 2012], we tested the hypothesis to challenge the *Pank2*$^{-/-}$ mouse model with a diet containing high fat levels. Ketogenic diet consists of a low glucose and high lipid content, stimulating lipid use by mitochondrial beta-oxidation and ketone body production in the liver. We demonstrate that the introduction of the ketogenic diet resulted in the onset of a severe phenotype in *Pank2*$^{-/-}$ mice characterized by motor dysfunctions, neurological impairment with feet-clasping, and exacerbated mitochondrial alterations. It is reported that the compound pantethine can work as a precursor of CoA in PKAN model of Drosophila, even in the presence of severely reduced levels of functional pantothenate kinase and that it was able to rescue brain degeneration, mitochondrial dysfunction and locomotor disabilities [Rana et al., 2010]. In *Pank2*$^{-/-}$ mice on a ketogenic diet, we have observed the rescue of the clinical phenotype including the movement disorder, the amelioration of the mitochondrial dysfunctions, and the extension of the lifespan after pantethine administration. Treatment with pantethine dramatically improved both the histological features of neurodegeneration and the ultrastructural mitochondrial damage in *Pank2*$^{-/-}$ mice fed a ketogenic diet. We have also demonstrated that pantethine administration was able to rescue the mitochondrial phenotype in neurons derived from *Pank2*$^{-/-}$ mice on a standard diet, indicating that its effectiveness was not dependent on or influenced by the ketogenic treatment. It is known that pantethine is rapidly converted into cysteamine and pantothenate by the vanin enzyme, also known as pantetheine hydrolase or pantetheinase [Kaskow et al., 2012]. Although pantethine is not able to cross the blood brain barrier, it was demonstrated that cysteamine can cross the blood brain barrier and can exert its positive effects [Bousquet et al. 2010]. Cysteamine is able to upregulate the expression of the brain derived neurotrophic factor (BDNF). These neuroprotective effects of cysteamine have been hypothesized to reflect the positive actions of this compound in Parkinson's disease [Sun et al., 2010; Gibrat and Cicchetti, 2011] and Huntington's disease [Borrell-Pages et al., 2006]. In agreement with these data, we can hypothesize that the beneficial effects of pantethine in our model system were due to its conversion into pantothenate and cysteamine. Moreover, it is important to consider that environmental factors, such as food intake, together with genetic background could modulate the disease presentation by worsening or, on the contrary, stabilizing the progression of the symptoms. This could also explain the variability of the clinical presentation of the disease, with a spectrum of syndromes ranging

from rapid to slowly progressive. We finally suggest that pantethine administration to patients with PKAN should be considered as a possible, safe and non-toxic therapeutic approach.

In conclusion, we have demonstrated that an altered lipid metabolism, as a result of CoA biosynthesis defect, could represent one of the main causes of NBIA disease. It is also possible, as demonstrated by the presence of mitochondrial alteration in mouse model, in the muscle and skin fibroblasts derived from PKAN patients and in CoPAN yeast model, that mitochondria play a relevant role or could be a concurrent cause in the pathogenic mechanism of NBIA.

References

Aghajanian, S. and Worrall, D.M. (2002). Identification and characterization of the gene encoding the human phosphopantetheine adenylyltransferase and dephospho-CoA kinase bifunctional enzyme (CoA synthase). Biochem. J. 365, 13–18.

Agrimi, G., Russo, A., Scarcia, P., Palmieri, F. (2012) The human gene*SLC25A17* encodes a peroxisomal transporter of coenzyme A, FAD andNAD+ . Biochem. J. 443, 241–247.

Alazami, A.M., Al-Saif, A., Al-Semari, A., Bohlega, S., Zlitni, S., Alzahrani, F., Bavi, P., Kaya, N., Colak, D., Khalak, H., Baltus, A., Peterlin, B., Danda, S., Bhatia, K.P., Schneider, S.A., Sakati, N., Walsh, C.A, Al-Mohanna, F., Meyer, B., Alkuraya, F.S. (2008) Mutations in C2orf37, encoding a nucleolar protein, cause hypogonadism, alopecia, diabetes mellitus, mental retardation, and extrapyramidal syndrome. Am. J. Hum. Genet. 83, 684–91.

Alderson, N.L., Rembiesa, B.M., Walla, M.D., Bielawska, A., Bielawski, J., Hama, H. (2004) The human FA2H gene encodes a fatty acid 2-hydroxylase. J. Biol. Chem. 279, 48562–8.

Arber, C.E., LI, A., Houlden, H.,Wray, S. (2015) Insights into molecular mechanisms of disease in neurodegeneration with brain iron accumulation: unifying theories. Neuropathol. Appl. Neurobiol. 2015.

Balsinde, J. and Balboa, M.A.. (2005) Cellular regulation and proposed biological functions of group VIA calcium-independent phospholipase A2 in activated cells. Cell Signal. 17, 1052–62.

Baraibar, M. A., Muhoberac, B. B., Garringer, H. J., Hurley, T. D., Vidal, R. (2010) Unraveling of the E-helices and disruption of 4-fold pores are associated with iron mishandling in a mutant ferritin causing neurodegeneration. J. Biol. Chem. 285, 1950–1956.

Beck, G., Sugiura, Y., Shinzawa, K., Kato, S., Setou, M., Tsujimoto, Y., Sakoda, S., Sumi-Akamaru, H. (2011) Neuroaxonal dystrophy in calcium-independent phospholipase A2βdeficiency results from insufficient remodeling and degeneration of mitochondrial and presynaptic membranes. J. Neurosci. 31, 11411–20.

Borrell-Pages, M., Canals, J.M., Cordelieres, F.P., Parker, J.A., Pineda, J.R., Grange, G., Bryson, E.A., Guillermier, M., Hirsch, E., Hantraye, P., Cheetham, M.E., Néri, C., Alberch, J., Brouillet, E., Saudou, F., Humbert, S. (2006) Cystamine and cysteamine increase brain levels of BDNF in Huntington disease via HSJ1b and transglutaminase. J. Clin. Invest. 116, 1410–24.

Bosveld, F., Rana, A., Van der Wouden, P.E., Lemstra, W., Ritsema, M., Kampinga, H.H., Sibon, O.C. (2008) De novo CoA biosynthesis is required to maintain DNA integrity during development of the Drosophila nervous system. um Mol Genet. 17, 2058-69.

Bousquet, M., Gibrat, C., Ouellet, M., Rouillard, C., Calon, F., Cicchetti F. (2010) Cystamine metabolism and brain transport properties: clinical implications for neurodegenerative diseases. J. Neurochem. 114, 1651–8.

Bras, J., Singleton, A., Cookson, M.R., Hardy, J. (2008) Emerging pathways in genetic Parkinson's disease: potential role of ceramide metabolism in Lewy body disease. FEBS. J. 275, 5767–73.

Bras, J., Verloes, A., Schneider, S.A., Mole, S.E., Guerreiro, R.J. (2012) Mutation of the parkinsonism gene ATP13A2 causes neuronal ceroid-lipofuscinosis. Hum. Mol. Genet. 21, 2646–50.

Brissot, P., Ropert, M., Le Lan, C., Loréal, O. (2012) Non-transferrin bound iron: a key role in iron overload and iron toxicity. Biochim. Biophys. Acta. 1820, 403–10.

Broekemeier, K.M., Iben, J.R., LeVan, E.G., Crouser, E.D., Pfeiffer, D.R. (2002) Pore Formation and Uncoupling Initiate a Ca2+ -Independent Degradation of Mitochondrial Phospholipids. Biochemistry. 41, 7771–80.

Brunetti, D., Dusi, S., Morbin, M., Uggetti, A., Moda, F., D'Amato, I., Giordano, C., d'Amati, G., Cozzi, A., Levi, S., Hayflick, S., Tiranti, V. (2012) Pantothenate kinase-associated neurodegeneration: altered mitochondria membrane potential and defective respiration in Pank2 knock-out mouse model. Hum Mol Genet. 21, 5294-305.

Burn, J. and Chinnery, P.F. (2006) Neuroferritinopathy. Semin. Pediatr. Neurol. 13, 176–181.

Campanella, A., Privitera, D., Guaraldo, M., Rovelli, E., Barzaghi, C., Garavaglia, B., Santambrogio, P., Cozzi, A., Levi, S. (2012) Skin fibroblasts from pantothenate kinase-associated neurodegeneration patients show altered cellular oxidative status and have defective iron-handling properties. Hum Mol Genet. 21, 4049-59.

Cossu, G., Abbruzzese, G., Matta, G., Murgia, D., Melis, M., Ricchi, V., Galanello, R., Barella, S., Origa, R., Balocco, M., Pelosin, E., Marchese, R., Ruffinengo, U., Forni, G.L. (2014) Efficacy and safety of deferiprone for the treatment of pantothenate kinase-associated neurodegeneration (PKAN) and neurodegeneration with brain iron accumulation **(**NBIA**):** results from a four years follow-up. Parkinsonism. Relat. Disord. 20, 651-4.

Curtis, A.R., Fey, C., Morris, C.M., Bindoff, L.A., Ince, P.G., Chinnery, P.F., Coulthard, A., Jackson, M.J., Jackson, A.P., McHale, D.P., Hay, D., Barker, W.A., Markham, A.F., Bates, D., Curtis, A., Burn, J. (2011) Mutation in the gene encoding ferritin light polypeptide causes dominant adult-onset basal ganglia disease. Nat. Genet. 28, 350–4.

Dall'Armi, C., Devereaux, K.A., Di Paolo, G. (2013) The role of lipids in the control of autophagy. Curr. Biol. 23, R33–45.

Dan, P., Edvardson, S., Bielawski, J., Hama, H., Saada, A. (2011) 2-Hydroxylated sphingomyelin profiles in cells from patients with mutated fatty acid 2-hydroxylase. Lipids Health Dis. 10, 84.

Daugherty, M., Polanuyer, B., Farrell, M., Scholle, M., Lykidis, A., de Crécy-Lagard, V., Osterman, A. (2002). Completere constitution of the human coenzyme A biosynthetic pathway via comparative genomics. J. Biol. Chem. 277, 21431–21439.

Di Fonzo, A., Chien, H.F., Socal, M., Giraudo, S., Tassorelli, C., Iliceto, G., Fabbrini, G., Marconi, R., Fincati, E., Abbruzzese, G., Marini, P., Squitieri, F., Horstink, M.W., Montagna, P., Libera, A.D., Stocchi, F., Goldwurm, S., Ferreira, J.J., Meco, G., Martignoni, E., Lopiano, L., Jardim, L.B., Oostra, B.A., Barbosa, E.R, Bonifati, V. (2007) ATP13A2 missense mutations in juvenile parkinsonism and young onset Parkinson disease. Neurology. 68, 1557–62.

Dusi, S., Valletta, L., Haack, T.B., Tsuchiya, Y., Venco, P., Pasqualato, S., Goffrini, P., Tigano, M., Demchenko, N., Wieland, T., Schwarzmayr, T., Strom, T.M., Invernizzi, F., Garavaglia, B., Gregory, A., Sanford, L., Hamada, J., Bettencourt, C., Houlden, H., Chiapparini, L., Zorzi, G., Kurian, M.A., Nardocci, N., Prokisch, H., Hayflick, S., Gout, I., Tiranti, V. (2014) Exome sequence reveals mutations in CoA synthase as a cause of neurodegeneration with brain iron accumulation. Am. J. Hum. Genet. 94, 11-22.

Eckhardt, M., Yaghootfam, A., Fewou, S.N., Zöller, I., Gieselmann, V. (2005) A mammalian fatty acid hydroxylase responsible for the formation of alpha-hydroxylated galactosylceramide in myelin. Biochem. J. 388, 245–54.

Fiermonte, G., Paradies, E., Todisco, S., Marobbio, C.M., Palmieri, F. (2009) A novel member of solute carrier family 25 (SLC25A42) is a transporter of coenzyme A and adenosine 3',5'-diphosphate in human mitochondria. J. Biol. Chem. 284, 18152–18159.

Friedman, A., Arosio, P., Finazzi, D., Koziorowski, D., Galazka-Friedman, J. (2011) Ferritin as an important player in neurodegeneration. Parkinsonism Relat. Disord. 17, 423–430.

Gadd, M.E., Broekemeier, K.M., Crouser, E.D., Kumar, J., Graff, G., Pfeiffer, D.R. (2006) Mitochondrial iPLA2 activity modulates the release of cytochrome c from mitochondria and influences the permeability transition. J. Biol. Chem. 281, 6931–9.

Gall, J., JJr, Skrha, Buchal, R., Sedlackova, E., Verebova, K., Platenik, J. (2012) Induction of the mitochondrial permeability transition (MPT) by micromolar iron: liberation of calcium is more important than NAD(P)H oxidation. Biochim. Biophys. Acta. 1817, 1537–1549.

Gibrat, C. and Cicchetti, F. (2011) Potential of cystamine and cysteamine in the treatment of neurodegenerative diseases. Prog. Neuropsychopharmacol. Biol. Psychiatry. 35, 380–9.

Gonzalez-Cuyar, L.F., Perry, G., Miyajima, H., Atwood, C.S., Riveros-Angel. M., Lyons, P.F., Siedlak, S.L., Smith, M.A., Castellani, R.J. (2008) Redox active iron accumulation in aceruloplasminemia. Neuropathology. 28, 466–71.

Green, J.T., Orr, S.K., Bazinet, R.P. (2008) The emerging role of group VI calcium-independent phospholipase A2 in releasing docosahexaenoic acid from brain phospholipids. J. Lipid. Res. 49, 939–44.

Gregory, A. and Hayflick, S.J. (2011) Genetics of neurodegeneration with brain iron accumulation. Curr. Neurol. Neurosci. Rep. 11, 254–261.

Gregory, A. and Hayflick, S.J. (2013) Pantothenate Kinase-Associated Neurodegeneration. Gene Reviews: 1993-2015.

Grünewald, A., Arns, B., Seibler, P., Rakovic, A., Münchau, A., Ramirez, A., Sue, C.M., Klein, C. (2012) ATP13A2 mutations impair mitochondrial function in fibroblasts from patients with Kufor-Rakeb syndrome. Neurobiol. Aging. 33, 1843, e1–7.

Haack, T.B., Hogarth, P., Kruer, M.C., Gregory, A., Wieland, T., Schwarzmayr, T., Graf, E., Sanford, L., Meyer, E., Kara, E., Cuno, S.M., Harik, S.I., Dandu, V.H., Nardocci, N., Zorzi, G., Dunaway, T., Tarnopolsky, M., Skinner, S., Frucht, S., Hanspal, E., Schrander-Stumpel, C., Héron, D., Mignot, C., Garavaglia, B., Bhatia, K., Hardy, J., Strom,

T.M., Boddaert, N., Houlden, H.H., Kurian, M.A., Meitinger, T., Prokisch, H., Hayflick, S.J. (2012) Exome sequencing reveals de novo *WDR45* mutations causing a phenotypically distinct, X-linked dominant form of NBIA. *Am. J. Hum. Genet.* 91, 1144–1149.

Hama, H. (2010) Fatty acid 2-Hydroxylation in mammalian sphingolipid biology. Biochim. Biophys. Acta. 1801, 405–14.

Hartig, M.B., Iuso., A., Haack, T., Kmiec, T., Jurkiewicz, E., Heim, K., Roeber, S., Tarabin, V., Dusi, S., Krajewska-Walasek, M., Jozwiak, S., Hempel, M., Winkelmann, J., Elstner, M., Oexle, K., Klopstock, T., Mueller-Felber, W., Gasser, T., Trenkwalder, C., Tiranti, V., Kretzschmar, H., Schmitz, G., Strom, T.M., Meitinger, T., Prokisch, H. (2011) Absence of an orphan mitochondrial protein, c19orf12, causes a distinct clinical subtype of neurodegeneration with brain iron accumulation. Am. J. Hum. Genet. 89, 543–50.

Hayflick, S.J., Kruer, M.C., Gregory, A., Haack, T.B., Kurian, M.A., Houlden, H.H., Anderson, J., Boddaert, N., Sanford, L., Harik, S.I., Dandu, V.H., Nardocci, N., Zorzi, G., Dunaway, T., Tarnopolsky, M., Skinner, S., Holden, K.R., Frucht, S., Hanspal, E., Schrander-Stumpel, C., Mignot, C., Héron, D., Saunders, D.E., Kaminska, M., Lin, J-P., Lascelles, K., Cuno, S.M., Meyer, E., Garavaglia, B., Bhatia, K., de Silva, R., Crisp, S., Lunt, P., Carey, M., Hardy, J., Meitinger, T., Prokisch, H., Hogarth, P. (2013) β-Propeller protein-associated neurodegeneration: a new X-linked dominant disorder with brain iron accumulation. Brain. 136, 1708–17.

Hayflick, S.J.,Westaway, S.K., Levinson, B., Zhou, B., Johnson, M.A., Ching, K.H., Gitschier, J. (2003). Genetic, clinical, and radiographic delineation of Hallervorden-Spatz syndrome. N. Engl. J. Med. 348, 33–40.

Hogarth, P., Gregory, A., Kruer, M.C., Sanford, L., Wagoner, W., Natowicz, M.R., Egel, R.T., Subramony, S.H., Goldman. J.G., Berry-Kravis, E., Foulds, N.C., Hammans, S.R., Desguerre, I., Rodriguez, D., Wilson, C., Diedrich, A., Green, S., Tran, H., Reese, L., Woltjer, R.L., Hayflick, S.J. (2013) New NBIA subtype: genetic, clinical, pathologic, and radiographic features of MPAN. Neurology. 80, 268–75.

Itoh, K., Negishi, H., Obayashi, C., Hayashi, Y., Hanioka, K., Imai, Y., Itoh, H. (1993) Infantile neuroaxonal dystrophy – immunohistochemical and ultrastructural studies on the central and peripheral nervous systems in infantile neuroaxonal dystrophy. Kobe. J. Med. Sci. 39, 133–46.

Iuso, A., Sibon, O.C.M., Gorza, M., Heim, K., Organisti, C., Meitinger, T., Prokisch, H. (2014) Impairment of Drosophila orthologs of the human orphan protein C19orf12 induces bang sensitivity and neurodegeneration. PLoS ONE. 9, e89439.

Jana, A., Hogan, E.L., Pahan, K. (2009) Ceramide and neurodegeneration: susceptibility of neurons and oligodendrocytes to cell damage and death. J. Neurol. Sci. 278, 5–15.

Jeong, S.Y. and David, S. (2006) Age-related changes in iron homeostasis and cell death in the cerebellum of ceruloplasmindeficient mice. J. Neurosci. 26, 9810–19.

Jeong, S.Y. and David, S. Glycosylphosphatidylinositol-anchored ceruloplasmin is required for iron efflux from cells in the central nervous system. J. Biol. Chem. 278, 27144–27148.

Jin, J., Arias, E.E, Chen, J., Harper, J.W., Walter, J.C. (2006) A family of diverse Cul4-Ddb1-interacting proteins includes Cdt2, which is required for S phase destruction of the replication factor Cdt1. Mol. Cell. 23, 709–21.

Kandel, E. R., Schwartz, J. H., Jessel, T. M., Siegelbaum, S. A., Hudspeth, A. J. (2013) Principles of neural science. Fifth edition.

Kaneko, K., Hineno, A., Yoshida, K., Ohara, S., Morita, H., Ikeda, S. (2012) Extensive brain pathology in a patient with aceruloplasminemia with a prolonged duration of illness. Hum. Pathol. 43, 451–6.

Kaskow, B.J., Proffitt, J.M., Blangero, J., Moses, E.K., Abraham, L.J. (2012) Diverse biological activities of the vascular non-inflammatory molecules - the Vanin pantetheinases. Biochem. Biophys. Res. Commun. 417, 653–8

Kondo, M., Shibata, T., Kumagai, T., Osawa, T., Shibata, N., Kobayashi, M., Sasaki, S., Iwata, M., Noguchi, N., Uchida, K. (2002). 15-Deoxy-Delta(12,14)-prostaglandin J(2): the endogenous electrophile that induces neuronal apoptosis. Proc. Natl. Acad. Sci. USA. 99, 7367–72

Kono, S. and Miyajima, H. (2006) Molecular and pathological basis of aceruloplasminemia. Biol. Res. 39, 15–23.

Kono, S., Suzuki, H., Oda, T., Miyajima, H., Takahashi, Y., Shirakawa, K., Ishikawa, K., Kitagawa, M. (2006) Biochemical features of ceruloplasmin gene mutations linked to aceruloplasminemia. Neuromolecular. Med. 8, 361–74.

Kruer, M.C., Boddaert, N., Schneider, S.A., Houlden, H., Bhatia, K.P., Gregory, A., Anderson, J.C., Rooney, W.D., Hogarth, P., Hayflick, S.J. (2012). Neuroimaging features of neurodegeneration with brain iron accumulation. AJNR Am. J. Neuroradiol. 33, 407–414.

Kruer, M.C., Hiken, M., Gregory, A., Malandrini, A., Clark, D., Hogarth, P., Grafe, M., Hayflick, S.J., Woltjer, R.L. (2011) Novel histopathologic findings in molecularly-confirmed pantothenate kinase-associated neurodegeneration. Brain. 134, 947-58.

Kruer, M.C., Paisán-Ruiz, C., Boddaert, N., Yoon, M.Y., Hama, H., Gregory, A., Malandrini, A., Woltjer, R.L., Munnich, A., Gobin, S., Polster, B.J., Palmeri, S., Edvardson, S., Hardy, J., Houlden, H., Hayflick, S.J. (2010) Defective FA2H leads to a novel form of neurodegeneration with brain iron accumulation (NBIA). Ann. Neurol. 68, 611–18.

Kühlbrandt, W. (2004) Biology, structure and mechanism of P-type ATPases. Nat. Rev. Mol. Cell. Biol. 5, 282–95.

Kuo, Y.M., Duncan, J.L., Westaway, S.K., Yang, H., Nune, G., Xu, E.Y., Hayflick, S.J., Gitschier, J. (2005) Deficiency of pantothenate kinase 2 (Pank2) in mice leads to retinal degeneration and azoospermia. Hum. Mol. Genet. 14, 49–57.

Kuo, Y.M., Hayflick, S.J., Gitschier, J. (2007) Deprivation of pantothenic acid elicits a movement disorder and azoospermia in a mouse model of pantothenate kinase-associated neurodegeneration. J. Inherit. Metab. Dis. 30, 310–317.

Larsson, P.K.A., Claesson, H.E., Kennedy. B.P. (1998) Multiple splice variants of the human calcium-independent phospholipase A2 and their effect on enzyme activity. J. Biol. Chem. 273, 207–14.

Lei, X., Zhang, S., Bohrer, A., Barbour, S.E., Ramanadham, S. (2012) Role of calcium-independent phospholipase A(2)β in human pancreatic islet β-cell apoptosis. Am. J. Physiol. Endocrinol. Metab. 303, E1386–95.

Leonardi, R., Rock, C.O., Jackowski, S., Zhang, Y-M. (2007) Activation of human mitochondrial pantothenate kinase 2 by palmitoylcarnitine. Proc Natl Acad Sci. 104, 1494–9.

Leonardi, R., Zhang, Y.M., Rock, C.O., Jackowski, S. (2005) Coenzyme A: back in action. Prog. Lipid Res. 44, 125–153.

Leoni, V., Strittmatter, L., Zorzi, G., Zibordi, F., Dusi, S., Garavaglia, B., Venco, P., Caccia, C., Souza, A.L., Deik, A., Clish, C.B., Rimoldi, M., Ciusani, E., Bertini, E., Nardocci, N., Mootha, V.K., Tiranti, V. (2012) Metabolic consequences of mitochondrial coenzyme A deficiency in patients with PANK2 mutations. Mol Genet Metab. 105, 463–71.

Levi, S. and Rovida, E. (2009). The role of iron in mitochondrial function. Biochim. Biophys. Acta. 1790, 629–636.

Li, A., Paudel, R., Johnson, R., Courtney, R., Lees, A.J., Holton, J.L., Hardy, J., Revesz, T., Houlden, H. (2012) Pantothenate kinasea ssociated neurodegeneration is not a synucleinopathy. Neuropathol. Appl. Neurobiol. 39, 121–31.

Liou, J.Y., Aleksic, N., Chen, S.F., Han, T.J., Shyue, S.K., Wu, K.K.. (2005) Mitochondrial localization of cyclooxygenase-2 and calcium-independent phospholipase A2 in human cancer cells: implication in apoptosis resistance. Exp. Cell. Res. 306, 75–84.

Lu, Q., Yang, P., Huang, X., Hu, W., Guo, B., Wu, F., Lin, L., Kovács, A.L., Yu, L., Zhang, H. (2011) The WD40 repeat PtdIns(3)P-binding protein EPG-6 regulates progression of omegasomes to autophagosomes. Dev. Cell. 21, 343–57.

Lu, C.S., Lai, S.C., Wu, R.M., Weng, Y.H., Huang, C.L., Chen, R.S., Chang, H.C., Wu-Chou, Y.H., Yeh, T.H. (2012) PLA2G6 mutations in PARK14-linked young-onset parkinsonism and sporadic Parkinson's disease. Am. J. Med. Genet. B Neuropsychiatr. Genet. 159B, 183-91.

Mahadevan, A., Santosh, V., Gayatri, N., Ratnavalli, E., NandaGopal, R., Vasanth, A., Roy, A.K., Shankar, S.K. (2000) Infantile neuroaxonal dystrophy and giant axonal neuropathy – overlap diseases of neuronal cytoskeletal elements in childhood? Clin. Neuropathol 2000. 19, 221–9.

Mancuso, M.M., Davidzon, G.M., Kurlan, R.M.M., Tawil, R.M., Bonilla, E.M., Di Mauro, S.M., Powers, J.M.M. (2005) Hereditary ferritinopathy: a novel mutation, its cellular pathology, and pathogenetic insights. J. Neuropathol. Exp. Neurol. 64, 280–94.

McNeill, A. and Chinnery, P.F. (2011) Neurodegeneration with brain iron accumulation. Handb. Clin. Neurol.. 100, 161–172.

Morgan, N.V., Westaway, S.K., Morton, J.E.V., Gregory, A., Gissen, P., Sonek, S., Cangul, H., Coryell, J., Canham, N., Nardocci, N., Zorzi, G., Pasha, S., Rodriguez, D., Desguerre, I., Mubaidin, A., Bertini, E., Trembath, R.C., Simonati, A., Schanen, C., Johnson, C.A., Levinson, B., Woods, C.G., Wilmot, B., Kramer, P., Gitschier, J., Maher, E.R., Hayflick, S.J. (2006) PLA2G6, encoding a phospholipase A2, is mutated in neurodegenerative disorders with high brain iron. Nat. Genet. 38, 752–4.

Nemazanyy, I., Panasyuk, G., Breus, O., Zhyvoloup, A., Filonenko, V., Gout, I.T. (2006). Identification of a novel CoA synthase isoform, which is primarily expressed in the brain. Biochem. Biophys. Res. Commun. 341, 995–1000.

Nemazanyy, I., Panasyuk, G., Zhyvoloup, A., Panayotou, G., Gout, I.T., Filonenko, V. (2014) Specific interaction between S6K1 and CoA synthase: a potential link between the mTOR/S6K pathway, CoA biosynthesis and energy metabolism. FEBS Lett. 578, 357-62.

Nunnari, J., and Suomalainen, A. (2012) Mitochondria: in sickness and in health. Cell. 148, 1145-59.

Paisán-Ruiz, C., Li, A., Schneider, S.A., Holton, J.L., Johnson, R., Kidd, D., Chataway, J., Bhatia, K.P., Lees, A.J., Hardy, J., Revesz, T., Houlden, H. (2012) Widespread Lewy body and tau accumulation in childhood and adult onset dystoniaparkinsonism cases with PLA2G6 mutations. Neurobiol. Aging. 33, 814–23.

Pandey, A., Pain, J., Ghosh, A.K., Dancis, A., Pain, D. (2015) Fe–S cluster biogenesis in isolated mammalian mitochondria: coordinated use of persulfide sulfur and iron and requirements for GTP, NADH, and ATP. J. Biol. Chem. 290, 640–657.

Poli, M., Derosas, M., Luscieti, S., Cavadini, P., Campanella, A., Verardi, R., Finazzi, D., Arosio, P. (2010) Pantothenate kinase-2 (Pank2) silencing causes cell growth reduction, cell-specific ferroportin upregulation and iron deregulation. Neurobiol. Dis. 39, 204-10.

Potter, K.A., Kern, M.J., Fullbright, G., Bielawski, J., Scherer, S.S., Yum, S.W., Li, J.J., Cheng, H., Han, X., Venkata, J.K., Khan, P.A.A., Rohrer, B., Hama, H. (2011) Central nervous system dysfunction in a mouse model of FA2H deficiency. Glia. 59, 1009–21.

Prohl, C., Pelzer, W., Diekert, K., Kmita, H., Bedekovics, T., Kispal, G., Lill, R. (2001) The yeast mitochondrial carrier Leu5p and its human homologue Graves' disease protein are required for accumulation of coenzyme A in the matrix. Mol. Cell. Biol. 21, 1089–1097.

Rana, A., Seinen, E., Siudeja, K., Muntendam, R., Srinivasan, B., Van der Want, J.J., Hayflick, S., Reijngoud, D.J., Kayser, O., Sibon, O.C. (2010) Pantethine rescues a Drosophila model for pantothenate kinase-associated neurodegeneration. Proc. Natl. Acad. Sci. USA. 107, 6988-93.

Ross, B.M., Moszczynska, A., Erlich, J., Kish, S.J. (2002) Phospholipid-metabolizing enzymes in Alzheimer's disease: increased lysophospholipid acyltransferase activity and decreased phospholipase A2 activity. J. Neurochem. 70, 786–93.

Rouault, T.A. (2013) Iron metabolism in the CNS: implications for neurodegenerative diseases. Nat. Rev. Neurosci. 14, 551-6.

Roy, S., Zhang, B., Lee, V.M-Y, Trojanowski, J.Q. (2005) Axonal transport defects: a common theme in neurodegenerativedise ases. Acta Neuropathol. 109, 5–13.

Saitsu, H., Nishimura, T., Muramatsu, K., Kodera, H., Kumada, S., Sugai, K., Kasai-Yoshida, E., Sawaura, N., Nishida, H., Hoshino, A., Ryujin, F., Yoshioka, S., Nishiyama, K., Kondo, Y., Tsurusaki, Y., Nakashima, M., Miyake, N., Arakawa, H., Kato, M., Mizushima, N., Matsumoto, N. (2013) De novo mutations in the autophagy gene WDR45 cause static encephalopathy of childhood with neurodegeneration in adulthood. Nat. Genet. 45, 445–9, 449e1.

Schneider, S.A., Paisan-Ruiz, C., Quinn, N.P., Lees, A.J., Houlden, H., Hardy, J., Bhatia, K.P. (2010) ATP13A2 mutations (PARK9) cause neurodegeneration with brain iron accumulation. Mov. Disord. 25, 979–84.

Seleznev, K., Zhao, C., Zhang, X.H., Song, K., Ma, Z.A. (2006) Calcium-independent phospholipase A2 localizes in and protects mitochondria during apoptotic induction by staurosporine. J. Biol. Chem. 281, 22275–88.

Sian-Hulsmann, J., Mandel, S., Youdim, M. B., Riederer, P. (2011) The relevance of iron in the pathogenesis of Parkinson's disease. J. Neurochem. 118, 939-957.

Song, H., Bao, S., Lei, X., Jin, C., Zhang, S., Turk, J., Ramanadham, S. (2010) Evidence for proteolytic processing and stimulated organelle redistribution of iPLA(2)beta. Biochim. Biophys. Acta. 1801, 547–58.

Srinivasan, B., Baratashvili, M., Van der Zwaag, M., Kanon, B., Colombelli, C., Lambrechts, R.A., Schaap, O., Nollen, E.A., Podgoršek, A., Kosec, G., Petković, H., Hayflick, S., Tiranti, V., Reijngoud, D.J., Grzeschik, N.A., Sibon, O.C. (2015) Extracellular 4'-phosphopantetheine is a source for intracellular coenzyme A synthesis. Nat. Chem. Biol. 11, 784-92.

Stehling, O., Wilbrecht, C., Lill, R. (2014) Mitochondrial iron–sulfur protein biogenesis and human disease. Biochimie 100, 61–77.

Strauss, E. and Begley, T.P. (2005) The selectivity for cysteine over serine in coenzyme A biosynthesis. Chem. Bio. Chem 6, 284–286.

Strokin, M., Sergeeva, M., Reiser, G. (2007) Prostaglandin synthesis in rat brain astrocytes is under the control of the n-3 docosahexaenoic acid, released by group VIB calciumindependent phospholipase A2. J. Neurochem. 102, 1771–82.

Sun, L., Xu, S., Zhou, M., Wang, C., Wu, Y., Chan, P. (2010) Effects of cysteamine on MPTP-induced dopaminergic neurodegeneration in mice. Brain Res. 1335, 74–82.

Tahiliani, A. G. and Beinlich, C.J. (1991) Pantothenic acid in health and disease. Vitam. Horm. 46, 165-228

Tan, J., Zhang, T., Jiang, L., Chi, J., Hu, D., Pan, Q., Wang, D., Zhang, Z. (2011) Regulation of intracellular manganese homeostasis by Kufor-Rakeb syndrome-associated ATP13A2 protein. J. Biol. Chem. 286, 29654–62.

Tsunemi, T. and Krainc, D. (2014) Zn2+ dyshomeostasis caused by loss of ATP13A2/PARK9 leads to lysosomal dysfunction and alpha-synuclein accumulation. Hum. Mol. Genet. 23, 2791–801.

Usenovic, M., Tresse, E., Mazzulli, J.R., Taylor, J.P., Krainc, D. (2012) Deficiency of ATP13A2 leads to lysosomal dysfunction, α-synuclein accumulation, and neurotoxicity. J. Neurosci. 32, 4240–6.

Venco, P., Bonora, M., Giorgi, C., Papaleo, E., Iuso, A., Prokisch, H., Pinton, P., Tiranti, V. (2015) Mutations of C19orf12, coding for a transmembrane glycine zipper containing mitochondrial protein, cause mis-localization of the protein, inability to respond to oxidative stress and increased mitochondrial Ca^{2+}. Front Genet. 6, 185.

Vidal, R., Miravalle, L., Gao, X., Barbeito, A.G., Baraibar, M.A., Hekmatyar, S.K., Widel, M., Bansal, N., Delisle, M.B., Ghetti, B. (2008) Expression of a mutant form of the ferritin light chain gene induces neurodegeneration and iron overload in transgenic mice. J. Neurosci. 28, 60–67.

Vidal, R.P., Ghetti, B.M., Takao, M.M., Brefel-Courbon, C.M., Uro-Coste, E.M.D.P., Glazier, B.S., Siana, V.M., Benson, M.D.M., Calvas, P.M.D.P., Miravalle, L.P., Rascol, O.M.D.P., Delisle, M.B.M. (2004) Intracellular ferritin accumulation in neural and extraneural tissue characterizes a neurodegenerative disease associated with a mutation in the ferritin light polypeptide gene. J. Neuropathol. Exp. Neurol. 63, 363–80.

Weinreb, O., Amit, T., Mandel, S., Kupershmidt, L., Youdim, M. B. (2010) Neuroprotective multifunctional iron chelators: from redox-sensitive process to novel therapeutic opportunities. Antioxid. Redox Signal. 13, 919-949.

Wu, Z., Li, C., Lv, S., Zhou, B. (2009) Pantothenate kinase-associated neurodegeneration: insights from a Drosophila model. Hum. Mol. Genet. 18, 3659–3672.

Zhang, Y-M., Rock, C.O., Jackowski, S. (2006) Biochemical properties of human pantothenate kinase 2 isoforms and mutations linked to pantothenate kinase-associated neurodegeneration. J. Biol. Chem. 281, 107–14.

Zhao, Y.G., Sun, L., Miao, G., Ji, C., Zhao, H., Sun, H., Miao, L., Yoshii, S.R., Mizushima, N., Wang, X., Zhang, H. (2015) The autophagy gene Wdr45/Wipi4 regulates learning and memory function and axonal homeostasis. Autophagy. 11, 881-90.

Zhou, B.,Westaway, S.K., Levinson, B., Johnson, M.A., Gitschier, J., Hayflick, S.J. (2001). A novel pantothenate kinase gene (PANK2) is defective in Hallervorden-Spatz syndrome. Nat. Genet. 28, 345–349.

Acknowledgements

I would like to thank my supervisor Dr. Valeria Tiranti for her scientific support and her cordiality in these years. I also would like to thank the members of my Thesis Committee Prof. Marco Muzi Falconi and Prof. Giacomo Comi, and finally Prof. Gianni Dehò.

Many thanks also to our collaborators Holger Prokisch, Tobias Haack, Ivan Gout, Yugo Tsuchiya, Sebastiano Pasqualato, Paola Goffrini, Camilla Ceccatelli Berti, Sonia Levi and Paolo Santambrogio.

Last but not least, I would like to thank my past and present colleagues Paola Venco, Cristina Colombelli, Alice Segnali, Lorella Valletta, Manar Aoun and Dario Brunetti, for their scientific and moral support, and for the funny moments shared in these years.

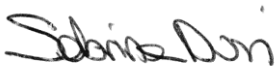

Section II

Published papers

Brunetti D, **Dusi S**, Giordano C, Lamperti C, Morbin M, Fugnanesi V, Marchet S, Fagiolari G, Sibon O, Moggio M, d'Amati G, Tiranti V. **Pantethine treatment is effective in recovering the disease phenotype induced by ketogenic diet in a pantothenate kinase-associated neurodegeneration mouse model**. Brain. 2014 Jan;137(Pt 1):57-68.

Dusi S, Valletta L, Haack TB, Tsuchiya Y, Venco P, Pasqualato S, Goffrini P, Tigano M, Demchenko N, Wieland T, Schwarzmayr T, Strom TM, Invernizzi F, Garavaglia B, Gregory A, Sanford L, Hamada J, Bettencourt C, Houlden H, Chiapparini L, Zorzi G, Kurian MA, Nardocci N, Prokisch H, Hayflick S, Gout I, Tiranti V. **Exome sequence reveals mutations in CoA synthase as a cause of neurodegeneration with brain iron accumulation**. Am J Hum Genet. 2014 Jan 2;94(1):11-22.

Santambrogio P, **Dusi S**, Guaraldo M, Rotundo LI, Broccoli V, Garavaglia B, Tiranti V, Levi S. **Mitochondrial iron and energetic dysfunction distinguish fibroblasts and induced neurons from pantothenate kinase-associated neurodegeneration patients.** Neurobiol Dis. 2015 Mar 30. pii: S0969-9961(15)00098-4.

Ceccatelli Berti C, Dallabona C, Lazzaretti M, **Dusi S**, Tosi E, Tiranti V, Goffrini P. **Modeling human Coenzyme A synthase mutation in yeast reveals altered mitochondrial function, lipid content and iron metabolism**. Microbial Cell 2015, Vol. 2, No. 4, pp. 126 - 135.

Brain Advance Access published December 6, 2013

BRAIN
A JOURNAL OF NEUROLOGY

Pantethine treatment is effective in recovering the disease phenotype induced by ketogenic diet in a pantothenate kinase-associated neurodegeneration mouse model

Dario Brunetti,[1] Sabrina Dusi,[1] Carla Giordano,[2] Costanza Lamperti,[1] Michela Morbin,[3] Valeria Fugnanesi,[3] Silvia Marchet,[1] Gigliola Fagiolari,[4] Ody Sibon,[5] Maurizio Moggio,[4] Giulia d'Amati[2] and Valeria Tiranti[1]

1 Unit of Molecular Neurogenetics, Foundation IRCCS Neurological Institute C. Besta, Milan, Italy
2 Department of Radiology, Oncology and Pathology, Sapienza University, Policlinico Umberto I, Rome, Italy
3 Unit of Neuropathology and Neurology, Foundation IRCCS Neurological Institute C. Besta, Milan, Italy
4 Unit of Neuromuscular and Rare Disorders, Foundation IRCCS Ca' Granda Ospedale Maggiore Policlinico, Department of Neurological Sciences, Milan, "Dino Ferrari" Centre, Milan University, Italy
5 Department of Cell Biology, University Medical Centre Groningen, University of Groningen, The Netherlands

Correspondence to: Valeria Tiranti,
Unit of Molecular Neurogenetics,
IRCCS Foundation Neurological Institute "C. Besta",
Via Temolo, 4,
20126 Milan, Italy,
E-mail: tiranti@istituto-besta.it

Pantothenate kinase-associated neurodegeneration, caused by mutations in the *PANK2* gene, is an autosomal recessive disorder characterized by dystonia, dysarthria, rigidity, pigmentary retinal degeneration and brain iron accumulation. *PANK2* encodes the mitochondrial enzyme pantothenate kinase type 2, responsible for the phosphorylation of pantothenate or vitamin B5 in the biosynthesis of co-enzyme A. A *Pank2* knockout (*Pank2*$^{-/-}$) mouse model did not recapitulate the human disease but showed azoospermia and mitochondrial dysfunctions. We challenged this mouse model with a low glucose and high lipid content diet (ketogenic diet) to stimulate lipid use by mitochondrial beta-oxidation. In the presence of a shortage of co-enzyme A, this diet could evoke a general impairment of bioenergetic metabolism. Only *Pank2*$^{-/-}$ mice fed with a ketogenic diet developed a pantothenate kinase-associated neurodegeneration-like syndrome characterized by severe motor dysfunction, neurodegeneration and severely altered mitochondria in the central and peripheral nervous systems. These mice also showed structural alteration of muscle morphology, which was comparable with that observed in a patient with pantothenate kinase-associated neurodegeneration. We here demonstrate that pantethine administration can prevent the onset of the neuromuscular phenotype in mice suggesting the possibility of experimental treatment in patients with pantothenate kinase-associated neurodegeneration.

Keywords: pantothenate kinase-associated neurodegeneration (PKAN); mitochondria; ketogenic diet; pantethine

Abbreviation: PKAN = pantothenate kinase-associated neurodegeneration

Received July 19, 2013. Revised September 6, 2013. Accepted October 5, 2013.

Introduction

The common feature of a group of genetic disorders, termed neurodegeneration with brain iron accumulation, is brain iron overload identified by radiological and histopathological examinations (Kruer *et al.*, 2012). Different subtypes of neurodegeneration with brain iron accumulation have been defined at the genetic level but pantothenate kinase-associated neurodegeneration (PKAN) syndrome is the most frequent form.

PKAN is caused by mutations in the *PANK2* gene, which codes for the mitochondrial enzyme pantothenate kinase 2. This enzyme is involved in the co-enzyme A biosynthetic pathway, catalysing the phosphorylation of vitamin B5 or pantothenate (Hayflick, 2003). PKAN usually manifests in childhood with gait disturbances and rapidly progresses to a severe movement deficit with dystonia, dysarthria and dysphagia. The hallmark of this disease is the eye-of-the-tiger signal in the globus pallidus on T_2-weighted MRI (Hayflick *et al.*, 2003; Gregory *et al.*, 2009)

To date, the mechanistic connection linking PANK2 dysfunction, neurodegeneration and alteration of iron homeostasis has not been understood, thus preventing our comprehension of the pathogenesis of the disease and the design of efficient therapeutic strategies. It has been proposed that reduced PANK2 enzymatic activity determines the accumulation of cysteine, which may chelate iron thus promoting the formation of free radicals (Gregory *et al.*, 2008); alternatively, defects in co-enzyme A and, as a consequence, in phospholipid metabolism may damage the membranes and lead to increased oxidative stress, which may alter iron homeostasis (Leonardi *et al.*, 2007).

The mouse models of PKAN display incomplete phenotypes, including hardly any brain iron accumulation. *Pank2*$^{-/-}$ mice show growth reduction, retinal degeneration, male infertility because of azoospermia (Kuo *et al.*, 2005), and mitochondrial dysfunctions (Brunetti *et al.*, 2012) under standard diet conditions. Retinal degeneration (Kuo *et al.*, 2005) was not confirmed in a recent *Pank2* knockout mouse (Garcia *et al.*, 2012) and this phenotype is uncertain. A movement disorder was present in mice on a pantothenic acid-deficient diet (Kuo *et al.*, 2007). A *Pank1* knockout mouse (Leonardi *et al.*, 2010) displayed a metabolic disorder characterized by altered fatty acid oxidation and gluconeogenesis, causing mild hypoglycaemia. An additional mouse model consisting of a double *Pank1/Pank2* knockout (Garcia *et al.*, 2012) showed a severe phenotype characterized by hypoglycaemia and hyperketonaemia leading to dysfunctional post-natal development and premature death at 17 days.

Based on the role of co-enzyme A in several crucial cellular metabolic pathways, we tested the hypothesis to stress the *Pank2*$^{-/-}$ mouse model with a high-fat ketogenic diet. Ketone bodies produced by the ketogenic diet through fatty acid oxidation bypass glycolysis and enter the citric acid cycle to produce oxidative phosphorylation (OXPHOS) substrate. Mice on a ketogenic diet use mainly fatty acid oxidation and OXPHOS for ATP production as compared to mice on a standard diet (Laffel, 1999). We observed that only ketogenic diet-fed *Pank2*$^{-/-}$ mice presented typical signs of neurological and motor impairment, as well as neuropathological findings, resembling the phenotype observed in patients with PKAN. Moreover, these mice showed muscular dysfunctions with mitochondrial morphological alterations, which were also detected in the muscle of a patient with PKAN.

Recently, a PANK2 knockout *Drosophila* model has shown that panthethine can serve as a compound to bypass the block due to severe impairment of pantothenate kinase and that it is able to rescue brain degeneration, mitochondrial dysfunction and locomotor disabilities (Rana *et al.*, 2010).

To determine if pantethine was able to counteract the disease phenotype elicited in ketogenic diet-fed *Pank2*$^{-/-}$ mice, we continuously administered pantethine in drinking water during the ketogenic treatment. Our data indicated that pantethine treatment was safe, with no side effects and was able to ameliorate both the majority of the symptoms in the nervous and muscular systems and the morphological features of neuronal and mitochondrial damage.

Materials and methods

Animals and diets

Animal studies were approved by the Ethics Committee of the Foundation IRCCS Neurological Institute C. Besta, in accordance with guidelines of the Italian Ministry of Health: Project no. BT4/2011. The use and care of animals followed the Italian Law D.L. 116/1992 and the EU directive 86/609/CEE.

Standard diet (Mucedola), ketogenic diet (E15149-30, ssniff Spezialdiaten) and water were given *ad libitum*. Ketogenic diet composition: 79.2 % fat; 8% protein; 5% crude fibre; 4.5 % crude ash; 0.6% starch; 0.7% sugar (31.6 MJ/kg), with multi-vitamin addition. Pantethine (Sigma) was administered at a concentration of 15 mg/kg/day in drinking water. The JM129/SvJ-C57BL/6 *Pank2*$^{+/-}$ mice used in this study were kindly provided by Professor Hayflick (Kuo *et al.*, 2005).

Animals were housed two or three in a cage, in a temperature-controlled (21°C) room with a 12 h light-dark cycle and ~60% relative humidity.

The experimental design included four groups of mice: (i) the 'standard diet' group composed of eight *Pank2*$^{-/-}$ mice (four male and four female) and nine *Pank2*$^{+/+}$ (five male and four female) on a standard diet for 2 months; (ii) the 'standard diet + pantethine' group composed of eight *Pank2*$^{-/-}$ mice (four male and four female) and 12 *Pank2*$^{+/+}$ (five male and seven female) on a standard diet with the concomitant administration of pantethine for 2 months; (iii) the 'ketogenic diet' group composed of 20 *Pank2*$^{-/-}$ mice (nine male and 11 female) and 26 *Pank2*$^{+/+}$ (11 male and 15 female) on an *ad libitum* ketogenic diet for 2 months; and (iv) the 'ketogenic diet + pantethine' group composed of 13 *Pank2*$^{-/-}$ mice (five male and eight female) and 16 *Pank2*$^{+/+}$ (five male and 11 female) on an *ad libitum* ketogenic diet with the concomitant administration of pantethine.

Behavioural and motor skills analysis

The different groups were monitored weekly for onset of postural abnormalities, loss of weight and general behavioural changes. We detected spontaneous motor activity over a continuous period of 15 h (at any time between 17:00 pm and 08:00 am) in an activity cage (Ugo Basile) for four single-gender groups of 3-month-old *Pank2*$^{+/+}$ and *Pank2*$^{-/-}$ mice, each comprising three mice of each genotype. In total 12 *Pank2*$^{+/+}$ and 12 *Pank2*$^{-/-}$ mice were analysed.

Measure of motor exercise endurance was evaluated using a treadmill apparatus (Columbus Instruments) counting the number of falls in the motivational grid during a gradually accelerating program with speed initially at 3.8 m/min and increasing by 3 m/min every 2 min. The test was terminated by exhaustion, defined by >10 falls/min into the motivational grid.

A footprint test was performed by painting hindlimbs with non-toxic ink and placing mice at one end of an enclosed, dark tunnel on white paper. Mice walked along a 28 cm long, 7 cm wide strip; stride length and width of consecutive steps were measured. These tests were carried out in 3-month-old mice to monitor the phenotype.

Histology, histochemistry and immunohistochemistry

Histological, histochemical and immunohistochemical analyses were performed on formalin-fixed and paraffin-embedded brain tissues from the following treatment groups: standard diet *Pank2*$^{+/+}$ ($n = 2$); standard diet *Pank2*$^{-/-}$ ($n = 2$); ketogenic diet *Pank2*$^{+/+}$ ($n = 4$); ketogenic diet *Pank2*$^{-/-}$ ($n = 5$); ketogenic diet + pantethine *Pank2*$^{+/+}$ ($n = 3$); ketogenic diet + pantethine *Pank2*$^{-/-}$ ($n = 3$). Briefly, whole formalin-fixed brains were cut in 2-mm thick slices along the sagittal plane, and embedded in formalin. Five to 10-μm thick serial sections were stained with haematoxylin-eosin, periodic acid Schiff, Luxol fast blue and Perls' stain. Immunohistochemistry was performed using antibodies against amyloid precursor protein (Abcam, 1:200), heavy molecular weight neurofilament (Abcam, 1:2000); ubiquitin (Dako, 1:50); phosphorylated tau (Abcam, 1:50), alpha synuclein phospho specific (Covance, 1:200), NeuN (Millipore, 1:500), and glial fibrillary acidic protein (GFAP; Dako, 1:100).

Left quadricep skeletal muscle biopsies were performed in patients according to a protocol approved by the Foundation IRCCS Neurological Institute C. Besta. Morphological analysis in patient and mouse skeletal muscle tissue was carried out on 8 μm cryostat sections using standard histological and histochemical techniques (Dubowitz *et al.* 1973). The reactions for COX and SDH were performed as previously described (Sciacco and Bonilla, 1996). The following treatment groups were analysed: standard diet *Pank2*$^{+/+}$ ($n = 2$); standard diet *Pank2*$^{-/-}$ ($n = 2$); ketogenic diet *Pank2*$^{+/+}$ ($n = 2$); ketogenic diet *Pank2*$^{-/-}$ ($n = 2$); ketogenic diet + pantethine *Pank2*$^{+/+}$ ($n = 2$); and ketogenic diet + pantethine *Pank2*$^{-/-}$ ($n = 2$).

Evaluation of mitochondrial bioenergetics

We analysed mitochondrial energy metabolism in isolated mitochondria derived from brains of standard diet *Pank2*$^{+/+}$ ($n = 3$); standard diet *Pank2*$^{-/-}$ ($n = 3$); standard diet + pantethine *Pank2*$^{+/+}$ ($n = 3$); and standard diet + pantethine *Pank2*$^{-/-}$ ($n = 3$) mice, using an XF96 Extracellular Flux Analyzer (Seahorse Bioscience) as previously reported (Brunetti *et al.*, 2012).

Derivation of neurons from sciatic nerve and analysis of mitochondrial membrane potential

Detection of mitochondrial potential was performed using JC1 staining kit on neurons derived from sciatic nerves isolated from adult mouse as previously described (Brunetti *et al.*, 2012).

Electron microscopy analysis

Sciatic nerve analysis was performed on the following treatment groups: standard diet *Pank2*$^{+/+}$ ($n = 1$); standard diet *Pank2*$^{-/-}$ ($n = 1$); ketogenic diet *Pank2*$^{+/+}$ ($n = 3$); ketogenic diet *Pank2*$^{-/-}$ ($n = 3$); ketogenic diet + pantethine *Pank2*$^{+/+}$ ($n = 3$); and ketogenic diet + pantethine *Pank2*$^{-/-}$ ($n = 3$). Sciatic nerves were surgically removed and processed for epoxy resin embedding as previously described (Brunetti *et al.*, 2012). In particular, each sciatic nerve was cut in proximal, middle and distal segments and dehydrated separately. Ultrastructural analyses were conducted on each stump. Brain ultrastructural analysis was performed on the following treatment groups: standard diet *Pank2*$^{+/+}$ ($n = 1$); standard diet *Pank2*$^{-/-}$ ($n = 1$); ketogenic diet *Pank2*$^{+/+}$ ($n = 3$); ketogenic diet *Pank2*$^{-/-}$ ($n = 3$); ketogenic diet + pantethine *Pank2*$^{+/+}$ ($n = 3$); and ketogenic diet + pantethine *Pank2*$^{-/-}$ ($n = 3$). Sagittally spliced brains were fixed by immersion in glutaraldehyde (2.5% in phosphate buffer). After fixation, serial sagittal slides of 1-mm thick were obtained. Selected areas of interest were sampled, post-fixed in osmium tetroxide and embedded in Epon^{TM} epoxy resin. Thin sections (80–90 nm) were stained with uranyl acetate and lead citrate and examined with a CM10 Philips electron microscope.

Patient and mouse muscle tissues were fixed in 2.5% glutaraldehyde, processed as previously described (Napoli *et al.*, 2011) and post-fixed in 2% osmium tetroxide for 1 h. After dehydration, the specimens were embedded in epoxy resin. Ultrathin sections were cut and stained with uranyl acetate and lead citrate, then examined with a Zeiss electron microscope.

Results

Mice phenotyping

We constantly monitored the weight of *Pank2*$^{+/+}$ and *Pank2*$^{-/-}$ mice during the administration of standard or ketogenic diet. As also previously reported (Kuo *et al.*, 2005) *Pank2*$^{-/-}$ mice under standard diet showed a slight weight reduction as compared with *Pank2*$^{+/+}$ mice, whereas during ketogenic treatment *Pank2*$^{-/-}$ mice showed a fast and progressive weight loss (Fig. 1A and B). Moreover, only *Pank2*$^{-/-}$ mice fed a ketogenic diet manifested kyphosis with hunched position, (Fig. 1C), feet clasping (Fig. 1D), whitening of the fur and rigidity of the tail (Fig. 1E), as well as dystonic limb positioning (Fig. 1F).

We asked whether these signs could have been prevented by pantethine administration. To this aim we treated a group of *Pank2*$^{+/+}$ and *Pank2*$^{-/-}$ mice ('ketogenic diet + pantethine' group) with a ketogenic diet and the concomitant administration of pantethine (15 mg/kg/day) in drinking water. This concentration was established based on a dosage of 900 mg/day in an adult individual ($n = 14$) considering an average weight of 60 kg. We also tested various concentrations of pantethine in mice over 3 weeks and determined that a dose of up to 480 mg/kg/day was tolerated without any side effects on weight and drinking intake (Supplementary Fig. 1).

We observed that, with pantethine administration to mice fed a ketogenic diet, the weight of *Pank2*$^{-/-}$ mice was similar to that of *Pank2*$^{+/+}$ mice (Fig. 1G), no signs of kyphosis or feet clasping were present (Fig. 1H) and body size approached that of *Pank2*$^{-/-}$ mice

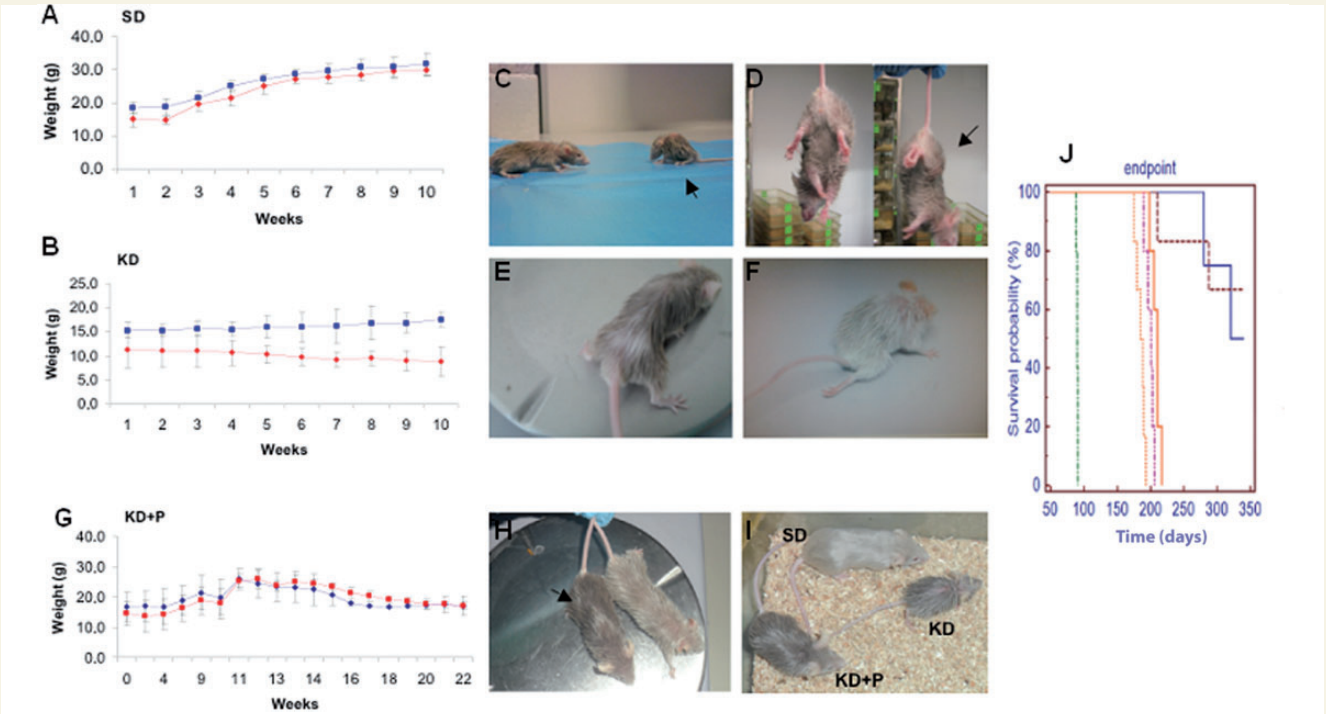

Figure 1 Mice phenotype. (**A**) Body weight of *Pank2*$^{+/+}$ and *Pank2*$^{-/-}$ mice fed a standard diet (SD). (**B**) Body weight of *Pank2*$^{+/+}$ and *Pank2*$^{-/-}$ mice on a ketogenic diet (KD). (**C**) Kyphosis with hunched position; (**D**) feet clasping in ketogenic diet-fed *Pank2*$^{-/-}$ (arrow); (**E**) whitening of the fur and rigidity of the tail in ketogenic diet-fed *Pank2*$^{-/-}$; (**F**) dystonic hindlimb position. (**G**) Body weight of *Pank2*$^{-/-}$ mice was similar to that of *Pank2*$^{+/+}$ fed a ketogenic diet with pantethine administration (KD + P). (**H**) No sign of kyphosis or feet clasping were present in *Pank2*$^{-/-}$ mice on a ketogenic diet with pantethine administration (arrow). (**I**) Comparison of *Pank2*$^{-/-}$ body size in mice on standard (SD), ketogenic (KD) and ketogenic + pantethine (KD + P) diets (**J**) Survival curves for different diet conditions: *Pank2*$^{-/-}$ mice fed a ketogenic diet died after 2 months (dotted green line); *Pank2*$^{+/+}$ mice fed a ketogenic (dotted yellow line); *Pank2*$^{+/+}$ mice fed a ketogenic diet with pantethine (dotted pink line); *Pank2*$^{-/-}$ mice fed a ketogenic diet with pantethine administration prolonged their survival by up to 5 months (orange line); *Pank2*$^{-/-}$ mice fed a standard diet (dotted brown line); and *Pank2*$^{+/+}$ mice fed a standard diet (blue line). In **A**, **B** and **G**, the red symbols indicate *Pank2*$^{-/-}$; blue symbols indicate *Pank2*$^{+/+}$.

fed a standard diet (Fig. 1I). Most importantly, *Pank2*$^{-/-}$ mice fed a ketogenic diet died after 2 months whereas the administration of pantethine prolonged their survival for up to 5 months (Fig. 1J). We could not verify the recovery of retina degeneration as this initial observation (Kuo *et al.*, 2005) was not confirmed by our own investigations and also not reported in another *Pank2* knockout mouse model (Garcia *et al.*, 2012). On the contrary, azoospermia was confirmed in mice fed a standard diet and ketogenic diet but was not rescued by pantethine treatment during the period of our observation and with the dose used.

Motor performance evaluation

Pank2$^{-/-}$ mice fed a ketogenic diet were lethargic and showed a significant reduction of spontaneous movements as compared with *Pank2*$^{+/+}$ mice fed a ketogenic diet, whereas no differences were observed when fed a standard diet (Fig. 2A).

Quantitative motor tests revealed significantly lower activity in *Pank2*$^{-/-}$ mice on a ketogenic diet as compared with *Pank2*$^{+/+}$ mice; no differences were evident on a standard diet (Fig. 2B). The footprint patterns were assessed quantitatively by measuring stride length and hind base width. We found that *Pank2*$^{-/-}$ mice on a ketogenic diet exhibited shorter stride lengths and hind paw width, and an irregular gait as compared with *Pank2*$^{+/+}$ mice on a ketogenic diet (Fig. 2C). All of these abnormalities were recovered by pantethine treatment and *Pank2*$^{-/-}$ mice behaved in the same way as their control littermates (Fig. 2A–C).

Neuropathology of *Pank2*$^{-/-}$ mice fed a ketogenic diet

On histological and immunohistochemical analysis of the whole brains we did not observe massive neural loss, gliosis or demyelination in Pank2$^{-/-}$ mice on a standard diet or a ketogenic diet (data not shown). However, we noticed the presence of small, scattered groups of neurons with eosinophilic, periodic acid Schiff-positive round cytoplasmic inclusions (Fig. 3A–C). These features were observed only in *Pank2*$^{-/-}$ mice on a ketogenic diet, and were located mostly in the midbrain, putamen and amygdala. On immunohistochemistry, the inclusions were sharply positive for ubiquitin (Fig. 3D and F) and negative for amyloid precursor protein, phosphorylated tau, α-synuclein, and high molecular weight neurofilaments (not shown). In addition, ubiquitin

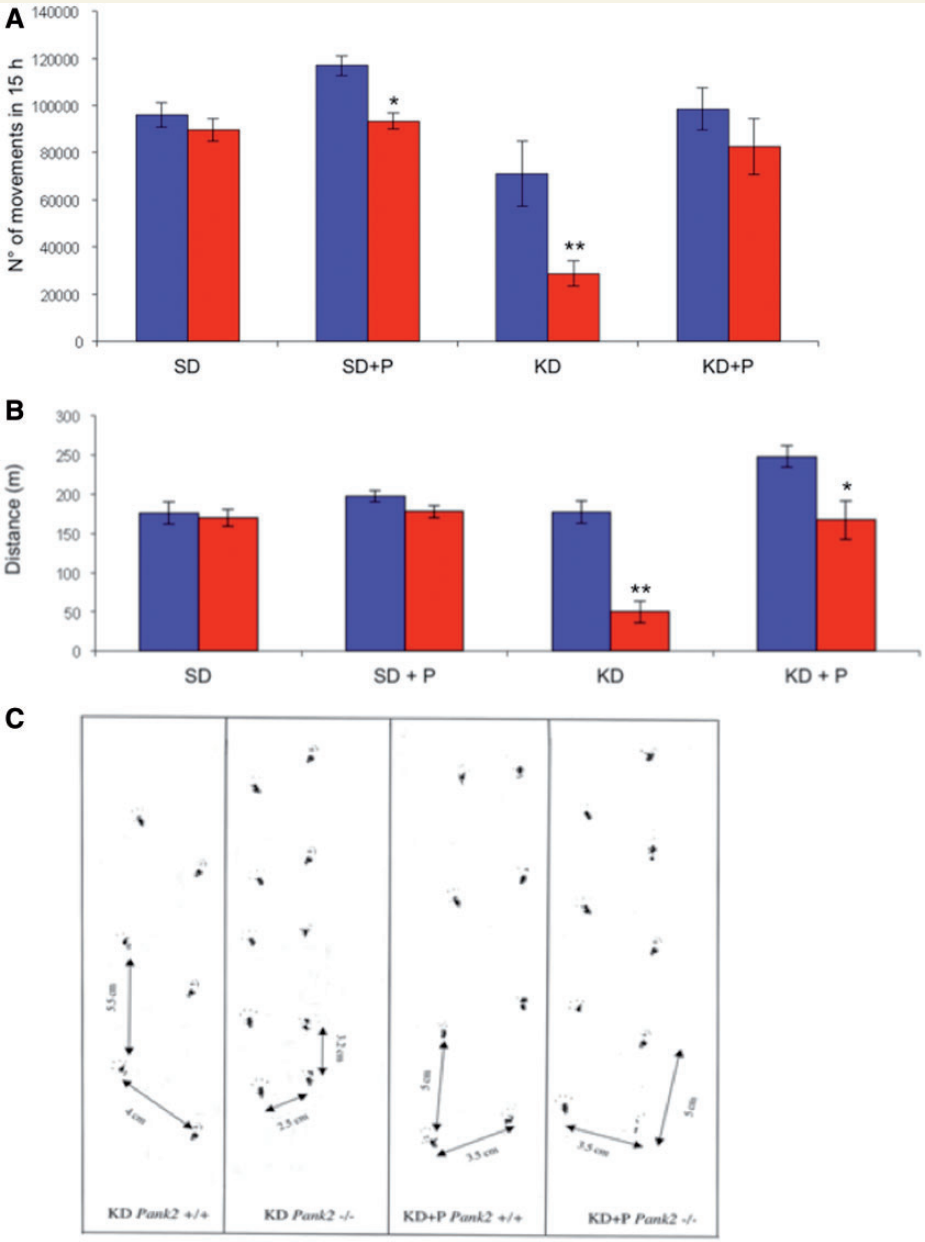

Figure 2 Motor performance evaluation. (**A**) Activity cage: no differences were observed in *Pank2*$^{+/+}$ and *Pank2*$^{-/-}$ mice on a standard diet (SD) or with pantethine (SD + P); *Pank2*$^{+/+}$mice were more active with pantethine treatment (*$P < 0.05$, two-tailed, unpaired Student's *t*-test). *Pank2*$^{-/-}$ mice fed a ketogenic diet were lethargic and showed a significant reduction of spontaneous movements as compared with *Pank2*$^{+/+}$ mice on a ketogenic diet (**$P < 0.001$, two-tailed, unpaired Student's *t*-test). Pantethine treatment (KD + P) rescues the reduced movements. (**B**) Treadmill test: no differences in the distance travelled by *Pank2*$^{+/+}$ and *Pank2*$^{-/-}$ mice on a standard diet (SD) or with pantethine (SD + P). *Pank2*$^{-/-}$ mice on a ketogenic diet ran only 50 m as compared to 180 m of *Pank2*$^{+/+}$ mice (**$P < 0.001$, two-tailed, unpaired Student's *t*-test). Pantethine treatment (KD + P) restored the running capability in *Pank2*$^{-/-}$ mice and increased the performance in *Pank2*$^{+/+}$ mice (*$P < 0.05$, two-tailed, unpaired Student's *t*-test). (**C**) Footprint pattern: *Pank2*$^{-/-}$ mice fed a ketogenic diet showed shorter stride lengths and hind paw width, and an irregular gait as compared with *Pank2*$^{+/+}$ mice fed a ketogenic diet. Pantethine treatment (KD + P) abolishes the movement disorders. In **A** and **B**, the red bars indicate *Pank2*$^{-/-}$ mice and blue bars indicate *Pank2*$^{+/+}$ mice, respectively.

stain highlighted finely granular cytoplasmic deposits in several neurons, as well as large, ubiquitin positive degenerating neurons (Fig. 3D and E). Iron deposits were not observed with Perl's stain (data not shown).

Pantethine treatment of *Pank2*$^{-/-}$ mice on a ketogenic diet led to the disappearance of neuronal cytoplasmic inclusion on haematoxylin-eosin and periodic acid Schiff stain. Ubiquitin was merely detectable by immunohistochemistry after treatment (Fig. 3G) and

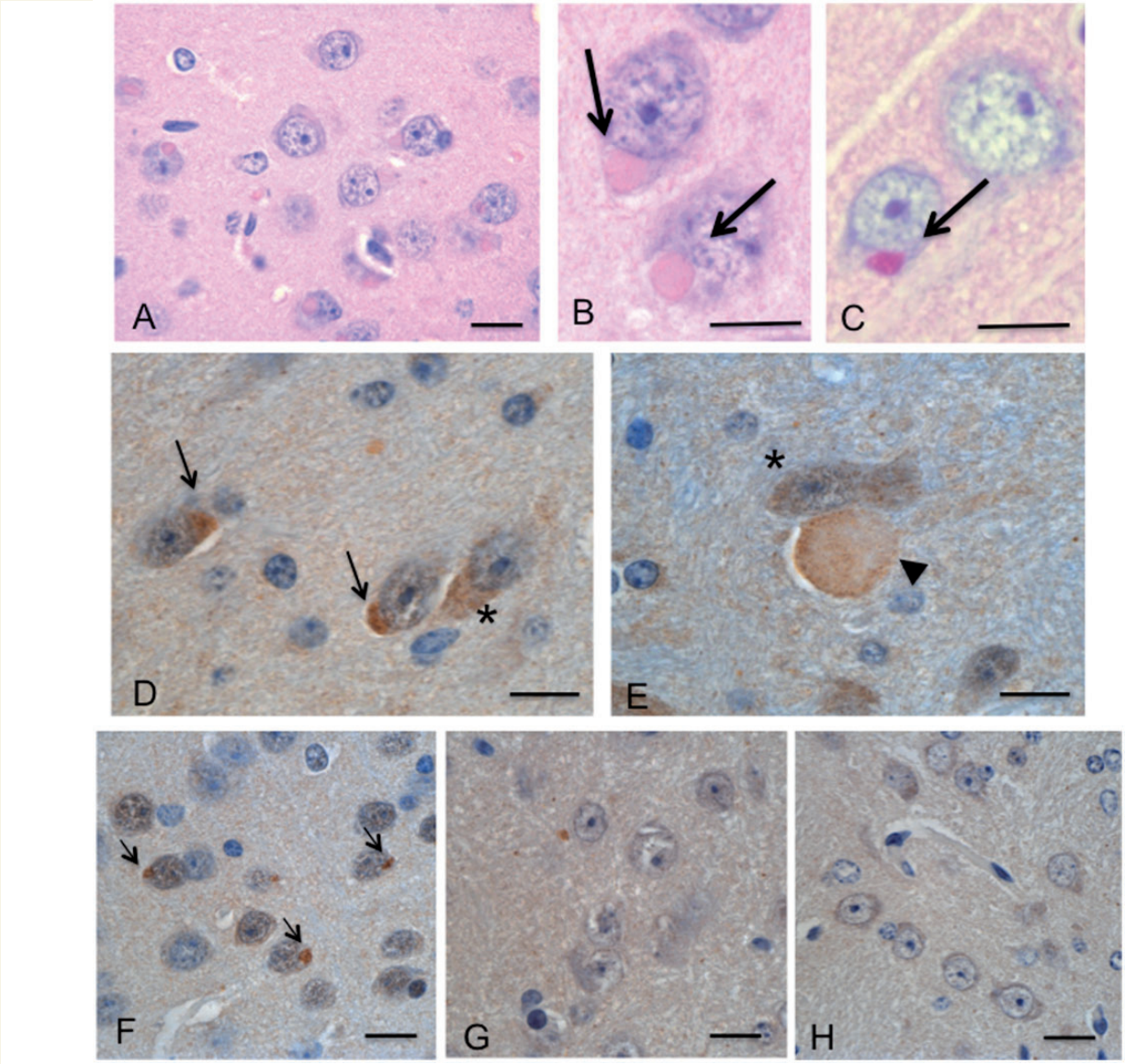

Figure 3 Histology and immunohistochemistry of brains from *Pank2*$^{-/-}$ mice fed a ketogenic diet and a ketogenic diet with pantethine. The analysed animals were 3 months old. Round, eosinophilic, periodic acid Schiff-positive cytoplasmic inclusions were present in neurons of *Pank2*$^{-/-}$ mice fed a ketogenic diet (**A–C**, arrows in **B** and **C**). Cytoplasmic bodies are markedly positive on ubiquitin immunostain (**D** and **F**, arrows). Scattered neurons showed a finely granular cytoplasmic stain for ubiquitin (**D** and **E**, asterisks). There were large degenerating neurons with a diffuse positivity for ubiquitin (**E**, arrowhead). Ubiquitin stain was barely detected in neurons from *Pank2*$^{-/-}$ mice fed a ketogenic diet with pantethine (**G**), which show histological and immunohistochemical features similar to their wild-type littermates (**H**). Scale bars = 25 μm.

completely absent in ketogenic diet-*Pank2*$^{+/+}$ mice brain (Fig. 3H).

Ultrastructural features of central and peripheral nervous systems

Ultrastructural analysis was performed on basal ganglia and peripheral nerve of *Pank2*$^{-/-}$ and *Pank2*$^{+/+}$ mice under different diet conditions. In the basal ganglia, *Pank2*$^{-/-}$ animals on a standard diet showed the presence of numerous mitochondria with abnormal, swollen cristae (Fig. 4). These features were worsened by a ketogenic diet, which led to focal loss of cristae (Fig. 4). *Pank2*$^{-/-}$ animals fed a ketogenic diet also showed cytoplasmic deposits of lipofuscin (data not shown). Notably, pantethine administration completely rescued the mitochondrial morphology of *Pank2*$^{-/-}$ animals on a standard diet, which were indistinguishable from the wild-type littermates (Fig. 4), and ameliorated the morphology of ketogenic diet-fed *Pank2*$^{-/-}$ mice (Fig. 4).

Ultrastructural analysis of peripheral nerve of *Pank2*$^{-/-}$ animals on a ketogenic diet showed the presence of swollen mitochondria, characterized by cristae degeneration and by the presence of amorphous material in the matrix (Fig. 5). Pantethine

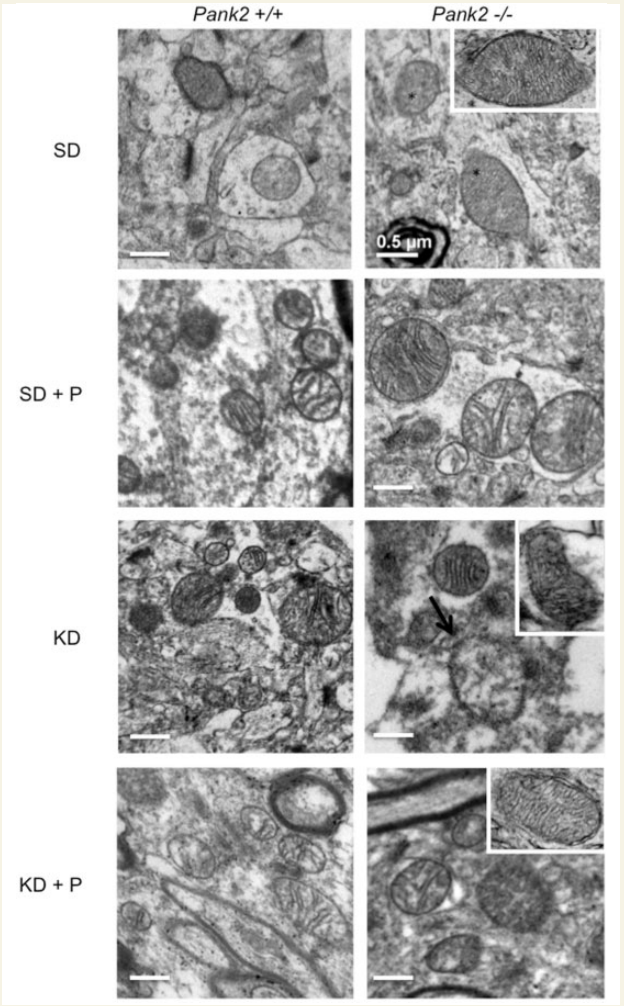

Figure 4 Electron microscopy of basal ganglia in *Pank2*$^{+/+}$ and *Pank2*$^{-/-}$ mice under different diet conditions. The analysed animals were 3 months old. *Pank2*$^{+/+}$ mice on a standard diet (SD), a standard diet + pantethine (SD + P), ketogenic diet (KD) and ketogenic diet + pantethine (KD + P) show normal mitochondria. *Pank2*$^{-/-}$ mice on a standard diet show mitochondria with swollen cristae (asterisks and insert). With a ketogenic diet the mitochondrial morphology is worsened with focal loss of cristae (arrow and insert). *Pank2*$^{-/-}$ mice on standard diet with pantethine were similar to wild-type littermates; with a ketogenic diet with pantethine there is a prevalence of mitochondria with normal cristae morphology, although a few mitochondria still showed swollen cristae.

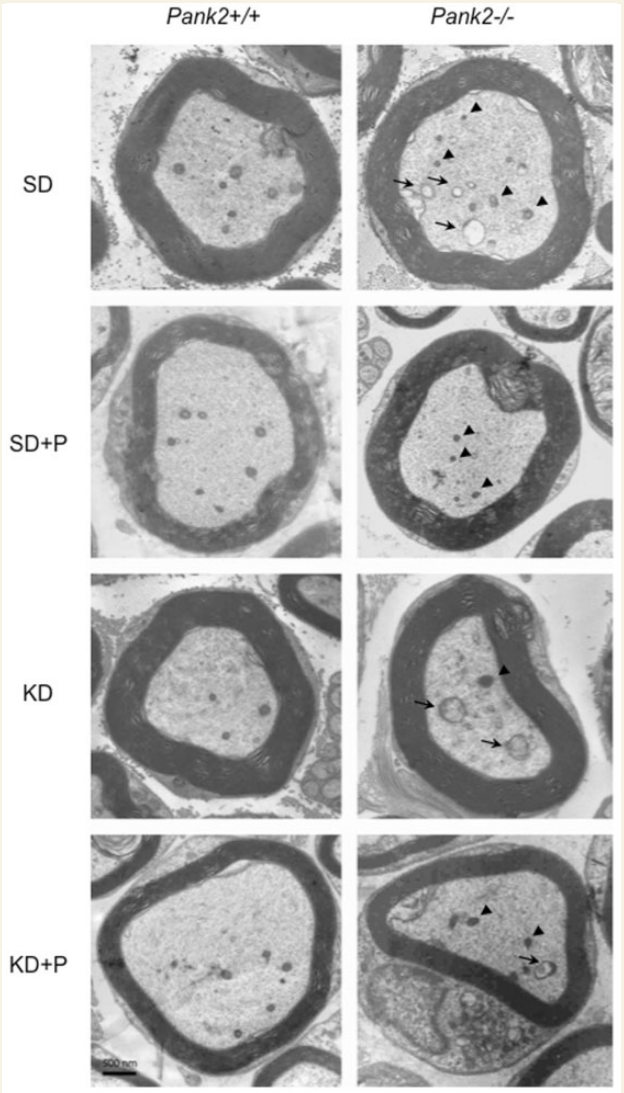

Figure 5 Electron microscopy of peripheral nerve in *Pank2*$^{+/+}$ and *Pank2*$^{-/-}$ mice under different diet conditions. The analysed animals were 3 months old. Sciatic nerve axons of *Pank2*$^{+/+}$ mice on a standard diet (SD), standard diet + pantethine (SD + P), ketogenic diet (KD) and ketogenic diet + pantethine (KD + P) contain morphologically normal mitochondria. Sciatic nerve axons of *Pank2*$^{-/-}$ mice on a standard diet and ketogenic diet show swollen mitochondria with altered cristae (arrows). Sciatic nerve axons of *Pank2*$^{-/-}$ mice on a standard diet + pantethine and ketogenic diet + pantethine show a high prevalence of normally-shaped mitochondria with regular cristae organization (arrowheads). Scale bars = 500 μm.

administration was able to completely rescue the mitochondrial morphology both in the PNS and CNS. No ultrastructural alterations were observed in *Pank2*$^{+/+}$ mice fed with standard or ketogenic diets (Figs 4 and 5).

Pantethine restores mitochondrial membrane potential of *Pank2*$^{-/-}$ neurons

To evaluate mitochondrial membrane potential we used JC1 staining. As shown in Fig. 6, neurons derived from *Pank2*$^{+/+}$ animals treated with a standard or ketogenic diet presented red fluorescent aggregates indicating the preservation of the mitochondrial membrane potential. On the contrary, neurons derived from *Pank2*$^{-/-}$ mice treated with a standard or ketogenic diet presented with a diffuse green fluorescence (Fig. 6) confirming the presence of a defective mitochondrial membrane potential. Interestingly, neurons derived from *Pank2*$^{-/-}$ mice under

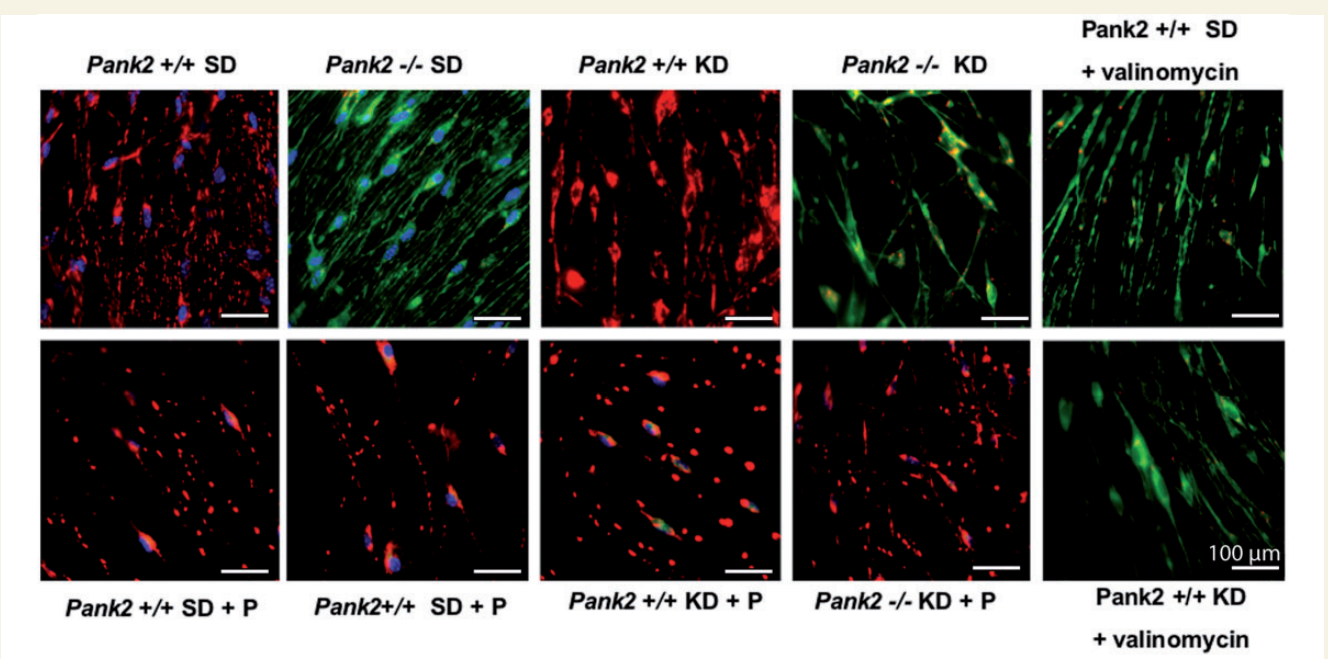

Figure 6 Membrane potential in *Pank2*$^{+/+}$ and *Pank2*$^{-/-}$ neurons derived from mice under different diet conditions. Neurons derived from *Pank2*$^{+/+}$ animals treated with a standard (SD) or ketogenic diet (KD), with or without pantethine (P) presented red fluorescent aggregates indicating the preservation of the mitochondrial membrane potential. Neurons derived from *Pank2*$^{-/-}$ mice treated with a standard or ketogenic diet presented with a diffuse green fluorescence confirming the presence of a defective mitochondrial membrane potential. Neurons derived from *Pank2*$^{-/-}$ mice with standard and ketogenic treatment plus the addition of pantethine, showed predominantly red fluorescence aggregates, indicating preservation of mitochondrial membrane potential. Scale bars = 100 µm.

standard and ketogenic treatment plus the addition of pantethine in drinking water, showed predominantly red fluorescence aggregates indicating that the mitochondrial membrane potential was preserved.

Pantethine improves mitochondrial respiration

We evaluated respiration with microscale oxygraphy on mitochondria isolated from brains of *Pank2*$^{+/+}$ and *Pank2*$^{-/-}$ mice treated with pantethine and we compared the results with untreated mice. Measurement was not performed in mitochondria derived from mice under ketogenic treatment because of technical difficulties, probably due to the presence of increased fat levels in the brain. We measured basal oxygen consumption rate, and oxygen consumption rate after ADP addition, and after oligomycin addition. We observed that pantethine was able to significantly increase oxygen consumption rate under all conditions tested in both *Pank2*$^{+/+}$ and *Pank2*$^{-/-}$ mitochondria (Fig. 7). In particular, pantethine determines a doubling in oxygen consumption rate after ADP stimulation suggesting a tightly coupled respiration with ATP production.

These differences were statistically significant as demonstrated by an unpaired, two-sided Student's *t*-test, assuming unequal variance. Values for statistical significance were set at $P < 0.05$.

Comparison of muscle derived from *Pank2*$^{-/-}$ mice on a ketogenic diet versus a patient with pantothenate kinase-associated neurodegeneration

COX histochemical reaction of the muscle derived from *Pank2*$^{-/-}$ mice fed a ketogenic diet revealed a peculiar staining pattern, likely because of the presence of abnormal mitochondria (Fig. 8A). We had the opportunity to study the muscle biopsy of a 6-year-old patient with PKAN (*PANK2* mutations: N500I + IVS2-1G > A). We did not observe any defects in the respiratory chain enzymatic activities apart from a succinate dehydrogenase (SDH) activity below the lower control value (not shown), but we found the same COX staining pattern (Fig. 8B) observed in mice. To characterize these mitochondria further we performed electron microscopy, which highlighted the presence of giant mitochondria spanning the sarcomere between two neighbouring Z-lines and showing irregularly shaped cristae (Fig. 8C).

The histological alterations of the *Pank2*$^{-/-}$ muscle highlighted by both trichrome and COX staining were absent in pantethine-treated mice (Fig. 9). Moreover, no histological abnormalities were evident in standard diet or ketogenic diet *Pank2*$^{+/+}$ muscle (Fig. 9).

Plasma analysis

Plasma analysis showed an increase of cholesterol (Supplementary Fig. 2A) and triglycerides (Supplementary Fig. 2B) in mice on a

ketogenic diet. As expected, pantethine was able to reduce the levels of both (Supplementary Fig. 2A and B). A decrease of glucose levels was detected in mice fed a ketogenic diet and a ketogenic + pantethine diet (Supplementary Fig. 2C). Ketosis was observed in mice fed a ketogenic diet and was maintained during pantethine administration (Supplementary Fig. 2D).

Discussion

The *Pank2*$^{-/-}$ mouse model did not recapitulate the clinical and neuropathological features of the human condition (Kuo *et al.*, 2005; Brunetti *et al.*, 2012). Based on the role of co-enzyme A in several crucial metabolic pathways and considering the data obtained by a metabolomics approach in patients with PKAN, indicating the presence of impairment in lipid metabolism, we tested the hypothesis to challenge this mouse model with a diet containing high fat levels. Ketogenic diet consists of a low glucose and high lipid content, stimulating lipid use by mitochondrial beta-oxidation and ketone body production in the liver. Ketone bodies are high-energy-content compounds that can be used as an energy source by the brain, heart and skeletal muscle. We administered a low carbohydrate high-fat ketogenic diet to 2-month-old *Pank2*$^{-/-}$ and *Pank2*$^{+/+}$ mice and evaluated the clinical and biochemical phenotype.

We demonstrate here that the introduction of the ketogenic diet resulted in the onset of a severe phenotype in *Pank2*$^{-/-}$ mice characterized by motor dysfunctions, neurological impairment with feet-clasping, and exacerbated mitochondrial alterations, which were also present in the brain and PNSs of 12-month-old *Pank2*$^{-/-}$ mice on a standard diet (Brunetti *et al.*, 2012). Moreover, this diet caused the premature death of *Pank2*$^{-/-}$ mice.

Pank2$^{-/-}$ mice fed a ketogenic diet did show the clinical signs present in patients with PKAN, namely more severe movement disorder and neurodegeneration. Importantly, these animals showed histological and immunohistochemical features of neurodegeneration, with cytoplasmic accumulation of abnormal, ubiquinated proteins as observed in the brains of patients with PKAN (Kruer *et al.*, 2011). However, the exact nature of the ubiquitinated proteins in our model remains to be elucidated. As observed in humans, cytoplasmic inclusions in *Pank2*$^{-/-}$ mice were negative for α-synuclein, confirming that PKAN neuropathological findings are different from other forms of neurodegeneration with brain iron accumulation.

We did not observe iron accumulation in *Pank2*$^{-/-}$ mice on a ketogenic diet, in contrast to that observed in human PKAN brains. We cannot exclude that iron levels could be below the detection level for the histological technique or that iron accumulates over a period of time beyond our observation. These aspects are still to be clarified and require further investigation.

The induction of a PKAN-like phenotype in *Pank2*$^{-/-}$ mice fed with a ketogenic diet, allowed us to have a model in which to test therapeutic compounds. Recently, in the *Drosophila* dPANK/*fbl* mutants it was shown that panthethine can work as a precursor of co-enzyme A, even in the presence of severely reduced levels of

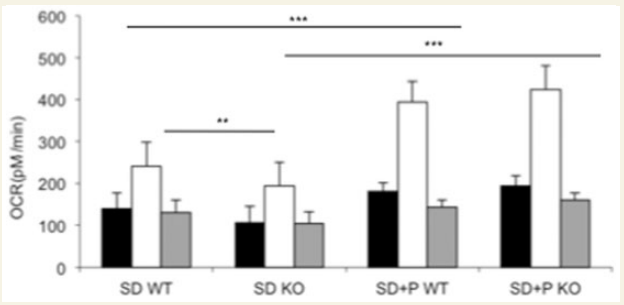

Figure 7 Evaluation of mitochondrial bioenergetics status. Oxygen consumption rate (OCR) in mitochondria isolated from brains of *Pank2*$^{+/+}$ and *Pank2*$^{-/-}$ mice treated with pantethine and compared with untreated mice. We measured basal oxygen consumption rate (OCR-B) after ADP addition (OCR-ADP), and after oligomycin addition (OCR-O). Pantethine was able to significantly increase oxygen consumption rate in both *Pank2*$^{+/+}$ and *Pank2*$^{-/-}$ mitochondria, especially ADP-induced respiration. Black, white and grey histograms indicate OCR-B, -ADP, and -O, respectively. Bars indicate the standard deviation (SD). $^{**}P < 0.01$; $^{***}P < 0.001$ (unpaired, two-tail Student's *t*-test). WT = wild-type; KO = knock-out.

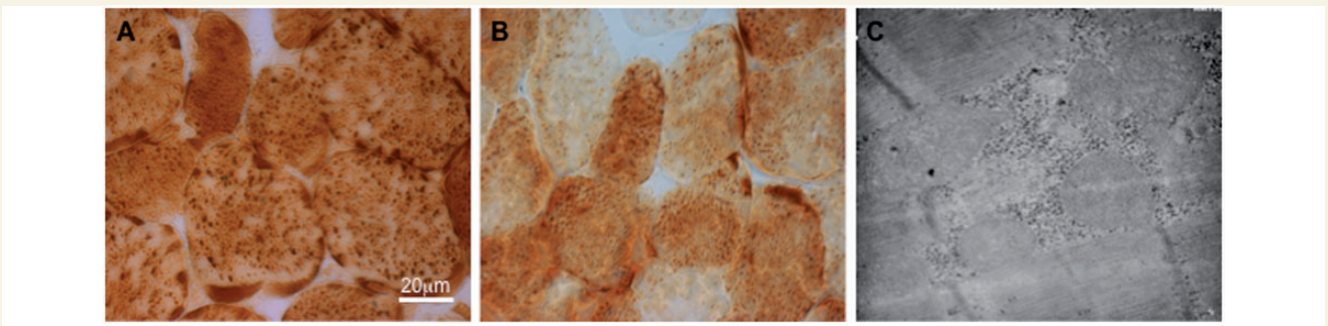

Figure 8 Muscle COX (cytochrome *c* oxidase) histochemical reaction and electron microscopy. (**A**) *Pank2*$^{-/-}$ mice on a ketogenic diet. (**B**) Patient with PKAN revealed the same peculiar staining pattern as mice fed a ketogenic diet. (**C**) Electron microscopy highlighted the presence of giant mitochondria spanning the sarcomere between two neighbouring Z-lines and showing irregularly shaped cristae ($\times$20 000).

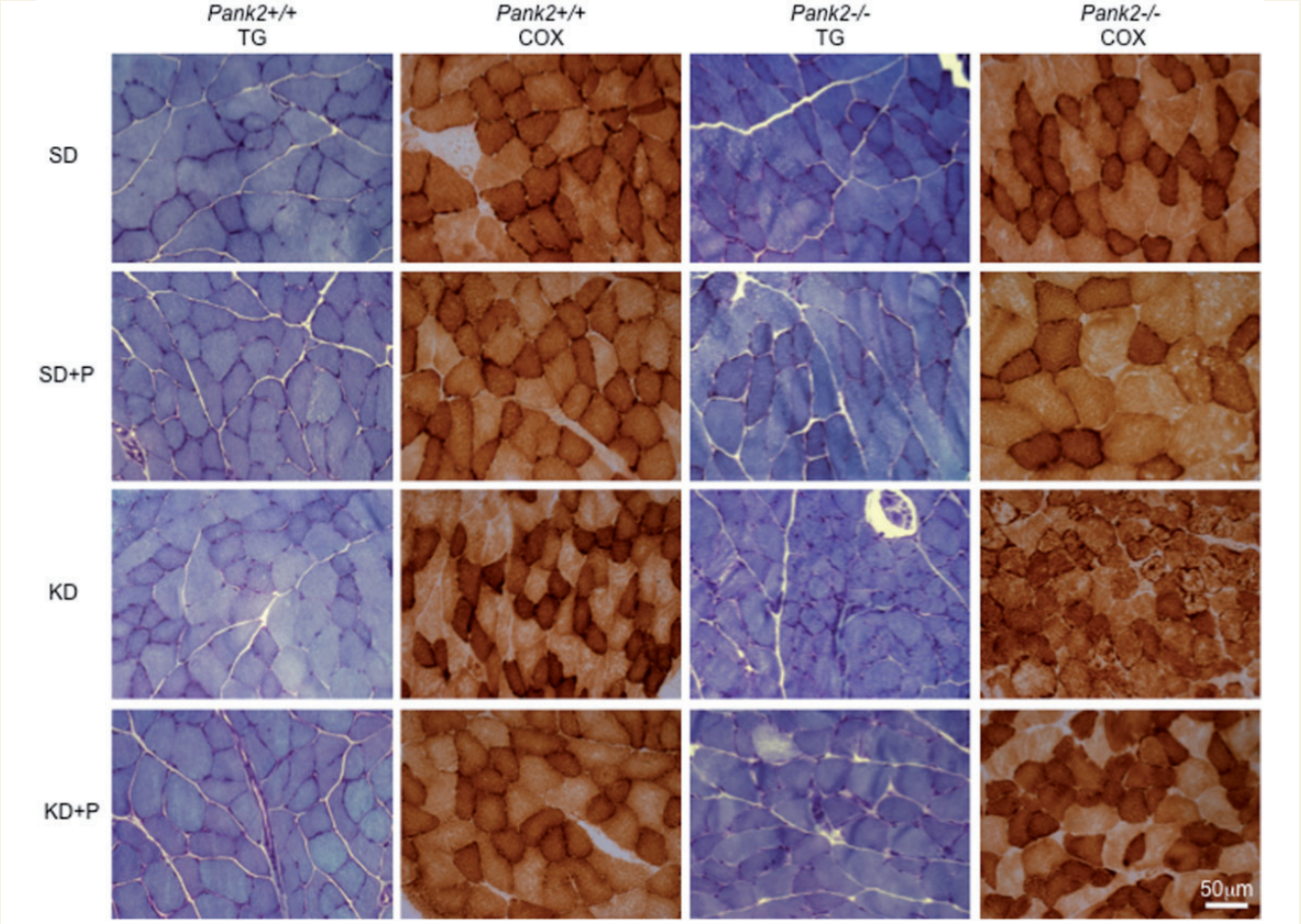

Figure 9 Gomori trichrome (TG) and COX histochemical reactions in muscle of *Pank2*$^{+/+}$ and *Pank2*$^{-/-}$ mice under different diet conditions. No alterations were present in *Pank2*$^{+/+}$ mice. Ketogenic diet (KD) induced muscle histological abnormalities in *Pank2*$^{-/-}$ mice (see also Fig. 8A) characterized by the presence of enlarged mitochondria. These alterations were rescued by pantethine administration (KD + P). Magnification × 400. SD = standard diet.

functional pantothenate kinase and that it was able to rescue brain degeneration, mitochondrial dysfunction and locomotor disabilities (Rana *et al.*, 2010). By reasoning on these data we decided to administer pantethine to mice under ketogenic treatment and, as an internal control, to mice on a standard diet. In *Pank2*$^{-/-}$ mice on a ketogenic diet, we observed the rescue of the clinical phenotype including the movement disorder, the amelioration of the mitochondrial dysfunctions, and the extension of the lifespan as previously demonstrated in *Drosophila* (Rana *et al.*, 2010). Treatment with pantethine dramatically improved both the histological features of neurodegeneration and the ultrastructural mitochondrial damage in *Pank2*$^{-/-}$ mice fed a ketogenic diet. We did not observe rescue of the azoospermic phenotype in mice. Fertility was not thoroughly investigated in patients with PKAN because of the severity of their clinical presentation and shortened lifespan. However, analysis of sperm samples in two affected individuals showed aberrant morphology and altered motility (Gregory and Hayflick, 2005).

We also demonstrated that pantethine administration was able to rescue the mitochondrial phenotype in neurons derived from *Pank2*$^{-/-}$ mice on a standard diet, indicating that its effectiveness was not dependent on or influenced by the ketogenic treatment. It is known that pantethine is rapidly converted into cysteamine and pantothenate by the vanin enzyme, also known as pantetheine hydrolase or pantetheinase (Kaskow *et al.*, 2012). Although pantethine is not able to cross the blood–brain barrier, Bousquet *et al.* (2010) demonstrated that cysteamine can cross the blood–brain barrier and in so doing can exert positive effects on the striatum and substantia nigra (Gibrat and Cicchetti, 2011). Cysteamine is able to enhance the expression of tyrosine hydroxylase protein and of the *Nurr1* gene (now known as *Nr4a2*), and to upregulate the expression of the Brain Derived Neurotrophic Factor (BDNF). These neuroprotective effects of cysteamine and of its dimer cystamine have been hypothesized to reflect the positive actions of this compound in Parkinson's disease (Sun *et al.*, 2010; Gibrat and Cicchetti, 2011) and Huntington's disease (Borrell-Pages *et al.*, 2006).

It has been observed that cysteamine and pantethine in drinking water have beneficial effects in MPTP-induced mouse models of Parkinson's disease (Cornille *et al.*, 2010; Sun *et al.*, 2010) and

would prevent neuronal degeneration in animal models of Parkinson's disease (Stack *et al.*, 2008; Gibrat and Cicchetti, 2011). Moreover, in animal models of Huntington's disease, cysteamine exerts its neuroprotective effects by prolonging lifespan and decreasing motor symptoms (Dedeoglu *et al.*, 2002; Karpuj *et al.*, 2002).

In agreement with these data, we can hypothesize that the beneficial effects of pantethine in our model system were due to its conversion into pantothenate and cysteamine. In fact, pantethine is rapidly hydrolyzed to pantothenic acid and cysteamine as it could not be detected in plasma after oral administration (Wittwer *et al.*, 1985). Cysteamine, the reduced form of cystamine (2-aminoethanethiol) is approved by the FDA for the treatment of cystinosis, a childhood disorder, which causes renal failure through cystine intracellular accumulation (Dohil *et al.*, 2010) and in 2006 a small trial with this compound was initiated in patients with Huntington's disease (Dohil *et al.*, 2010).

However, cysteamine causes side effects (Corden *et al.*, 1981) whereas pantethine has low toxicity (Knott *et al.*, 1957; Schwartz and Bagdon, 1964) and might act as a neutral systemic carrier that would target cysteamine into the brain, avoiding toxicity and maximizing its efficacy.

The metabolism of cysteamine generates several intermediates including hypotaurine and taurine. In addition to being the major bile salt, in the form of taurocholate (Bouckenooghe *et al.*, 2006), taurine crosses the blood–brain barrier and is involved in brain physiological activities such as inhibitory neurotransmission and long-term potentiation (Muramatsu *et al.*, 1978; Pasantes-Morales *et al.*, 1981). Recently, we observed a reduction of the bile acids tauro and glycol cholate (Leoni *et al.*, 2012) and an alteration of lipid metabolism in plasma derived from patients with PKAN, likely because of co-enzyme A shortage causing, among others, dysfunctional fat assimilation.

Together with the data obtained in mice fed a high-fat diet, these observations suggest that it is possible to trace a parallel between patients with PKAN and *Pank2*$^{-/-}$ mice under stressful conditions. Moreover, it is important to consider that environmental factors, such as food intake, together with genetic background could modulate the disease presentation by worsening or, on the contrary, stabilizing the progression of the symptoms. This could also explain the variability of the clinical presentation of the disease, with a spectrum of syndromes ranging from rapid to slowly progressive.

Interestingly, we have analysed for the first time the muscle histology of a genetically defined patient with PKAN. The first neuromuscular examination was performed by Malandrini *et al.* (1995) in two adult cases of clinically-defined Hallerworden-Spatz disease, which showed the presence of subsarcolemmal myeloid structures, features characteristic of inflammatory myopathies.

In our study we demonstrated that the muscle of a 6-year-old patient with PKAN showed giant mitochondria with a mild alteration of the cristae and was histologically comparable with the muscle of *Pank2*$^{-/-}$ mice fed a ketogenic diet. These alterations were rescued in mice after pantethine administration. This is a relevant observation when considering the option of pantethine administration to patients, as muscle analysis could represent the quantitative read-out to evaluate the effect of the compound with a minimal invasive procedure.

Taken together, these data strongly suggest that pantethine administration to patients with PKAN should be considered as a possible, safe and non-toxic therapeutic approach. Moreover, our data clearly demonstrate that an altered lipid metabolism, as a result of co-enzyme A shortage, could represent one of the underlining causes of the disease. It is also possible, as demonstrated by the presence of mitochondrial alteration in the mouse model and in the muscle of a patient with PKAN, that mitochondria play a relevant role or could be a concurrent cause in the pathogenic mechanism of the disease. Interestingly, the presence of giant mitochondria in muscle, although with slight morphological differences, resembles the picture present in another human disorder caused by mutations in the *CHKB* gene and mainly characterized by muscular dystrophy and mental retardation (Quinlivan *et al.*, 2013). *CHKB* encodes an enzyme catalysing the first step in *de novo* phosphatidylcholine synthesis (Mitsuhashi *et al.*, 2013). CHKB and PANK2 are clearly part of different metabolic pathways but they converge on phospholipid biosynthesis. It is tempting to speculate that dysfunction of lipid metabolism is indeed the common culprit of the generation of mitochondrial muscle alteration observed in both disorders (Lamari *et al.*, 2013).

We believe that the modulation of the diet composition in *Pank2* knockout mice has generated a useful model system in which to test not only pantethine, but also additional compounds, which could be beneficial for patients.

Acknowledgements

We would like to thank Stefano D'Arrigo for the clinical data of the patient with PKAN. A special thank to Emilio Ciusani, Stefania Saccucci and Anil Rana for technical support.

Funding

The financial support of Telethon GGP11088 to V.T. is gratefully acknowledged. This work was supported by TIRCON project of the European Commission's Seventh Framework Programme (FP7/2007-2013, HEALTH-F2-2011, grant agreement No. 277984).

Supplementary material

Supplementary material is available at *Brain* online.

References

Borrell-Pages M, Canals JM, Cordelieres FP, Parker JA, Pineda JR, Grange G, et al. Cystamine and cysteamine increase brain levels of BDNF in Huntington disease via HSJ1b and transglutaminase. J Clin Invest 2006; 116: 1410–24.

Bouckenooghe T, Remacle C, Reusens B. Is taurine a functional nutrient? Curr Opin Clin Nutr Metab Care 2006; 9: 728–33.

Bousquet M, Gibrat C, Ouellet M, Rouillard C, Calon F, Cicchetti F. Cystamine metabolism and brain transport properties: clinical

implications for neurodegenerative diseases. J Neurochem 2010; 114: 1651–8.
Brunetti D, Dusi S, Morbin M, Uggetti A, Moda F, D'Amato I, et al. Pantothenate kinase-associated neurodegeneration: altered mitochondria membrane potential and defective respiration in Pank2 knock-out mouse model. Hum Mol Genet 2012; 21: 5294–305.
Corden BJ, Schulman JD, Schneider JA, Thoene JG. Adverse reactions to oral cysteamine use in nephropathic cystinosis. Dev Pharmacol Ther 1981; 3: 25–30.
Cornille E, Abou-Hamdan M, Khrestchatisky M, Nieoullon A, de Reggi M, Gharib B. Enhancement of L-3-hydroxybutyryl-CoA dehydrogenase activity and circulating ketone body levels by pantethine. Relevance to dopaminergic injury. BMC Neurosci 2010; 11: 51.
Dedeoglu A, Kubilus JK, Jeitner TM, Matson SA, Bogdanov M, Kowall NW, et al. Therapeutic effects of cystamine in a murine model of Huntington's disease. J Neurosci 2002; 22: 8942–50.
Dohil R, Fidler M, Gangoiti JA, Kaskel F, Schneider JA, Barshop BA. Twice-daily cysteamine bitartrate therapy for children with cystinosis. J Pediatr 2010; 156: 71–5e1–3.
Dubowitz V, Brooke MH. Muscle biopsy: a modern approach. London; Philadelphia, USA: Sanders; 1973.
Garcia M, Leonardi R, Zhang YM, Rehg JE, Jackowski S. Germline deletion of pantothenate kinases 1 and 2 reveals the key roles for CoA in postnatal metabolism. PLoS One 2012; 7: e40871.
Gibrat C, Cicchetti F. Potential of cystamine and cysteamine in the treatment of neurodegenerative diseases. Prog Neuropsychopharmacol Biol Psychiatry 2011; 35: 380–9.
Gregory A, Hayflick SJ. Neurodegeneration with brain iron accumulation. Folia Neuropathol 2005; 43: 286–96.
Gregory A, Polster BJ, Hayflick SJ. Clinical and genetic delineation of neurodegeneration with brain iron accumulation. J Med Genet 2009; 46: 73–80.
Gregory A, Westaway SK, Holm IE, Kotzbauer PT, Hogarth P, Sonek S, et al. Neurodegeneration associated with genetic defects in phospholipase A(2). Neurology 2008; 71: 1402–9.
Hayflick SJ. Pantothenate kinase-associated neurodegeneration (formerly Hallervorden-Spatz syndrome). J Neurol Sci 2003; 207: 106–7.
Hayflick SJ, Westaway SK, Levinson B, Zhou B, Johnson MA, Ching KH, et al. Genetic, clinical, and radiographic delineation of Hallervorden-Spatz syndrome. N Engl J Med 2003; 348: 33–40.
Karpuj MV, Becher MW, Springer JE, Chabas D, Youssef S, Pedotti R, et al. Prolonged survival and decreased abnormal movements in transgenic model of Huntington disease, with administration of the transglutaminase inhibitor cystamine. Nat Med 2002; 8: 143–9.
Kaskow BJ, Proffitt JM, Blangero J, Moses EK, Abraham LJ. Diverse biological activities of the vascular non-inflammatory molecules—the Vanin pantetheinases. Biochem Biophys Res Commun 2012; 417: 653–8.
Knott RP, Tsao DP, McCutcheon RS, Cheldelin VH, King TE. Toxicity of pantetheine. Proc Soc Exp Biol Med 1957; 95: 340–1.
Kruer MC, Boddaert N, Schneider SA, Houlden H, Bhatia KP, Gregory A, et al. Neuroimaging features of neurodegeneration with brain iron accumulation. Am J Neuroradiol 2012; 33: 407–14.
Kruer MC, Hiken M, Gregory A, Malandrini A, Clark D, Hogarth P, et al. Novel histopathologic findings in molecularly-confirmed pantothenate kinase-associated neurodegeneration. Brain 2011; 134 (Pt 4): 947–58.
Kuo YM, Duncan JL, Westaway SK, Yang H, Nune G, Xu EY, et al. Deficiency of pantothenate kinase 2 (Pank2) in mice leads to retinal degeneration and azoospermia. Hum Mol Genet 2005; 14: 49–57.
Kuo YM, Hayflick SJ, Gitschier J. Deprivation of pantothenic acid elicits a movement disorder and azoospermia in a mouse model of pantothenate kinase-associated neurodegeneration. J Inherit Metab Dis 2007; 30: 310–7.
Laffel L. Ketone bodies: a review of physiology, pathophysiology and application of monitoring to diabetes. Diabetes Metab Res Rev 1999; 15: 412–26.
Lamari F, Mochel F, Sedel F, Saudubray JM. Disorders of phospholipids, sphingolipids and fatty acids biosynthesis: toward a new category of inherited metabolic diseases. J Inherit Metab Dis 2013; 36: 411–25.
Leonardi R, Rehg JE, Rock CO, Jackowski S. Pantothenate kinase 1 is required to support the metabolic transition from the fed to the fasted state. PLoS One 2010; 5: e11107.
Leonardi R, Rock CO, Jackowski S, Zhang YM. Activation of human mitochondrial pantothenate kinase 2 by palmitoylcarnitine. Proc Natl Acad Sci USA 2007; 104: 1494–9.
Leoni V, Strittmatter L, Zorzi G, Zibordi F, Dusi S, Garavaglia B, et al. Metabolic consequences of mitochondrial coenzyme A deficiency in patients with PANK2 mutations. Mol Genet Metab 2012; 105: 463–71.
Malandrini A, Bonuccelli U, Parrotta E, Ceravolo R, Berti G, Guazzi GC. Myopathic involvement in two cases of Hallervorden-Spatz disease. Brain Dev 1995; 17: 286–90.
Mitsuhashi S, Nishino I. Megaconial congenital muscular dystrophy due to loss-of-function mutations in choline kinase β. Curr Opin Neurol 2013; 26: 536–43.
Muramatsu M, Kakita K, Nakagawa K, Kuriyama K. A modulating role of taurine on release of acetylcholine and norepinephrine from neuronal tissues. Jpn J Pharmacol 1978; 28: 259–68.
Napoli L, Crugnola V, Lamperti C, Silani V, Di Mauro S, Bresolin N, et al. Ultrastructural mitochondrial abnormalities in patients with sporadic amyotrophic lateral sclerosis. Arch Neurol 2011; 68: 1612–3.
Pasantes-Morales H, Chaparro H, Otero E. Clinical study on the effect of taurine on intractable epileptics (author's transl). Rev Invest Clin 1981; 33: 373–8.
Quinlivan R, Mitsuahashi S, Sewry C, Cirak S, Aoyama C, Mooore D, et al. Muscular dystrophy with large mitochondria associated with mutations in the CHKB gene in three British patients: extending the clinical and pathological phenotype. Neuromuscul Disord 2013; 23: 549–56.
Rana A, Seinen E, Siudeja K, Muntendam R, Srinivasan B, van der Want JJ, et al. Pantethine rescues a Drosophila model for pantothenate kinase-associated neurodegeneration. Proc Natl Acad Sci USA 2010; 107: 6988–93.
Schwartz E, Bagdon RE. Toxicity studies of some derivatives of pantothenic acid. Toxicol Appl Pharmacol 1964; 6: 280–3.
Sciacco M, Bonilla E. Cytochemistry and immunocytochemistry of mitochondria in tissue sections. Methods Enzymol 1996; 264: 509–21.
Stack EC, Ferro JL, Kim J, Del Signore SJ, Goodrich S, Matson S, et al. Therapeutic attenuation of mitochondrial dysfunction and oxidative stress in neurotoxin models of Parkinson's disease. Biochim Biophys Acta 2008; 1782: 151–62.
Sun L, Xu S, Zhou M, Wang C, Wu Y, Chan P. Effects of cysteamine on MPTP-induced dopaminergic neurodegeneration in mice. Brain Res 2010; 1335: 74–82.
Wittwer CT, Gahl WA, Butler JD, Zatz M, Thoene JG. Metabolism of pantethine in cystinosis. J Clin Invest 1985; 76: 1665–72.

Please cite this article in press as: Dusi et al., Exome Sequence Reveals Mutations in CoA Synthase as a Cause of Neurodegeneration with Brain Iron Accumulation, The American Journal of Human Genetics (2014), http://dx.doi.org/10.1016/j.ajhg.2013.11.008

ARTICLE

Exome Sequence Reveals Mutations in CoA Synthase as a Cause of Neurodegeneration with Brain Iron Accumulation

Sabrina Dusi,[1] Lorella Valletta,[1] Tobias B. Haack,[2,3] Yugo Tsuchiya,[4] Paola Venco,[1] Sebastiano Pasqualato,[5] Paola Goffrini,[6] Marco Tigano,[6] Nikita Demchenko,[4] Thomas Wieland,[3] Thomas Schwarzmayr,[3] Tim M. Strom,[2,3] Federica Invernizzi,[1] Barbara Garavaglia,[1] Allison Gregory,[7] Lynn Sanford,[7] Jeffrey Hamada,[7] Conceição Bettencourt,[8] Henry Houlden,[8] Luisa Chiapparini,[9] Giovanna Zorzi,[10] Manju A. Kurian,[11,12] Nardo Nardocci,[10] Holger Prokisch,[2,3] Susan Hayflick,[7] Ivan Gout,[4] and Valeria Tiranti[1,*]

Neurodegeneration with brain iron accumulation (NBIA) comprises a clinically and genetically heterogeneous group of disorders with progressive extrapyramidal signs and neurological deterioration, characterized by iron accumulation in the basal ganglia. Exome sequencing revealed the presence of recessive missense mutations in *COASY,* encoding coenzyme A (CoA) synthase in one NBIA-affected subject. A second unrelated individual carrying mutations in *COASY* was identified by Sanger sequence analysis. CoA synthase is a bifunctional enzyme catalyzing the final steps of CoA biosynthesis by coupling phosphopantetheine with ATP to form dephospho-CoA and its subsequent phosphorylation to generate CoA. We demonstrate alterations in RNA and protein expression levels of CoA synthase, as well as CoA amount, in fibroblasts derived from the two clinical cases and in yeast. This is the second inborn error of coenzyme A biosynthesis to be implicated in NBIA.

Introduction

The common pathological feature of a group of genetic disorders termed "neurodegeneration with brain iron accumulation" (NBIA) is brain iron overload.[1] Distinct subclasses of early-onset neurodegeneration with autosomal-recessive transmission are defined by mutations in specific genes: *PANK2* (MIM 606157) causes pantothenate kinase-associated neurodegeneration (PKAN);[2,3] *PLA2G6* (MIM 256600) causes phospholipase A_2-associated neurodegeneration (PLAN, also known as INAD);[4] *FA2H* (MIM 611026) causes fatty acid hydroxylase-associated neurodegeneration (FAHN);[5] and *C19orf12* (MIM 614297) causes mitochondrial membrane protein-associated neurodegeneration (MPAN).[6,7] More recently, a distinctive form of NBIA with X-linked dominant de novo mutations in *WDR45* (MIM 300894), coding for a protein with a putative role in autophagy, was reported.[8,9]

These genes account for ~70% of subjects with NBIA, leaving a significant fraction without an identified genetic defect. For this reason we performed exome sequence investigation in one individual with clinical presentation and neuroimaging suggestive of NBIA but without mutations in previously associated genes. By applying this approach we identified a homozygous missense mutation in *COASY*, coding for CoA synthase. We then performed traditional Sanger sequence analysis of a larger cohort of idiopathic NBIA cases, and we found a second individual harboring mutations in the same gene. CoA synthase is a bifunctional enzyme possessing 4′PP adenyltransferase (PPAT) and dephospho-CoA kinase (DPCK) activities, catalyzing the last two steps in the CoA biosynthetic pathway.[10] The enzyme is encoded by a single gene in mammals and *Drosophila*,[11,12] although two different genes code for PPAT and DPCK activities in yeast and bacteria.[13] In human there are three splice variants: COASY alpha is ubiquitously expressed and has a molecular weight of 60 kDa; COASY beta is predominantly expressed in the brain and possesses a 29 aa extension at the N terminus;[14] and COASY gamma is predicted to code for C-terminal region of CoA synthase corresponding to DPCK domain. Several studies have investigated the subcellular compartmentalization of the CoA biosynthetic pathway and have demonstrated that both PANK2, defective in the most common NBIA disorder, and CoA synthase alpha and beta are mitochondrial enzymes. PANK2 is mainly located in the intermembrane space[2,15,16] whereas CoA synthase alpha and beta are anchored to the outer

[1]Unit of Molecular Neurogenetics – Pierfranco and Luisa Mariani Center for the study of Mitochondrial Disorders in Children, IRCCS Foundation Neurological Institute "C. Besta," 20126 Milan, Italy; [2]Institute of Human Genetics, Technische Universität München, 81675 Munich, Germany; [3]Institute of Human Genetics, Helmholtz Zentrum München, 85764 Munich, Germany; [4]Institute of Structural and Molecular Biology, University College London, London WC1E 6BT, UK; [5]Crystallography Unit, Department of Experimental Oncology, European Institute of Oncology, IFOM-IEO Campus, 20139 Milan, Italy; [6]Department of Life Sciences, University of Parma, 43124 Parma, Italy; [7]Department of Molecular & Medical Genetics, Oregon Health & Science University, Portland, OR 97329, USA; [8]UCL Institute of Neurology and The National Hospital for Neurology and Neurosurgery, Queen Square, London WC1N 3BG, UK; [9]Unit of Neuroradiology, IRCCS Foundation Neurological Institute "C. Besta," 20133 Milan, Italy; [10]Unit of Child Neurology, IRCCS Foundation Neurological Institute "C. Besta," 20133 Milan, Italy; [11]Neurosciences Unit, UCL-Institute of Child Health, Great Ormond Street Hospital, London WC1N 3JH, UK; [12]Department of Neurology, Great Ormond Street Hospital, London WC1N 3JH, UK
*Correspondence: tiranti@istituto-besta.it
http://dx.doi.org/10.1016/j.ajhg.2013.11.008.

Please cite this article in press as: Dusi et al., Exome Sequence Reveals Mutations in CoA Synthase as a Cause of Neurodegeneration with Brain Iron Accumulation, The American Journal of Human Genetics (2014), http://dx.doi.org/10.1016/j.ajhg.2013.11.008

mitochondrial membrane by the N-terminal region[17] or localized within the mitochondrial matrix.[18] We here demonstrate that COASY is mainly located in the mitochondrial matrix and that the identified amino acid substitution causes instability of the protein with altered function of its enzymatic activity.

Subjects and Methods

Exome and Sanger Sequencing

Informed consent for participation in this study was obtained from all individuals involved and from their parents, in agreement with the Declaration of Helsinki, approved by the ethics committee of the Fondazione IRCCS (Istituto di Ricovero e Cura a Carattere Scientifico) Istituto Neurologico C. Besta (Milan, Italy) and by the ethics committees of the other institutes participating in the screening (Germany, UK, USA).

Exome sequencing and variant filtering was performed as described previously.[8] In brief, exonic DNA fragments were enriched with the SureSelect 50 Mb kit from Agilent and sequenced as 100 bp paired-end reads on a HiSeq 2500 system from Illumina. For sequencing statistics details see Table S1 available online. We predicted that causal mutations would be very rare and would alter the protein. We therefore searched for nonsynonymous variants with a frequency <0.1% in 2,700 control exomes analyzed in Munich and public databases that, given the reported consanguinity of the parents, were anticipated to be homozygous. This analysis left a total of 12 candidate genes (Table S2). The detailed list of these 12 genes is reported in Table S3. We first excluded the following genes because of the presence of additional subjects with compound heterozygous or homozygous mutations related with different clinical phenotypes: *HRNR*, *ADAM8*, *BZRAP1*, *C17orf47*, *LRP1B*, *EVC2*, *KIAA1797*, and *CACNB1*. Moreover, variants in *HRNR*, *CACNB1*, *C17orf47*, and *KIAA1797* were predicted to be benign by PolyPhen. Four remaining genes (*GUCA2A*, *FBXO47*, *COASY*, and *IFNW1*) were potentially good candidates carrying deleterious mutations.

By performing segregation analysis of the c.265G>T homozygous variant in *GUCA2A*, we found that also the healthy mother (subject I-2 of family 1) and one of the healthy sisters (subject II-4 of family 1) carried this variant.

Segregation analysis of c.490A>G in *IFNW1* showed that this change was present in homozygous state in the healthy mother (subject I-2 of family 1) and in two healthy sisters (subjects II-4 and II-5 in family 1). Altogether, this observation excluded both *GUCA2A* and *IFNW1* as potential candidate genes (see also Table S3).

FBXO47 was mainly expressed in kidney, liver, and pancreas and it was suggested to act as a tumor-suppressor gene in renal carcinoma and possibly other malignancies.[19] However, because this gene carries a splice site mutation, we decided to perform sequence analysis in a subgroup of 56 NBIA-affected individuals. We did not identify any pathogenic mutation in this cohort of subjects.

Based on these data and because *COASY* coded for an enzyme involved in Coenzyme A biosynthesis as *PANK2*, we concentrated our efforts on the analysis of this gene.

RNA Extraction and Real-Time PCR

Total RNA was isolated from fibroblasts (80% confluence) with the RNeasy Mini Kit (QIAGEN). RNA quantity was measured with the Nanodrop instrument (Nanodrop Technologies). RNA was used as a template to generate complementary DNA (cDNA) by GoScript Reverse Transcriptase protocol (Promega). Reverse transcriptase products were used in real-time PCR to evaluate the expression level of *COASY* with the Power SYBR Green PCR Master Mix (Applied Biosystems) system. The housekeeping gene used for data normalization was *GAPDH*. Primer sequences are as follows: *COASY*, forward 5′-AGTTGCGGTTTCTCCGTTAG-3′ and reverse 5′-ATCCTGGGAGGGGGAAAT-3′; *GAPDH*, forward 5′-CTCTG CTCCTCCTGTTCGAC-3′ and reverse 5′-ACGACCAAATCCGTT GA-3′.

Expression and Purification of Recombinant hDPCK in Bacteria

mRNA coding for human DPCK domain (COASY amino acid sequence from 355 to 564) was expressed with the N-terminal histidine-tag from pET30-a(+) (Novagen) at 37°C in *E. coli* strain BL21 (DE3), after induction with 0.2 mM IPTG.

Cells were lysed by a French press in 50 mM Tris-HCl (pH 8), 0.5 M NaCl, 1% Triton X-100, 20 mM imidazole, 1 mM phenylmethylsulfonyl fluoride (PMSF), 10 mM β-mercaptoethanol, and Roche Complete EDTA-free protease inhibitor cocktail. After clearing, the lysate was loaded on a Ni-NTA beads (QIAGEN) column. Bound proteins were eluted with an imidazole gradient. Fractions containing His-hDPCK were pooled, desalted, and loaded onto an anion-exchange (AE) Resource-S column (GE Healthcare) equilibrated in 50 mM Tris-HCl (pH 7.4), 2.5% glycerol, 20 mM β-mercaptoethanol. The protein was eluted with a NaCl gradient, concentrated by ultrafiltration, and further separated by size exclusion chromatography (SEC) on a Superdex-200 column (GE Healthcare) equilibrated in 10 mM Tris-HCl (pH 7.4), 0.15 M NaCl, 2.5% glycerol, 0.1 mM EDTA, and 1 mM DTT. The entire purification scheme was carried out at 4°C.

Mitochondria and Mitoplast Isolation from Cultured Cells

Isolated mitochondria from cultured cells were obtained according to the protocol described by Fernández-Vizarra.[20]

For mitoplast purification, mitochondria were dissolved in 1 ml Buffer A (MOPS 20 mM, sucrose 0.25 M [pH 7.4]). A total of 1 ml of 200 μg/ml digitonin in Buffer A was added to each sample. Samples were mixed and incubated on ice 5 min, then centrifuged 3 min at 8,000 rpm at 4°C. Supernatant was discarded and pellet dissolved in 1 ml Buffer B (MOPS 20 mM, sucrose 0.25 M, EDTA Na_4 1 mM [pH 7.4]). Samples were incubated on ice for 5 min, then centrifuged at 12,000 rpm at 4°C for 3 min. Separate fractions of mitochondria and mitoplasts were also treated with 0.04 μg of proteinase K (PK) for 15 min at 4°C or 37°C; PK digestion was blocked with PMSF. In some samples of mitochondria and mitoplasts, 0.1% Triton X-100 was added followed by incubation for 15 min at 37°C.

Immunoblot Analysis

Approximately 1×10^6 fibroblasts, grown in DMEM (EuroClone) were trypsinized, centrifuged at 1,200 rpm for 3 min, and solubilized in 200 μl of RIPA buffer (50 mM Tris-HCl [pH 7.5], 150 mM NaCl, 1% NP40, 0.5% NaDOC, 5 mM EDTA) with 1× Complete Mini Protease Inhibitor Cocktail Tablets (Roche) for 40 min at 4°C. 30 μg of proteins were used for each sample in denaturing sodium-dodecyl sulfate polyacrylamide gel electrophoresis (SDS-PAGE). Immunoblot analysis was performed as described[21] with the ECL-chemiluminescence kit (Amersham).

Antibodies

A rabbit monoclonal anti-COASY antibody was used at 1:1,000 dilution (EPR8246-Abcam). A mouse monoclonal anti-β-TUBULIN antibody was used at a final concentration of 1 μg/ml (Sigma-Aldrich). Secondary anti-rabbit and anti-mouse antibodies were used at 1:2,000 and 1:7,000 dilution, respectively.

HPLC Analysis of Dephospho-CoA, CoA, and AcetylCoA

HPLC analysis was performed on recombinant wild-type and mutant DPCK proteins, on fibroblast lysates derived from control and subjects carrying *COASY* variants, and on isolated yeast mitochondria.

The method employed a column (Kinetex 5u C18 100A New Column 250 × 4.6 mm from Phenomenex) eluted with 100 mmol/l NaH_2PO_4 and 75 mmol/l CH_3COONa (pH was adjusted to 4.6 by the addition of concentrated H_3PO_4)-acetonitrile (94:6, v/v) at a flow rate of 1.0 ml/min. The ultraviolet (UV) detector was set at 259 nm. To obtain standard solutions of 5 μM, dephospho-CoA and CoA were dissolved in 50 mmol/l KH_2PO_4-K_2HPO_4 buffer (pH 7.0). CoA and dephospho-CoA standards were eluted at approximately 4.5 and 8 min, respectively, and CoA compounds were quantified by comparison of peak areas with those of authentic standards.

In Vitro DPCK Activity

1 μg of purified wild-type or mutant protein was incubated for 2 hr at 37°C in 50 μl of reaction mixture containing 50 mM Tris-HCl (pH 8), 5 mM $MgCl_2$, 1 mM ATP, and 0.1 mM dephospho-CoA. After incubation, sample was treated with perchloric acid (PCA) 3%, vortexed, and centrifuged at 13,000 rpm at 4°C. Trietanolamine was added to the supernatant to a final concentration of 100 mM, and then the sample was neutralized with 5 M K_2CO_3.

Fibroblast Analysis

Fibroblasts, grown on 10 cm plates (approx. 80%–90% confluent), were washed with PBS and collected by trypsinization. 40 μl of ice-cold PCA (5%) was added to cells and samples were vortexed and centrifuged at 18,000 × g for 5 min at 4°C. The supernatant was collected and triethanolamine was added to a final concentration of 100 mM. The pH was adjusted to 6.5 with 5 M K_2CO_3 before centrifuging again at 18,000 × g for 3 min at 4°C to remove potassium perchlorate. Neutralized PCA extract was made up to 100 μl with $Na_2H_2PO_4$ (150 mM), Tris-(2-carboxyethyl) phosphine hydrochloride (TCEP) (10 mM), EDTA (5 mM), and methanol (9%) and filtered through a 0.2 μm PVDF filter, and 50 μl was injected for HPLC analysis of CoA compounds.

In Vitro PPAT/DPCK Assay of Cell Homogenates

Fibroblasts grown on 10 cm plates (approx. 80%–90% confluent) were washed with PBS and collected by trypsinization. Cells were homogenized in 150 μl buffer containing 50 mM Tris/HCl (pH 7.5), 150 mM NaCl, 10 mM 2-glycerophosphate, 1 mM EDTA, 0.5 mM TCEP, and protease inhibitor cocktail (Roche). Total protein concentration in the homogenate was measured by Bradford assay. 65 μg of homogenate protein was incubated with 2 mM ATP, 5 mM $MgCl_2$, and 5 mM 4-phosphopantetheine in a total volume of 50 μl at 30°C for 1 hr. 4-phosphopantetheine was prepared by phosphorylating pantetheine with bacterially expressed pantothenate kinase 1b. For control incubation, ATP and $MgCl_2$ were added to homogenate, but 4-phosphopantetheine was omitted. After the incubation, PCA (3.5% final) was added to the reaction mixtures before centrifugation at 18,000 × g for 5 min at 4°C. The pH of the PCA-soluble fraction was adjusted to 6.5 with TEA/K_2CO_3 and CoA compounds formed were analyzed by HPLC as described above.

Yeast Mitochondria Analysis

Mitochondrial suspensions were diluted to obtain about 0.5 μg/μl in a final volume of 150 μl of 5% 5-sulfosalicylic acid containing 50 μmole/l DTT and vortexed. The homogenates were centrifuged at 12,000 × g for 10 min at 4°C. The supernatant was passed through a 0.45 μm filter (Millipore) and the filtrate (40 μl) was injected directly into the HPLC system. We loaded equal amount of yeast mitochondrial proteins (40 μg) and we performed CoA quantification by evaluating peak's areas as compared to known concentration of internal standard.

Yeast Strains and Media

Yeast strains used in this study were W303-1B (MATα*ade2-1 leu2-3,112 ura3-1 his3*-11,15 *trp1-1 can1-100*) *ade2-1 leu2-3,112 ura3-1 trp1-1 his3-11,15,* its isogenic strain *cab5*::*KanMx4* that harbors plasmid pFl38-*CAB5* or pFl39-*CAB5*, and the strain *cab5*::*KanMx4* that harbors plasmid pYEX-BX-*COASY* (see below). Cells were cultured in minimal medium 40 supplemented with appropriate amino acids and bases for auxotrophy as previously described.[22] To obtain medium lacking pantothenate (40-Pan), a mixture of vitamins without pantothenate was prepared. Various carbon sources (Carlo Erba Reagents) were added at the indicated concentration. YP medium contained 1% Bacto-yeast extract and 2% Bacto-peptone (ForMedium). Media were solidified with 20 g/l agar (ForMedium) and strains were incubated at 23°C, 30°C, or 37°C.

Cloning Procedures and Plasmid Vectors

pFL38-*CAB5* was obtained by PCR amplification of *CAB5*, including the upstream and the downstream regions, from genomic DNA of strain W303-1B with primers as follows.

For *CAB5* (forward 5′-GGGGGGATCCCCATTGCTTAGAA TGGGCGG-3′ and reverse 5′-CCGCGGTACCGAGAACCCATA GAATTCGAC-3′), the oligos were modified at 5′ end in order to insert restriction sites for cloning in the centromeric plasmid pFL38 carrying the *URA3* marker.[23] pFL39-*CAB5* was obtained by subcloning *CAB5* into pFL39 vector carrying the *TRP1* marker.[23] Human *COASY* and human *COASY*^{Arg499Cys} were amplified by PCR from pcDNA3.1 constructs, containing wild-type and mutant cDNA, respectively, with primers described below.

For *COASY* (forward 5′-GGGGGGATCCATGGCCGTATT CCGGTCG-3′ and reverse 5′-CCGCGTCGACTCAGTCGAGGG CCTGATGAGTC-3′), the oligonucleotides contained appropriate restriction sites to allow cloning in the BamHI-SalI-digested pYEX plasmid under the control of *CUP1* promoter. All cloned fragments were sequenced to check the absence of mutations. Restriction-enzyme digestions, *Escherichia coli* transformation, and plasmid extractions were performed with standard methods.[24]

Site-Directed Mutagenesis and Generation of Yeast *cab5* Strains

The conserved human arginine 499 residue (RefSeq accession number NM_025233.6), which is replaced by a cysteine in human COASY, corresponds to arginine 146 (RefSeq NM_001180504.3) in the yeast protein. The *CAB5* mutant allele was obtained by site-directed mutagenesis (QuikChange II Site-Directed Mutagenesis Kit Stratagene) by introducing an AGA>TGT codon substitution, resulting in p.Arg146Cys amino acid change. The corresponding modified primers used to generate mutated allele are as follows.

For *COASY*^{Arg146Cys} (forward 5′-CGCAAGAATTGCAACTAGAA *TGT*TTAATGACAAGAAATCCTG-3′ and reverse 5′-CAGGATTTC TTGTCATTAA*ACA*TTCTAGTTGCAATTCTTGCG-3′), mutagenized insert was verified by sequencing of both strands.

The pFL38 plasmid-borne *CAB5* was transformed in the W303-1B by the lithium-acetate method[25] to allow cell viability and the resident *CAB5* was deleted with the *Kan*MX4 cassette amplified from plasmid pCXJKan by primers described below.

For *CAB5-Kan* (forward 5′-CAGATAGCCACAATTAAAATAT GCTGGTAGTGGGATTGACAGGTCGTACGCTGCAGGTCGAC-3′ and reverse 5′-GTAATTATAAGATATCAACCTTATACCCGCTGAA GACTTTTTATTTTGAAGATCGATGAATTGAGCTCG-3′), both of them contained a 5′ complementary stretch for an internal sequence of *CAB5* ORF and a 3′ complementary stretch (underlined in the sequences) for the extremities of the *KanMX4* cassette. Strains with engineered *CAB5* were selected on YP supplemented with 200 μg/ml geneticin and gene rearrangement was confirmed by PCR. Transformation of *cab5*::Kan^{R}/pFLl38*CAB5* strain with pfl39-*CAB5* and pFL39-*CAB5*^{Arg146Cys} constructs and plasmid shuffling on media supplemented with 5-FOA in order to select spontaneous events of Ura^{+} constructs loss were finally performed. Similarly, *cab5*::Kan^{R}/pFL39*CAB5* strain was transformed with *pYEX-BX-COASY* and *pYEX-BX-COASY*^{Arg499Cys} constructs; loss of Trp^{+} plasmids was induced by growing the transformants with tryptophan in the medium.

Yeast Mitochondria Isolation

Mitochondria were purified as previously reported.[26] In brief, cells cultured at 28°C in the 40 medium supplemented with 0.6% glucose were collected and washed. Spheroplasts were obtained after Zymoliase20T digestion (Nacalai Tesque) and disrupted with a glass-teflon potter homogenizer. Mitochondria were purified by differential centrifugation. Total protein concentrations were quantified according to Bradford (Bio-rad).

Results

Molecular and Biochemical Investigations

Exome-NGS analysis of one individual (subject II-3, family 1, Figure 1) affected by idiopathic NBIA resulted in the identification of 12 genes (Table S3) that carried variants potentially relevant for the disease. However, as described in detail in the Subjects and Methods section, several of these genes were not investigated further because (1) the identified variants were present in additional individuals and associated with other clinical phenotypes; (2) genetic segregation analysis was not compatible with clinical presentation of the subjects of family 1; or (3) gene function and tissue-specific expression could hardly explain the neurological presentation. The homozygous mutation in *COASY*, coding for a bifunctional enzyme converting 4′-phosphopantetheine into dephospho-CoA and then to Coenzyme A, was considered as potentially relevant for the disease and further investigated. By Sanger sequencing we confirmed the presence of the homozygous missense *COASY* mutation in the affected individual (Figure 1: subject II-3, family 1). The family had no history of neurological disorders and this subject was the youngest and the only affected of five siblings. She was born to consanguineous parents after an uneventful pregnancy and normal delivery. Birth weight was 3,850 g. There was no history of perinatal complications and she attained normal early developmental milestones. From 24 months of age, parents reported gait difficulties and persistent toe walking. At age 6, when she started primary school, she showed poor academic ability. At age 15, general physical examination was normal. Neurological evaluation showed mild oro-mandibular dystonia with dysarthria and also spastic dystonic paraparesis, but she was still able to walk unaided. Neuropsychological evaluation demonstrated cognitive impairment (total IQ = 49). The disease continued to progress slowly and at the age of 20 she became unable to ambulate independently. During the most recent examination at age 25, the clinical picture was dominated by a severe spastic bradykinetic-rigid syndrome associated with mild dystonia and with distal areflexia in the lower limbs. There were no clinical or psychometric data suggesting mental deterioration but behavioral disturbances with obsessive-compulsive symptoms and depression was evident. Funduscopic examination and visual evoked potential studies were normal and on electroretinogram there were no signs of retinopathy. Electromyographic and nerve conduction studies were consistent with a mild motor axonal neuropathy. Serial brain MRI showed bilateral hypointensity in the globi pallidi associated with a central region of hyperintensity in the antero-medial portion (Figure 1).

Identification of one Italian subject carrying *COASY* mutation prompted us to analyze the nine exons of this gene in a cohort of 280 NBIA-affected individuals of different ethnicity by using polymerase chain reaction and direct Sanger sequencing. Primer sequences and PCR conditions are described in Table S4. By this analysis we identified a second Italian case carrying *COASY* mutations (Figure 1: subject II-2, family 2). He is 20 years old and he was born at term of uneventful pregnancy from healthy nonconsanguineous parents. Psychomotor development was normal in the first year of life, but he was delayed in walking as a result of instability and toe walking. At age 3 the neurological picture was characterized by spastic tetraparesis with moderate mental and language impairment. The disease was progressive, with worsening of the motor signs in the lower limbs and progressive involvement of the upper limbs and oro-mandibular region. He lost independent ambulation at age 15. At age 17, the neurological examination showed mild oro-mandibular dystonia with dysarthria, spastic-dystonic tetraparesis with prevalent involvement of lower limbs, and parkinsonian features (rigidity and abnormal postural reflexes). Distal amyotrophia and areflexia with pes cavus were also evident. Cognitive impairment was severe (total IQ < 40) with obsessive-compulsive behavior and complex motor tics. On follow-up, 2 years later, the neurological picture was unchanged. Nerve conduction study and electromyography detected a motor axonal neuropathy more prominent in the lower limbs. There was no retinal or optic nerve

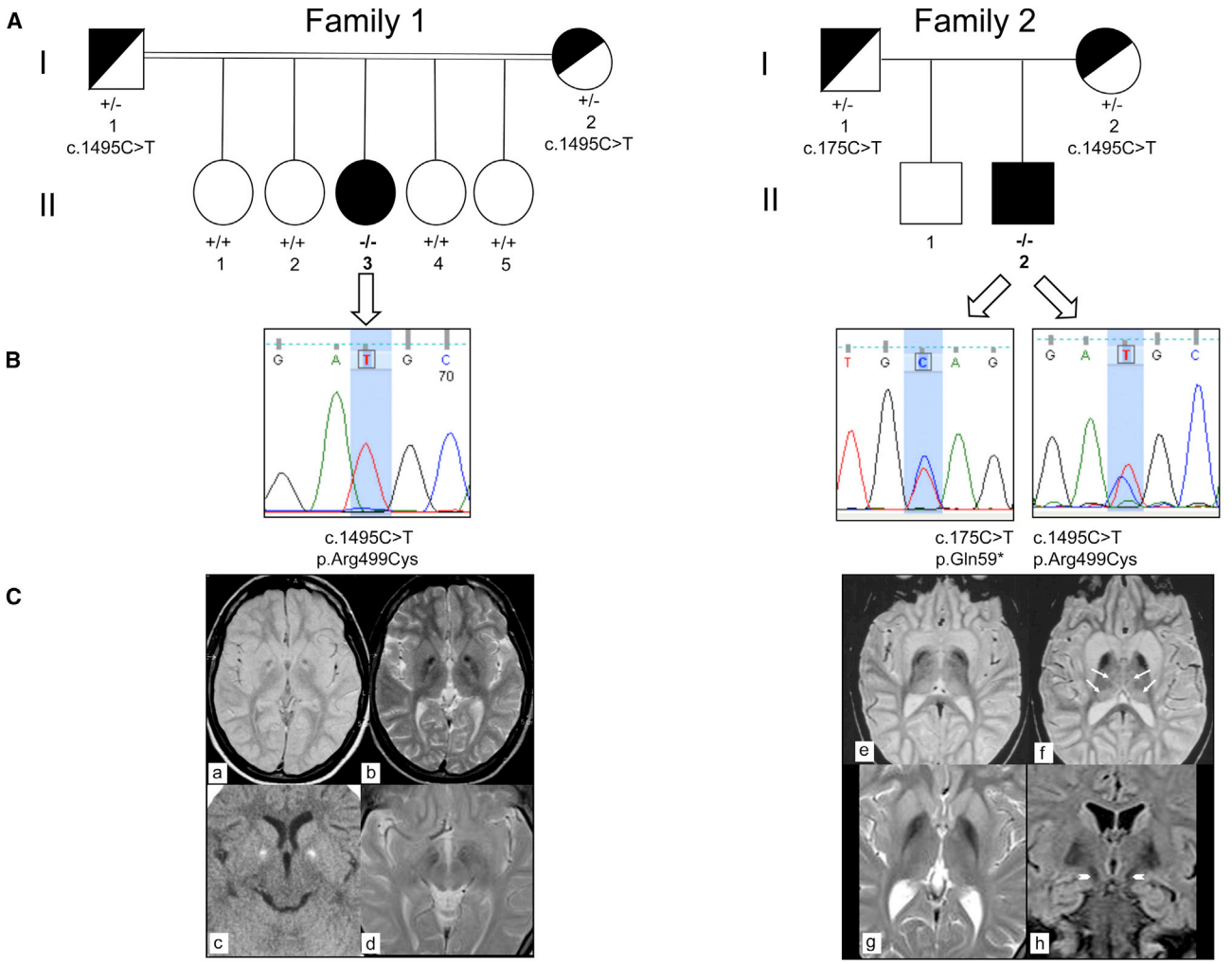

Figure 1. Genetics and MRI of Subjects Carrying *COASY* Mutations
(A) Pedigrees of family 1 (left) and family 2 (right). II-3, affected individual in family 1; II-2, affected individual in family 2. The presence of homozygous or compound heterozygous mutation is indicated by −/−; wild-type sequence by +/+; heterozygous mutation by +/−.
(B) Electropherograms show sequence variations in individual II-3 of family 1 (left) and in individual II-2 of family 2 (right).
(C) Left: MRI of individual II-3 of family 1 at 11 years of age (a–c). Axial MR (1.5 T) proton density and T2-weighted images (a, b) show bilateral low signal intensity in the globi pallidi (clearly visible in b) with a central region of high signal intensity located in the antero-medial portion of the nuclei ("eye-of-the-tiger" sign) and with a large central spot of low signal intensity. Axial CT (c) shows bilateral hyperdensities consistent with calcifications and corresponding to the central spot visible on MRI. Six years later (d), no changes were found. The hypointensity in the medial portion of the substantia nigra was also unchanged. Right: MRI of individual II-2 of family 2 at 9 years of age (e, f) and at age 19 (g, h). Axial T2-weighted 1.5 T MR images (e, f) reveal hypointensity in the pallida. Both caudate nuclei and putamina are swollen and hyperintense. Slight hyperintensity is also present in both medial and posterior thalami (arrows). Axial T2-weighted MR image (g) confirms bilateral symmetric low signal intensity and atrophy in the pallida. Both putamina and caudate nuclei are still slightly hyperintense with minimal swelling. Coronal FLAIR image (h) demonstrates low signal in both pallida and in the medial portion of the substantia nigra (arrowheads).

involvement, as demonstrated by normal funduscopic and evoked potential studies.

The first brain MRI performed at age 5 demonstrated hyperintensity and swelling of both caudate nuclei and putamina and mild hyperintensity in both thalami. Globi pallidi were normal. At ages 9 and 19, hypointensity in the globi pallidi was evident and no significant changes were found in the caudate nuclei, putamina, and thalami (Figure 1).

Subject II-3 of family 1 (Figure 1) carried a homozygous missense mutation, a c.1495C>T transition causing an amino acid change p.Arg499Cys (referral sequence NM_025233.6; numbering starts from the first methionine). Segregation analysis performed in family 1 indicated heterozygous state in the parents (Figure 1), and the four healthy sisters showed wild-type sequence (Figure 1).

Subject II-2 of family 2 (Figure 1) turned out to be a compound heterozygote for the same mutation, c.1495C>T (p.Arg499Cys), identified in subject II-3, and for a c.175C>T transition, resulting in a premature p.Gln59* stop codon in the N-terminal regulatory region of the protein. Segregation analysis in the parents demonstrated

Please cite this article in press as: Dusi et al., Exome Sequence Reveals Mutations in CoA Synthase as a Cause of Neurodegeneration with Brain Iron Accumulation, The American Journal of Human Genetics (2014), http://dx.doi.org/10.1016/j.ajhg.2013.11.008

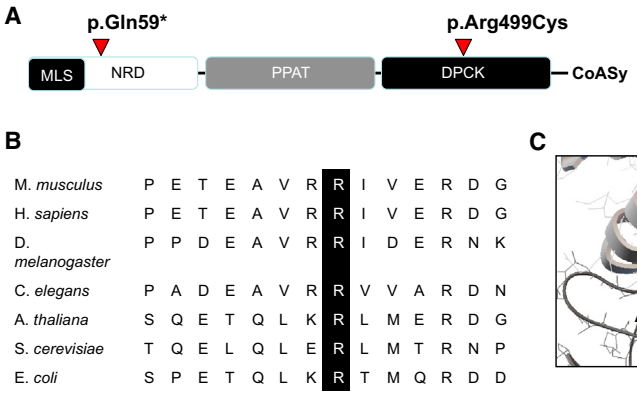

Figure 2. COASY: Conserved Domains, Phylogenetic Conservation, and Crystal Structure

(A) Schematic domain organization of human CoA synthase and location of point mutations. Abbreviations are as follows: MLS, mitochondrial localization signal; NRD, N terminus regulatory domain; PPAT, 4′PP adenylyltransferase domain; DPCK, dephospho-CoA kinase domain.

(B) Amino acid sequence alignment showing conservation of Arg499 across species.

(C) Crystal structure of *E. coli* DPCK (CoaE) (PDB ID 1VHL) showing the position of Arg140 (equivalent to Arg499 in human DPCK) in the nucleotide-binding site.

that the two mutations were on different alleles: one inherited from the mother and one from the father (Figure 1). The healthy brother was not available for genetic testing.

The missense substitution affected an amino acid residue Arg499, which is highly conserved in all available animal, plant, and yeast species, including *S. cerevisiae*, and is localized in the nucleotide-binding site of the DPCK domain (Figure 2). Furthermore, mutational analysis of Arg140, equivalent to Arg499, in the mycobacterial dephospho-CoA kinase (CoaE) revealed the importance of this residue in ATP binding and phosphotransfer reaction.[27,28]

The substitution was predicted to be pathogenic by in silico analysis according to Polyphen2 ($p = 1$) and MutPred ($p = 0.909$). Frequency of the mutation derived from the Exome Variant Server and calculated on European, American, and African population was 1 out of 13,005 analyzed cases.

To evaluate the impact of the two mutations on the stability of the transcript, we extracted mRNA from fibroblasts of subjects II-3 (family 1) and II-2 (family 2) and reverse transcribed it into cDNA. Quantitative real-time PCR showed that although in individual II-3 the amount of mutant *COASY* transcript was similar to that of the control sample (Figure 3A), it was reduced to 50% in individual II-2, suggesting RNA decay.

Next, we analyzed COASY level in total cell lysates obtained from both mutants and control fibroblasts by using a monoclonal anti-COASY antibody. We first tested the antibody specificity by verifying its cross-reactivity with the 62 kDa COASY alpha in vitro translation product (Figure 3B).

Immunoblot analysis revealed the presence of a normal protein content in three different control fibroblasts whereas a significant reduction of the protein amount was detected in fibroblasts of subject II-2 (family 2) carrying the premature stop codon and the missense p.Arg499Cys (Figure 3B). Interestingly, we also observed a minimally detectable immunoreactive band corresponding to COASY in subject II-3 (family 1) carrying the homozygous p.Arg499Cys substitution (Figure 3B). This suggests that the p.Arg499Cys change is associated with instability or accelerated degradation of the protein. Immunoblot analysis of fibroblasts derived from subject I-2 of family 1 and from both parents of family 2 (Figure 3B) showed a partial reduction of the protein level. As reported in Figure 3C, protein amount quantified by densitometry analysis with three different controls as standard resulted to be around 50% in subject I-2 of family 1 and in the parents of family 2 and less than 5% in both affected individuals.

Submitochondrial Localization of COASY

To better determine submitochondrial localization of COASY, we carried out immunoblot analysis of mitochondria and submitochondrial fractions derived from HeLa cells, using a commercially available antibody (see Subjects and Methods).

Immunoblotting of different cellular fractions revealed the presence of a band of the expected molecular weight in total lysate and intact mitochondria (Figure 4A). To determine whether the protein was present on the outer mitochondrial membrane, we treated mitochondria with proteinase K (PK) and demonstrated COASY resistance to degradation (Figure 4A). Efficiency of PK activity was demonstrated by treating mitochondria with Triton X-100, which dissolves the membranes and makes the protein accessible to PK digestion (Figure 4A). This result was further supported by hybridizing the same filter with control antibodies against proteins such as CORE1 or ETHE1, which are located in the inner mitochondrial membrane and in the mitochondrial matrix, respectively, or against VDAC1, which is located in the outer mitochondrial membrane (Figure 4A) facing the intermembrane space. We observed that COASY was also present in total lysates and not enriched in the mitochondrial fraction, suggesting that its localization might not be exclusively in mitochondria.

The protein was found in mitoplasts and was resistant to PK digestion. Further fractionation of mitoplasts demonstrated that the protein was mainly present in the matrix, probably anchored to the inner mitochondrial membrane (Figure 4B). The presence of trans-membrane domains was predicted by TMpred and PSIPRED software. We also observed the presence of VDAC in mitoplasts,

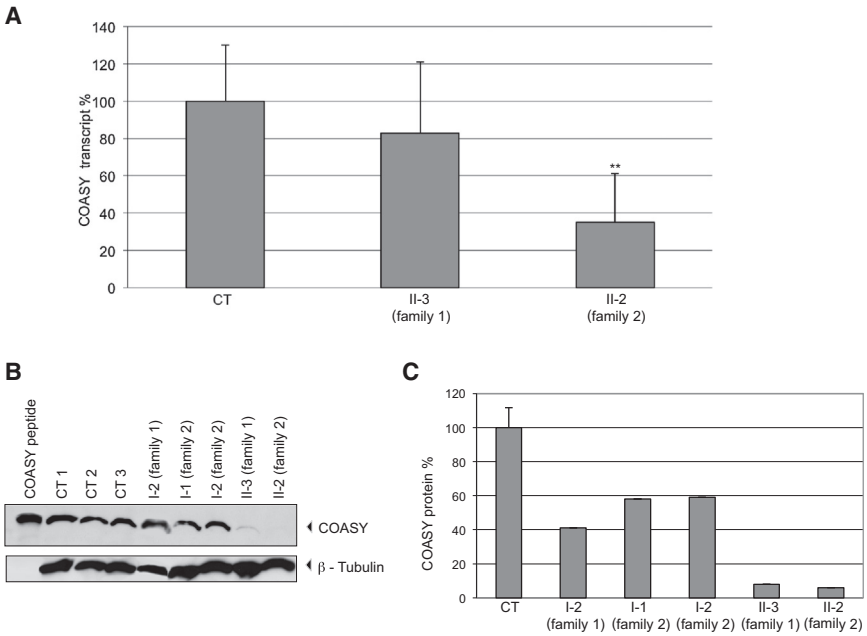

Figure 3. *COASY* mRNA Expression and Protein Accumulation in Skin Fibroblasts

(A) Quantification of *COASY* mRNA levels by real-time PCR in fibroblasts of subject II-3 and II-2 relative to the expression of glyceraldehyde 3-phosphate dehydrogenase (*GAPDH*). The amount of *COASY* transcript is reduced in subject II-2 versus control samples (CT), indicating mRNA decay. Data are represented as mean ± SD. Statistically significant differences with CT were determined by the Student's t test; $^{**}p < 0.02$.

(B) Immunoblot analysis of COASY in fibroblasts derived from three healthy subjects (CT 1, CT 2, CT 3), individual I-2 (family 1), individuals I-1 and I-2 (family 2), and affected subjects (II-3 and II-2). The same amount of protein (30 μg) was loaded. β-tubulin was used as a loading control. As a control, COASY in vitro translation product (COASY peptide) was loaded.

(C) Relative quantification of the protein amount: mean ± SD of three controls (CT); of individual I-2 (family 1); of individuals I-1 and I-2 (family 2); and of affected subjects II-3 and II-2. Histogram shows COASY amount quantified by densitometry and normalized on β-tubulin level.

suggesting that the outer mitochondrial membrane was not completely removed. However, VDAC was partially digested with PK and, most importantly, it was completely absent in the mitochondrial matrix.

HPLC Assays on Recombinant Protein and Fibroblasts Derived from Affected Subjects

To assess the effect of the p.Arg499Cys substitution on the DPCK activity, we expressed mRNA corresponding to the wild-type and mutant DPCK domain in bacteria as His-tag fusion proteins. Recombinant proteins were purified by NTA chromatography and 1 μg of each protein was loaded on an SDS-PAGE and stained with Coomassie blue (Figure 5A, top). To demonstrate that the recombinant proteins were recognized by the anti-COASY antibody, the gel was blotted and incubated with the specific antibody (Figure 5A, bottom). Activities of wild-type DPCK and of the mutant DPCK-Arg499Cys were measured in vitro by HPLC analysis via 1 μg of recombinant proteins.

This analysis evaluates dephospho-CoA conversion into CoA after incubation of wild-type and mutant DPCK proteins with ATP and dephospho-CoA. As indicated by the chromatogram in Figure 5B, the wild-type enzyme was able to completely convert dephospho-CoA into CoA, as demonstrated by the coincidence of the reaction mixture peak with that of CoA standard. On the contrary, the DPCK-Arg499Cys mutant did not have this enzymatic activity and the peak corresponding to CoA was not observed (Figure 5C). This finding suggests that CoA biosynthesis might be abolished in the presence of the p.Arg499Cys change.

We then analyzed CoA levels in fibroblasts derived from healthy and affected subjects by HPLC, but we did not observe a significant difference. However, a general reduction of acetyl-CoA and total CoA was observed in both affected individuals as compared to control, and this difference was statistically significant for acetyl-CoA in subject II-3 of family 1 (Figure 6A).

To examine whether skin fibroblasts from affected individuals were able to synthesize CoA, we performed an in vitro assay to evaluate CoA biosynthesis in cell homogenates with 4′PP (4′-phosphopantetheine) as substrate. HPLC analysis of reaction mixtures showed that dephospho-CoA and CoA were efficiently produced de novo from 4′PP in control fibroblasts (Figure 6B). We also observed residual de novo production of dephospho-CoA and CoA in skin fibroblasts from affected subjects, although the level of CoA was approximately 20% of that produced by control fibroblasts (Figure 6B). These findings suggest the existence of an alternative as yet uncharacterized pathway for CoA biosynthesis. However, we cannot exclude the possibility that the remaining COASY aberrant protein present in fibroblasts may still retain some catalytic activity.

Studies in Yeast *Saccharomyces cerevisiae*

To further test the pathogenic role of the *COASY* missense mutation, we used the yeast *Saccharomyces cerevisiae*. Biosynthesis of CoA in *S. cerevisiae* follows the same pathway described for mammalian cells: pantothenate, formed de novo from several amino acids or taken up from outside the cell, is converted in CoA in five reactions

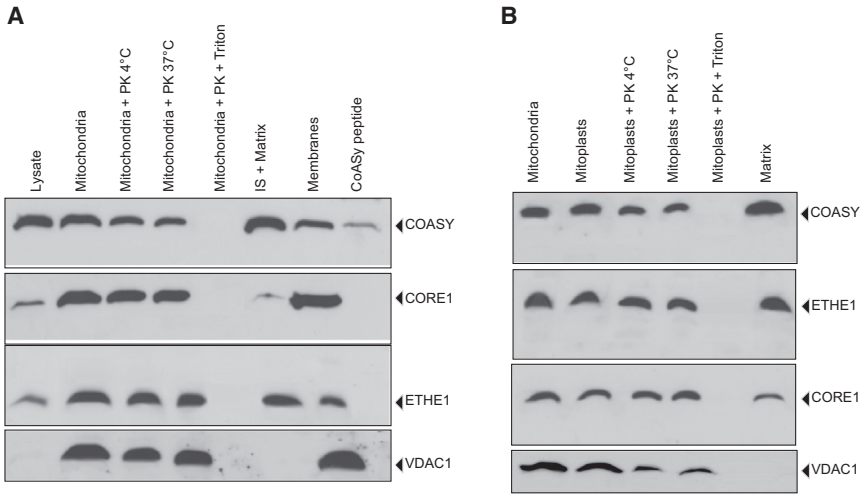

Figure 4. Mitochondrial Localization of COASY

(A) Immunoblot analysis on mitochondria and different submitochondrial fractions derived from HeLa cells. Mitochondria were treated for 15 min at 4°C or 37°C with proteinase K (PK) in presence or absence of triton. The filter was incubated with anti-COASY, anti-CORE1, anti-ETHE1, and anti-VDAC1 antibodies. As a control, COASY in vitro translation product (COASY peptide) was loaded.

(B) Immunoblot analysis on mitoplasts, matrix, and inner membrane isolated from HeLa cells. Mitoplasts were treated for 15 min at 4°C or 37°C with PK in presence or absence of triton. The filter was sequentially incubated with anti-COASY, anti-ETHE1, anti-CORE1, and anti-VDAC antibodies.

catalyzed by enzymes encoded by *CAB1* through *CAB5*.[29] With the exception of *CAB1*, the other genes of the pathway have been identified because of sequence similarity and their function in CoA biosynthesis assessed by heterologous complementation with bacterial genes. The only difference with human is that in yeast, as in *E. coli*, the PPAT and DPCK activities reside on different proteins encoded by *CAB4* and *CAB5* genes, respectively. Deletion of each *CAB* gene results in a lethal phenotype, indicating an essential role for this pathway in yeast.

Sequence analysis indicated that Arg499 is highly conserved from yeast to human and corresponds to Arg146 in the yeast Cab5p (see also Figure 2). By using the plasmid shuffling method, deletion strains expressing either the mutant alleles *cab5*^{Arg146Cys} and *COASY*^{Arg499Cys} or the *CAB5* and *COASY* wild-type genes were generated. The *Δcab5* lethal phenotype was rescued by the re-expression of either human *COASY* wild-type or human *COASY*^{Arg499Cys} and yeast *cab5*^{Arg146Cys}. No major defects of growth on different substrates or at different temperatures were observed (data not shown).

However, we noticed that the mutant *cab5*^{Arg146Cys} as well as the strain expressing *COASY*^{Arg499Cys} became auxotrophic for pantothenate and showed growth reduction. In fact, wild-type yeast can form colonies regardless of the presence of pantothenate at all tested temperatures (Figure 7A); by contrast, in the absence of pantothenate both mutants *cab5*^{Arg146Cys} and *COASY*^{Arg499Cys} failed to form colonies at 37°C and a significant impairment of growth was observed at both 23°C and 28°C when compared with that of the strain expressing the wild-type alleles (Figure 7B). This result supports the pathogenicity of the substitution p.Arg499Cys and suggests that the mutant enzyme requires a higher concentration of pantothenate to produce enough CoA to sustain yeast growth.

Because Cab5p as COASY is located into the mitochondria,[30] we measured the level of CoA in mitochondria isolated from wild-type, *COASY*^{Arg499Cys}, and *cab5*^{Arg146Cys} transformed yeasts grown in complete medium at 28°C with 0.6% glucose. We first verified, by immunoblot analysis, that COASY^{Arg499Cys} was expressed in yeast at a comparable level as in the wild-type enzyme (not shown). We could not verify cab5^{Arg146Cys} expression because the available antibody did not cross-react with the yeast protein. We observed that the level of CoA was reduced to 40% in yeast transformed with both the human *COASY*^{Arg499Cys} and yeast *cab5*^{Arg146Cys} mutant versions as compared to wild-type (Figure 8).

Discussion

We here report the second inborn error of CoA synthesis leading to a neurodegenerative disorder. The first defect discovered was due to *PANK2* mutations, causing the most prevalent NBIA subtype, PKAN.[2]

Coenzyme A (CoA) is a crucial cofactor in all living organisms and is involved in several enzymatic reactions. It is a key molecule for the metabolism of fatty acids, carbohydrates, amino acids, and ketone bodies. Its biosynthesis proceeds through a pathway conserved from prokaryotes to eukaryotes, involving five enzymatic steps, which utilize pantothenate (vitamin B5), ATP, and cysteine.

In the first step, catalyzed by pantothenate kinase, the product of *PANK2*, pantothenic acid is phosphorylated to generate 4′-phosphopantothenic acid. Then, this intermediate is converted into 4′-phosphopantothenoylcysteine, which is subsequently decarboxylated to 4′-phosphopantetheine. The last two steps are carried out by the bifunctional enzyme CoA synthase, which converts 4′-phosphopantetheine into dephospho-CoA and then CoA.[31]

We have identified mutations in the *COASY* in two subjects with clinical and MRI features typical of NBIA. They displayed a strikingly similar phenotype, more severe in subject II-2 of family 2, presenting with early-onset

Please cite this article in press as: Dusi et al., Exome Sequence Reveals Mutations in CoA Synthase as a Cause of Neurodegeneration with Brain Iron Accumulation, The American Journal of Human Genetics (2014), http://dx.doi.org/10.1016/j.ajhg.2013.11.008

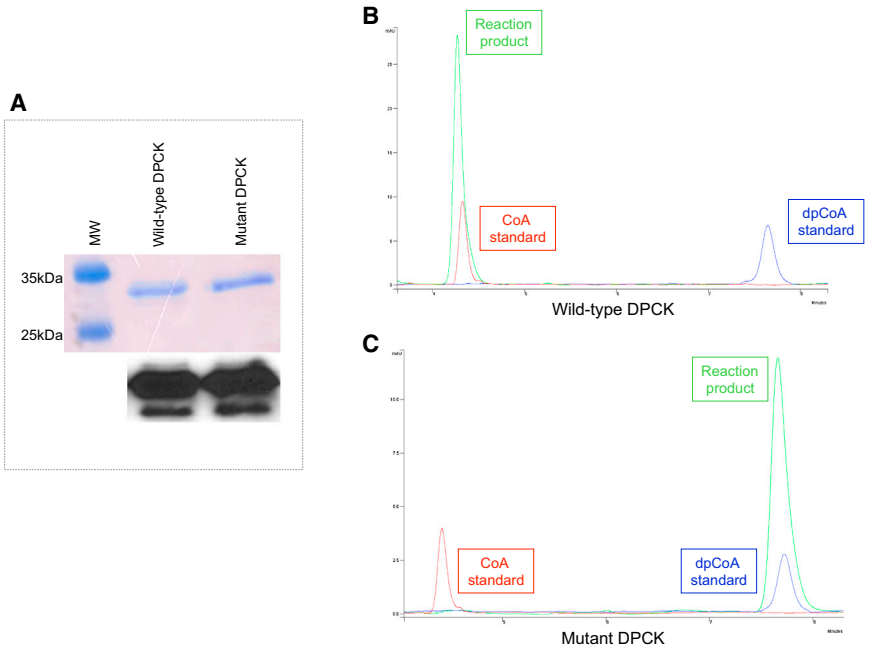

Figure 5. HPLC Analysis of CoA Production by Wild-Type and Mutant DPCK Recombinant Proteins

(A) Top: equal amount of purified wild-type and mutant DPCK proteins were loaded on a 12% SDS page and stained with Coomassie blue. Bottom: immunoblot analysis on the same gel showing that anti-COASY antibody is able to recognize both the wild-type and the mutant protein.

(B) Chromatogram showing the peak corresponding to the reaction product (green) obtained from incubation of wild-type DPCK recombinant protein with ATP and dephospho-CoA.

(C) Chromatogram showing the peak corresponding to the reaction product (green) obtained from incubation of mutant DPCK-Arg499Cys recombinant protein with ATP and dephospho-CoA. Red peak, CoA standard; blue peak, dephospho-CoA standard.

spastic-dystonic paraparesis with a later appearance of parkinsonian features, cognitive impairment, and pronounced obsessive-compulsive disorder. The disease was slowly progressive with loss of ambulation during adolescence and adulthood. This phenotype overlaps with other NBIA disorders, including the presence of an axonal neuropathy, which is commonly reported in phospholipase A_2-associated neurodegeneration (PLAN) and also in mitochondrial membrane protein-associated neurodegeneration (MPAN) cases.[32]

In subject II-3 of family 1, MR images are reminiscent of the "eye-of-the-tiger" sign even if with subtle features, which differentiate it from the typical appearance present in PKAN.[33,34] In subject II-2 of family 2, an isolated involvement of neostriatum, which usually hallmarks a metabolic rather than degenerative disorder, preceded the evidence of the typical increase of pallida iron content. Such features have not been previously reported, expanding the MR spectrum of NBIA disorders.

Both individuals presented with a severe neurological disorder but they have survived up to the third decade of life, suggesting the presence of residual amount of CoA as observed in cultured fibroblasts. The complete absence of CoA would be probably incompatible with life, and organisms have developed alternative strategies to counteract deleterious effects of mutations in CoA enzymatic pathway. For instance, mammals possess four closely related PANK isoforms,[2] 1α, 1β, 2, and 3, which exhibit a tissue-specific pattern of expression. This redundancy could explain why PKAN patients can survive into the first or second decade of life. Probably, the different isoforms can compensate each other to maintain adequate CoA level. This was clearly demonstrated in mice by the simultaneous knockout of two different *Pank* genes.[35]

COASY has been reported to code for three transcript variants resulting in tissue-specific isoforms.[14] The existence and functional significance of these variants are

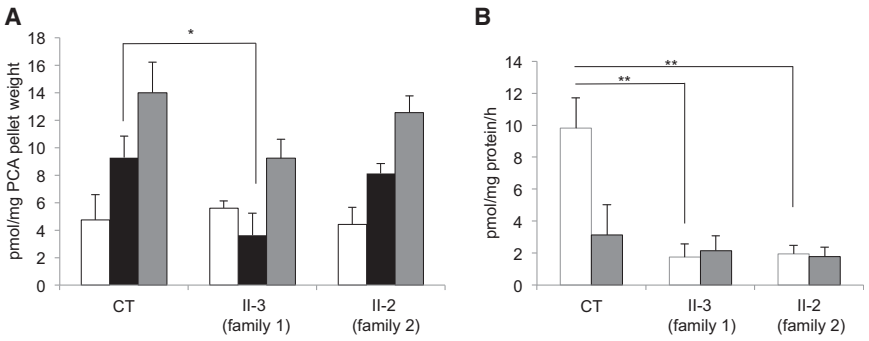

Figure 6. HPLC Analysis of CoA and CoA Derivatives in Fibroblasts

(A) CoA (white bar), acetyl-CoA (black bar), and total CoA (gray bar) levels in primary skin fibroblasts derived from a healthy control (CT) and from the two affected individuals (II-3, family 1; II-2, family 2). Results shown are mean ± SEM of four independent experiments. Statistically significant differences in acetyl-CoA amount between CT and subject II-3 (family 1) were determined by the Student's t test; *$p < 0.05$. This subject also shows a reduction in acetyl-CoA, which is not statistically significant. A reduction of total CoA was observed in both affected individuals, although not statistically significant.

(B) De novo synthesis of CoA and dephosphoCoA (dpCoA) in primary skin fibroblasts derived from a healthy control (CT) and from the two affected individuals (II-3, family 1; II-2, family 2). CoA (white bar) and dpCoA (gray bar) produced from 4′PP as substrate were quantified by HPLC after deproteinization of reaction mixture with PCA (3% final). Results shown are mean ± SEM of values from three independent experiments. Statistically significant differences with CT were determined by the Student's t test; **$p < 0.02$.

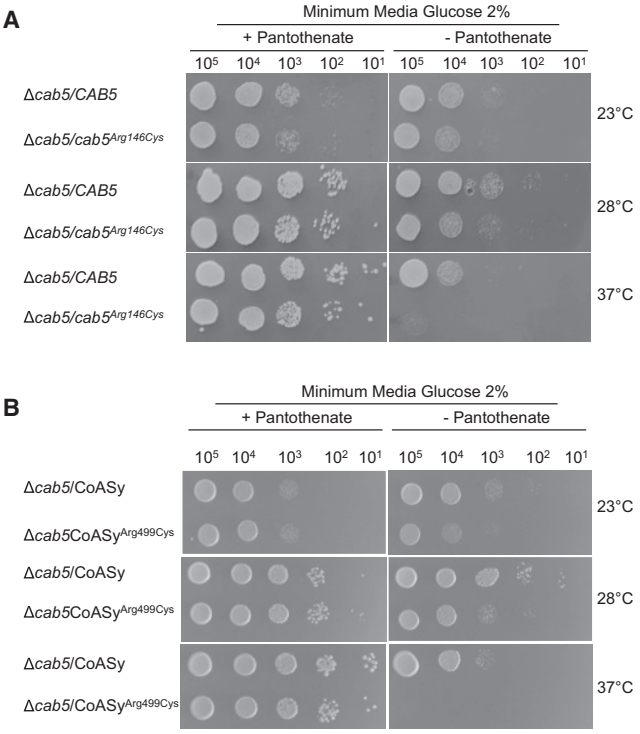

Figure 7. Growth of Yeast Strains in Presence or Absence of Pantothenate

The strain Δ*cab5* was transformed with pFL39 plasmid carrying the wild-type *CAB5* and the mutant allele *cab5*^{Arg146Cys} (A) or with pYEX-BX plasmid carrying *COASY* and *COASY*^{Arg499Cys} (B). Equal amounts of serial dilutions of cells from exponentially grown cultures (10^5, 10^4, 10^3, 10^2, 10^1 cells) were spotted onto minimum medium 40 plus 2% glucose, with or without pantothenate 1 mg l^{-1}. The growth was scored after 3 days of incubation at 23°C, 28°C, or 37°C. Each experiment of serial dilution grow test was done in triplicate starting from independent yeast cultures.

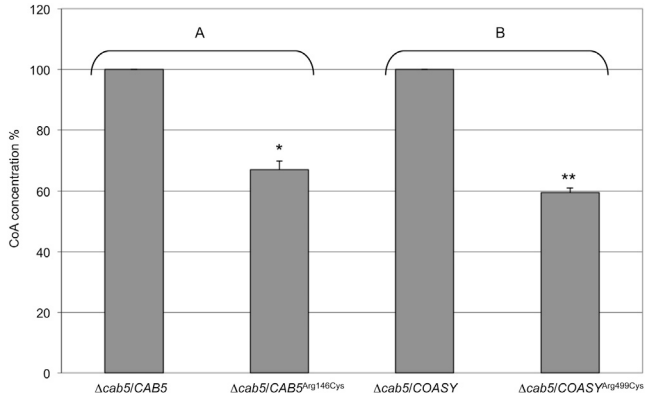

Figure 8. HPLC Analysis of CoA in Yeast Mitochondria

CoA level in mitochondria isolated from Δ*cab5* yeast transformed with wild-type (WT) or mutant (p.Arg146Cys) yeast *CAB5* (A), and with wild-type or mutant (p.Arg499Cys) human *COASY* (B). Equal amount of mitochondrial proteins (40 μg) were used in each assay. Results shown are mean ± SD of values from three independent experiments. Values of mutant samples are expressed as percentage of values obtained in wild-type samples taken as 100%. Statistically significant differences were determined by the Student's t test; *$p < 0.05$; **$p < 0.02$.

presently unknown but both mutations found in this study affect the protein sequence common to isoforms alpha and beta, predicting overall impairment of COASY function. Considering the ubiquitous presence of the enzymatic COASY activity, it remains unexplained why only the brain is affected and other organs are preserved. It is possible that a more severe impairment of CoA levels occurs in this organ, thus explaining the prevalence of neurological symptoms. At the cellular level CoA concentration is regulated by numerous factors, including hormones, glucocorticoids, nutrients, and cellular metabolites,[36,37] and a link between the complex signaling mTOR pathway, which is implicated in numerous metabolic and signaling processes, and CoA biosynthesis has been proposed.[38] Moreover, it is relevant to notice that the mutations targeted genes coding for pantothenate kinase[39] and PPAT activity of CoA synthase[36] are the two rate-limiting steps in CoA biosynthesis. All together these factors could contribute to modulate the clinical presentation of individuals carrying *COASY* mutations.

It is still unknown how mutations in genes involved in Coenzyme A enzymatic pathway cause neurodegeneration with iron accumulation in specific areas of the brain but whereas for *PANK2* it was hypothesized that cysteine accumulation may chelate iron and catalyze free radical formation,[40] a different mechanism could be involved in case of *COASY* mutations.

In *Drosophila* it has been demonstrated that abolishing the different genes of CoA biosynthetic pathway including the fumble/PANK2 and PPAT-DPCK activities causes a neurological phenotype characterized by brain vacuolization without iron accumulation.[12]

Identification of mutations in CoA synthase strongly reinforces the essential role of CoA biosynthetic pathway for the development and functioning of the nervous system. This also underlines the importance of further investigations on different subcellular pools of CoA available, because a specific mitochondrial pathway could exist considering that both PANK2 and CoA synthase are mitochondrial enzymes.[16–18] At present it is not understood whether CoA can pass from cytosol to mitochondria, even if a CoA-specific carrier has been identified in the inner mitochondrial membrane.[41] Moreover, it is not clear whether the regulation of the different pools is coordinated and whether the utilization could be modulated in response to different physiological or pathological conditions.

In conclusion, we have demonstrated that *COASY* mutations cause a distinctive NBIA subtype. This finding will require further investigation to understand the connection linking CoA metabolism to neurodegeneration, iron accumulation, and mitochondrial bioenergetics. We propose CoPAN, standing for COASY protein-associated neurodegeneration, as the acronym for NBIA caused by CoA synthase mutations to conform with the current nomenclature in use to classify these disorders.

Please cite this article in press as: Dusi et al., Exome Sequence Reveals Mutations in CoA Synthase as a Cause of Neurodegeneration with Brain Iron Accumulation, The American Journal of Human Genetics (2014), http://dx.doi.org/10.1016/j.ajhg.2013.11.008

Supplemental Data

Supplemental Data include four tables and can be found with this article online at http://www.cell.com/AJHG/.

Acknowledgments

We would like to thank Mario Savoiardo and Federica Zibordi for helpful neuroradiological and clinical support and Fabrizio Villa for experimental advice. The financial support of Telethon GGP11088 to V.T. is gratefully acknowledged. This work was supported by TIRCON project of the European Commission's Seventh Framework Programme (FP7/2007-2013, HEALTH-F2-2011, grant agreement no. 277984). We thank the Cell line and DNA bank of paediatric movement disorders of the Telethon Genetic Biobank Network (project no. GTB07001) and the Bank for the Diagnosis and Research of Movement Disorders (MDB) of the EuroBiobank. The financial support of Mariani Foundation of Milan is gratefully acknowledged. T.B.H. and S.H. were supported by the NBIA Disorders Association. M.A.K. is a Wellcome Trust Intermediate Clinical Fellow. H.H. and C.B. are grateful to the MRC UK (grant number G0802870) and Backman-Strauss Foundation.

Received: September 6, 2013
Accepted: November 14, 2013
Published: December 19, 2013

Web Resources

The URLs for data presented herein are as follows:

MutPred, http://mutpred.mutdb.org/
NHLBI Exome Sequencing Project (ESP) Exome Variant Server, http://evs.gs.washington.edu/EVS/
Online Mendelian Inheritance in Man (OMIM), http://www.omim.org/
PolyPhen-2, http://www.genetics.bwh.harvard.edu/pph2/
PSIPRED, http://bioinf.cs.ucl.ac.uk/psipred/
RefSeq, http://www.ncbi.nlm.nih.gov/RefSeq
TMpred, http://www.ch.embnet.org/software/TMPRED_form.html

References

1. Gregory, A., and Hayflick, S.J. (2011). Genetics of neurodegeneration with brain iron accumulation. Curr. Neurol. Neurosci. Rep. *11*, 254–261.
2. Zhou, B., Westaway, S.K., Levinson, B., Johnson, M.A., Gitschier, J., and Hayflick, S.J. (2001). A novel pantothenate kinase gene (PANK2) is defective in Hallervorden-Spatz syndrome. Nat. Genet. *28*, 345–349.
3. Hörtnagel, K., Prokisch, H., and Meitinger, T. (2003). An isoform of hPANK2, deficient in pantothenate kinase-associated neurodegeneration, localizes to mitochondria. Hum. Mol. Genet. *12*, 321–327.
4. Morgan, N.V., Westaway, S.K., Morton, J.E., Gregory, A., Gissen, P., Sonek, S., Cangul, H., Coryell, J., Canham, N., Nardocci, N., et al. (2006). PLA2G6, encoding a phospholipase A2, is mutated in neurodegenerative disorders with high brain iron. Nat. Genet. *38*, 752–754.
5. Kruer, M.C., Paisán-Ruiz, C., Boddaert, N., Yoon, M.Y., Hama, H., Gregory, A., Malandrini, A., Woltjer, R.L., Munnich, A., Gobin, S., et al. (2010). Defective FA2H leads to a novel form of neurodegeneration with brain iron accumulation (NBIA). Ann. Neurol. *68*, 611–618.
6. Hartig, M.B., Iuso, A., Haack, T., Kmiec, T., Jurkiewicz, E., Heim, K., Roeber, S., Tarabin, V., Dusi, S., Krajewska-Walasek, M., et al. (2011). Absence of an orphan mitochondrial protein, c19orf12, causes a distinct clinical subtype of neurodegeneration with brain iron accumulation. Am. J. Hum. Genet. *89*, 543–550.
7. Panteghini, C., Zorzi, G., Venco, P., Dusi, S., Reale, C., Brunetti, D., Chiapparini, L., Zibordi, F., Siegel, B., Garavaglia, B., et al. (2012). C19orf12 and FA2H mutations are rare in Italian patients with neurodegeneration with brain iron accumulation. Semin. Pediatr. Neurol. *19*, 75–81.
8. Haack, T.B., Hogarth, P., Kruer, M.C., Gregory, A., Wieland, T., Schwarzmayr, T., Graf, E., Sanford, L., Meyer, E., Kara, E., et al. (2012). Exome sequencing reveals de novo WDR45 mutations causing a phenotypically distinct, X-linked dominant form of NBIA. Am. J. Hum. Genet. *91*, 1144–1149.
9. Saitsu, H., Nishimura, T., Muramatsu, K., Kodera, H., Kumada, S., Sugai, K., Kasai-Yoshida, E., Sawaura, N., Nishida, H., Hoshino, A., et al. (2013). De novo mutations in the autophagy gene WDR45 cause static encephalopathy of childhood with neurodegeneration in adulthood. Nat. Genet. *45*, 445–449, e1.
10. Aghajanian, S., and Worrall, D.M. (2002). Identification and characterization of the gene encoding the human phosphopantetheine adenylyltransferase and dephospho-CoA kinase bifunctional enzyme (CoA synthase). Biochem. J. *365*, 13–18.
11. Bosveld, F., Rana, A., Lemstra, W., Kampinga, H.H., and Sibon, O.C. (2008). Drosophila phosphopantothenoylcysteine synthetase is required for tissue morphogenesis during oogenesis. BMC Res. Notes *1*, 75.
12. Bosveld, F., Rana, A., van der Wouden, P.E., Lemstra, W., Ritsema, M., Kampinga, H.H., and Sibon, O.C. (2008). De novo CoA biosynthesis is required to maintain DNA integrity during development of the Drosophila nervous system. Hum. Mol. Genet. *17*, 2058–2069.
13. Daugherty, M., Polanuyer, B., Farrell, M., Scholle, M., Lykidis, A., de Crécy-Lagard, V., and Osterman, A. (2002). Complete reconstitution of the human coenzyme A biosynthetic pathway via comparative genomics. J. Biol. Chem. *277*, 21431–21439.
14. Nemazanyy, I., Panasyuk, G., Breus, O., Zhyvoloup, A., Filonenko, V., and Gout, I.T. (2006). Identification of a novel CoA synthase isoform, which is primarily expressed in the brain. Biochem. Biophys. Res. Commun. *341*, 995–1000.
15. Johnson, M.A., Kuo, Y.M., Westaway, S.K., Parker, S.M., Ching, K.H., Gitschier, J., and Hayflick, S.J. (2004). Mitochondrial localization of human PANK2 and hypotheses of secondary iron accumulation in pantothenate kinase-associated neurodegeneration. Ann. N Y Acad. Sci. *1012*, 282–298.
16. Alfonso-Pecchio, A., Garcia, M., Leonardi, R., and Jackowski, S. (2012). Compartmentalization of mammalian pantothenate kinases. PLoS ONE *7*, e49509.
17. Zhyvoloup, A., Nemazanyy, I., Panasyuk, G., Valovka, T., Fenton, T., Rebholz, H., Wang, M.L., Foxon, R., Lyzogubov, V., Usenko, V., et al. (2003). Subcellular localization and regulation of coenzyme A synthase. J. Biol. Chem. *278*, 50316–50321.
18. Rhee, H.W., Zou, P., Udeshi, N.D., Martell, J.D., Mootha, V.K., Carr, S.A., and Ting, A.Y. (2013). Proteomic mapping of mitochondria in living cells via spatially restricted enzymatic tagging. Science *339*, 1328–1331.

19. Simon-Kayser, B., Scoul, C., Renaudin, K., Jezequel, P., Bouchot, O., Rigaud, J., and Bezieau, S. (2005). Molecular cloning and characterization of FBXO47, a novel gene containing an F-box domain, located in the 17q12 band deleted in papillary renal cell carcinoma. Genes Chromosomes Cancer *43*, 83–94.
20. Fernández-Vizarra, E., Ferrín, G., Pérez-Martos, A., Fernández-Silva, P., Zeviani, M., and Enríquez, J.A. (2010). Isolation of mitochondria for biogenetical studies: An update. Mitochondrion *10*, 253–262.
21. Tiranti, V., Galimberti, C., Nijtmans, L., Bovolenta, S., Perini, M.P., and Zeviani, M. (1999). Characterization of SURF-1 expression and Surf-1p function in normal and disease conditions. Hum. Mol. Genet. *8*, 2533–2540.
22. Magni, G.E., and Von Borstel, R.C. (1962). Different rates of spontaneous mutation during mitosis and meiosis in yeast. Genetics *47*, 1097–1108.
23. Bonneaud, N., Ozier-Kalogeropoulos, O., Li, G.Y., Labouesse, M., Minvielle-Sebastia, L., and Lacroute, F. (1991). A family of low and high copy replicative, integrative and single-stranded *S. cerevisiae/E. coli* shuttle vectors. Yeast *7*, 609–615.
24. Sambrook, J., and Russel, D.W. (2001). Molecular Cloning: A Laboratory Manual (Cold Spring Harbor: Cold Spring Harbor Laboratory Press).
25. Gietz, R.D., and Schiestl, R.H. (2007). Quick and easy yeast transformation using the LiAc/SS carrier DNA/PEG method. Nat. Protoc. *2*, 35–37.
26. Glick, B.S., and Pon, L.A. (1995). Isolation of highly purified mitochondria from *Saccharomyces cerevisiae*. Methods Enzymol. *260*, 213–223.
27. Walia, G., Gajendar, K., and Surolia, A. (2011). Identification of critical residues of the mycobacterial dephosphocoenzyme a kinase by site-directed mutagenesis. PLoS ONE *6*, e15228.
28. Walia, G., and Surolia, A. (2011). Insights into the regulatory characteristics of the mycobacterial dephosphocoenzyme A kinase: implications for the universal CoA biosynthesis pathway. PLoS ONE *6*, e21390.
29. Olzhausen, J., Schübbe, S., and Schüller, H.J. (2009). Genetic analysis of coenzyme A biosynthesis in the yeast *Saccharomyces cerevisiae*: identification of a conditional mutation in the pantothenate kinase gene *CAB1*. Curr. Genet. *55*, 163–173.
30. Reinders, J., Zahedi, R.P., Pfanner, N., Meisinger, C., and Sickmann, A. (2006). Toward the complete yeast mitochondrial proteome: multidimensional separation techniques for mitochondrial proteomics. J. Proteome Res. *5*, 1543–1554.
31. Leonardi, R., Zhang, Y.M., Rock, C.O., and Jackowski, S. (2005). Coenzyme A: back in action. Prog. Lipid Res. *44*, 125–153.
32. Hogarth, P., Gregory, A., Kruer, M.C., Sanford, L., Wagoner, W., Natowicz, M.R., Egel, R.T., Subramony, S.H., Goldman, J.G., Berry-Kravis, E., et al. (2013). New NBIA subtype: genetic, clinical, pathologic, and radiographic features of MPAN. Neurology *80*, 268–275.
33. Hayflick, S.J., Westaway, S.K., Levinson, B., Zhou, B., Johnson, M.A., Ching, K.H., and Gitschier, J. (2003). Genetic, clinical, and radiographic delineation of Hallervorden-Spatz syndrome. N. Engl. J. Med. *348*, 33–40.
34. Kruer, M.C., Boddaert, N., Schneider, S.A., Houlden, H., Bhatia, K.P., Gregory, A., Anderson, J.C., Rooney, W.D., Hogarth, P., and Hayflick, S.J. (2012). Neuroimaging features of neurodegeneration with brain iron accumulation. AJNR Am. J. Neuroradiol. *33*, 407–414.
35. Garcia, M., Leonardi, R., Zhang, Y.M., Rehg, J.E., and Jackowski, S. (2012). Germline deletion of pantothenate kinases 1 and 2 reveals the key roles for CoA in postnatal metabolism. PLoS ONE *7*, e40871.
36. Tahiliani, A.G., and Beinlich, C.J. (1991). Pantothenic acid in health and disease. Vitam. Horm. *46*, 165–228.
37. Smith, C.M., and Savage, C.R., Jr. (1980). Regulation of coenzyme A biosynthesis by glucagon and glucocorticoid in adult rat liver parenchymal cells. Biochem. J. *188*, 175–184.
38. Nemazanyy, I., Panasyuk, G., Zhyvoloup, A., Panayotou, G., Gout, I.T., and Filonenko, V. (2004). Specific interaction between S6K1 and CoA synthase: a potential link between the mTOR/S6K pathway, CoA biosynthesis and energy metabolism. FEBS Lett. *578*, 357–362.
39. Rock, C.O., Calder, R.B., Karim, M.A., and Jackowski, S. (2000). Pantothenate kinase regulation of the intracellular concentration of coenzyme A. J. Biol. Chem. *275*, 1377–1383.
40. Gregory, A., and Hayflick, S.J. (2005). Neurodegeneration with brain iron accumulation. Folia Neuropathol. *43*, 286–296.
41. Fiermonte, G., Paradies, E., Todisco, S., Marobbio, C.M., and Palmieri, F. (2009). A novel member of solute carrier family 25 (SLC25A42) is a transporter of coenzyme A and adenosine 3′,5′-diphosphate in human mitochondria. J. Biol. Chem. *284*, 18152–18159.

The American Journal of Human Genetics, Volume *93*

Supplemental Data

Exome Sequence Reveals Mutations in CoA Synthase as a Cause of Neurodegeneration with Brain Iron Accumulation

Sabrina Dusi, Lorella Valletta, Tobias B. Haack, Yugo Tsuchiya, Paola Venco, Sebastiano Pasqualato, Paola Goffrini, Marco Tigano, Nikita Demchenko, Thomas Wieland, Thomas Schwarzmayr, Tim M. Strom, Federica Invernizzi, Barbara Garavaglia, Allison Gregory, Lynn Sanford, Jeffrey Hamada, Conceição Bettencourt, Henry Houlden, Luisa Chiapparini, Giovanna Zorzi, Manju A. Kurian, Nardo Nardocci, Holger Prokisch, Susan Hayflick, Ivan Gout, and Valeria Tiranti

Table S1. Next generation Sequencing Statistics

Id	Type	Reads	Mapped	Percent	Seq (Gb)	on bait	Avg cov	Cov 1x	Cov 4x	Cov 8x	Cov 20x
#55633	SureSelect50Mb	87259289	80916002	92.73	8.81	73.85	93.96	99.61	98.79	97.3	92.4

Table S2. Variants Identified by Exome Sequencing

Variants filtering	
Synonymous variants	11846
NSV	11601
NSV with frequency <0.1% in ‘in-house and public databases	340
≥ 2NSV / gene	22
Genes carrying homozygous rare NSV	12

NSV = missense, nonsense, stop/loss, splice site disruption, insertions, deletions

Table S3: detailed list of the 12 genes carrying homozygous rare NSV

gene #	gene symbol	OMIM	chromosomal position of identified variant	UCSC transcript, predicted mutation at nucleotide and protein level	dbSNP (rs number)	prefunction	pph2	Sift	Occurence of predicted recessive-type variants in 3,159 samples with unrelated phenotypes	Other arguments against a causal role
1	GUCA2A	*139392	chr1:42629092-42629092	uc001chd.1, c.265G>T,p.Glu89*	rs147564899	nonsense		0.39	-	uc001chd.1, c.265G>T,p.Glu89* also found in healthy subjects I-2 and II-4 of family 1
2	HRNR	*114085	chr1:152189999-152189999	uc001ezt.1, c.4106G>T, p.Ser1369Phe		missense	benign	0.05	>1000 other patients with predicted recessive type mutations and unrelated phenotypes	
			chr1:152190002-152190002	uc001ezt.1, c.4103G>A, p.Gly1368Asp		missense	benign	0.3		
3	ADAM8	*602267	chr10:135082994-135082994	uc021qbe.1, c.1903T>G, p.Trp635Gly		missense	probably damaging		16 other patients with predicted recessive type mutations and unrelated phenotypes	
4	FBXO47	*609498	chr17:37118301-37118301	uc002hrc.2, c.182-1G>A, p.?		splice			absence of mutations in 56 NBIA subjects	Suggested role as a tumor supressor.
5	CACNB1	*114207	chr17:37353687-37353687	uc002hrm.2, c.62A>G, p.Glu21Gly		missense	benign	0.17	1 other patient with predicted compound heterozygous mutations and mental retardation.	
6	**COASY**	***609855**	**chr17:40717686-40717686**	**uc010cyj.3, c.1582C>T, p.Arg528Cys**	**rs140709867**	**missense**	**probably damaging**	**0**	-	
7	BZRAP1	*610764	chr17:56385086-56385086	uc002ivx.4, c.4869G->C, p.:Gln1623His	rs141226909	missense	possibly damaging	0.12	52 other patients with predicted recessive type mutations and unrelated phenotypes	
8	C17orf47	not available	chr17:56621291-56621291	uc002iwq.2, c.257C>T, p.Arg86Gln		missense	benign	0.28	2 other patients with predicted recessive type mutations and unrelated phenotypes	
9	LRP1B	*608766	chr2:141641491-141641491	uc002tvj.1, c.4064A>G, p.Asn1355Ser		missense	probably damaging	0.56	151 other patients with predicted recessive type mutations and unrelated phenotypes	
10	EVC2	*607261	chr4:5624616-5624616	uc003gij.3, p.2149C>G, p.His717Asp		missense	possibly damaging	0.32	25 other patients with predicted recessive type mutations and unrelated phenotypes	Associated with Ellis-van Creveld syndrome (MIM *607261)
			chr4:5667370-5667370	uc003gij.3, c.877C>T, p.Pro293Ser		missense	probably damaging	0.14		
11	KIAA1797	*614606	chr9:20885216-20885216	uc003zog.1, c.2612C>T, p.Ala871Val	rs187654100	missense	benign	0.29	16 other patients with predicted recessive type mutations and unrelated phenotypes	
12	IFNW1	*147553	chr9:21141080-21141080	uc003zol.1, c.490A>G, p.Trp164Arg	rs147009804	missense	probably damaging	0	-	uc003zol.1, c.490A->G, p.Trp164Arg also found in healthy subjects I-2, II-4 and II-5 of family 1

Table S4. Primer sequences and PCR conditions to amplify the 9 exons of *COASY* gene.

Exons	Forward primer	Reverse primer	DNA polymerase	Annealing Temp
1a	GATTTTTGGATCCCCAGCCC	CAAGAACCTCAAACGTGGCC	*AmpliTaq Gold*®	*58°C*
1b	TCCCATACAGGCCTCTGCC	GGCCTTAGCACCAATTGAGTG	*AmpliTaq Gold*®	*60°C*
2	TGCTTGCCTGTTTCTTCACCT	CGGGCAAACTGAGAACCAGTT	GoTaq® *Flexi*	59°C
3	GGAGCCTGGGTAGGAAGGG	CTCAGCCTCATGCCTGGG	GoTaq® *Flexi*	60°C
4	CCTGGCAATGCTGGAGAGTAG	GGCCTGGCTAGCTCCTCACT	GoTaq® *Flexi*	60°C
5	GGCCTCTGTGCTCAGTTGTCT	GCAAGGTGGTGTTGGGAACA	GoTaq® *Flexi*	60°C
6	CCCAGAATGCCATTTCCATT	GACGTTCTCCCAGGCAGAAC	GoTaq® *Flexi*	59°C
7	GAGGATGGCAACAGCTAAGGG	TTTGTCAGGAAGAATTCCAGCTC	GoTaq® *Flexi*	59°C
8	CCCCCCACACCATCCCTAC	GATGAGTCTTGGGAATGCGCT	GoTaq® *Flexi*	60°C
9	TACTGCCTGACCCTGCCCT	AAAGCTCGCCTCTGGCTAGC	*AmpliTaq Gold*®	*60°C*

GoTaq® *Flexi* DNA Polymerase (Promega); *AmpliTaq Gold*® (Life Technologies) were used. PCR conditions were: 94°C, 1min (1 cycle); 94°C 30sec, annealing time was 30sec at the indicated temperatures, 72°C 1min (30 cycles).

Neurobiology of Disease xxx (2015) xxx–xxx

Contents lists available at ScienceDirect

Neurobiology of Disease

journal homepage: www.elsevier.com/locate/ynbdi

Mitochondrial iron and energetic dysfunction distinguish fibroblasts and induced neurons from pantothenate kinase-associated neurodegeneration patients

Paolo Santambrogio [a], Sabrina Dusi [b], Michela Guaraldo [a,c], Luisa Ida Rotundo [a], Vania Broccoli [a], Barbara Garavaglia [b], Valeria Tiranti [b], Sonia Levi [a,c,*]

[a] San Raffaele Scientific Institute, Division of Neuroscience, 20132 Milano, Italy
[b] Molecular Neurogenetics Unit, Foundation IRCCS-Neurological Institute "Carlo Besta", 20126 Milano, Italy
[c] University Vita-Salute San Raffaele, 20132 Milano, Italy

ARTICLE INFO

Article history:
Received 5 December 2014
Revised 11 February 2015
Accepted 23 February 2015
Available online xxxx

Keywords:
Iron metabolism
Mitochondria
Reactive oxygen species
NBIA
PANK2
Induced neurons

ABSTRACT

Pantothenate kinase-associated neurodegeneration is an early onset autosomal recessive movement disorder caused by mutation of the pantothenate kinase-2 gene, which encodes a mitochondrial enzyme involved in coenzyme A synthesis. The disorder is characterised by high iron levels in the brain, although the pathological mechanism leading to this accumulation is unknown. To address this question, we tested primary skin fibroblasts from three patients and three healthy subjects, as well as neurons induced by direct fibroblast reprogramming, for oxidative status, mitochondrial functionality and iron parameters. The patients' fibroblasts showed altered oxidative status, reduced antioxidant defence, and impaired cytosolic and mitochondrial aconitase activities compared to control cells. Mitochondrial iron homeostasis and functionality analysis of patient fibroblasts indicated increased labile iron pool content and reactive oxygen species development, altered mitochondrial shape, decreased membrane potential and reduced ATP levels. Furthermore, analysis of induced neurons, performed at a single cell level, confirmed some of the results obtained in fibroblasts, indicating an altered oxidative status and signs of mitochondrial dysfunction, possibly due to iron mishandling. Thus, for the first time, altered biological processes have been identified in vitro in live diseased neurons. Moreover, the obtained induced neurons can be considered a suitable human neuronal model for the identification of candidate therapeutic compounds for this disease.

Introduction

Neurodegeneration with brain iron accumulation (NBIA) is a heterogeneous group of genetic disorders characterised by radiological evidence of focal accumulation of iron in the brain, usually in the basal ganglia and extrapyramidal dysfunction (Schneider et al., 2013; Levi and Finazzi, 2014). These disorders are characterised by early or late onset, with the main symptoms associated with problems in movement, spasticity and cognitive impairment. Approximately 50% of cases of NBIA can be explained by mutations in the *PANK2* gene that cause an autosomal–recessive form of the disease, termed pantothenate kinase-associated neurodegeneration (PKAN or NBIA type I; OMIM 234200) (Hayflick, 2014). Magnetic resonance imaging (MRI) is particularly useful for distinguishing the cases of PKAN from other NBIA forms. In the majority of PKAN patients, the T2-weighted images show a hyperintense lesion of the globus pallidus, surrounded by a hypointense area (Angelini et al., 1992). This combination of hyper- and hypointense areas in the globus pallidus gives rise to a pattern defined as the "eye of the tiger", which is almost pathognomonic of the disease. The brain regions in which iron accumulates at pathological levels are the globus pallidus and substantia nigra, where iron-positive spheroidal bodies are visible, usually in the vicinity of swollen axons. Other neuropathological signs include demyelination, neuronal loss and gliosis (Kruer et al., 2011).

PANK2 codes for the pantothenate kinase-2 (PANK2), a mitochondrial enzyme that catalyses the first limiting step of the de novo biosynthesis of coenzyme A (CoA). CoA is a key factor in several cellular processes, including mitochondrial energy metabolism, anabolism and catabolism of fatty acids, as well as protein biosynthesis (Leonardi et al., 2005). In humans, 4

Abbreviations: DCF, dichlorofluorescein; DFO, deferoxamine; DHR-123, dihydrorhodamine 123; FAC, ferric ammonium citrate; iNs, induced neurons; IRP1, iron regulatory protein 1; LIP, labile iron pool; NBIA, neurodegeneration with brain iron accumulation; PKAN, pantothenate kinase associated neurodegeneration; PIH, pyridoxal isonicotinoyl hydrazone; ROS, reactive oxygen species; RPA, rhodamine B-[(1,10-phenanthroline-5-yl)-aminocarbonyl]benzyl ester; RPAC, rhodamine B-[(phenanthren-9-yl)-aminocarbonyl]-benzylester; TMRM, tetramethylrhodamine methyl ester.

* Corresponding author at: Vita-Salute San Raffaele University and San Raffaele Scientific Institute, Via Olgettina 58, 20132 Milano, Italy. Fax: +39 02 26434844.
E-mail address: levi.sonia@hsr.it (S. Levi).

Available online on ScienceDirect (www.sciencedirect.com).

http://dx.doi.org/10.1016/j.nbd.2015.02.030

genes code for pantothenate kinases, but only PANK2 has mitochondrial localisation. Mutations in *PANK2*, which is located on chromosome 20, are spread over all 7 exons and include missense, nonsense, frameshift and splicing site mutations (Hartig et al., 2006). Mutations in *PANK2* result in enzyme deficiency, leading to insufficiency of the final product and accumulation of upstream substrates, such as N-pantotenoil-cysteine and pantetheine, which are potentially toxic (Leoni et al., 2012). In particular, cysteine is a potent iron chelator, and it has been proposed that high local levels of cysteine are the basis of the subsequent accumulation of iron, resulting in increased oxidative stress (Perry et al., 1985). The other hypothesis to explain the observed iron accumulation suggests that alterations in phospholipid metabolism due to CoA-deficiency may injure the membranes, with consequent oxidative stress that leads to iron dyshomeostasis (Leonardi et al., 2007). Different animal disease-models have been developed using *Drosophila melanogaster* and *Mus musculus*. *Drosophila* PKAN models partially recapitulate the human phenotype, showing locomotor dysfunction and neurodegeneration (Rana et al., 2010). In addition, a *Pank2* KO mouse model does not fully recapitulate the human phenotype (Kuo et al., 2005), unless particular dietary conditions are used (Brunetti et al., 2014). The double knock-out of more than one *Pank* in mice produces a very drastic phenotype resembling a metabolic syndrome (Garcia et al., 2012). However, these models do not show iron accumulation in the brain and are not useful for studying the pathogenetic mechanism leading to iron imbalance, which is hallmark sign in the brains of patients. Two in vitro studies on cellular models have attempted to explain the relationship between *PANK2* deficiency and iron deregulation. In HeLa, HepG2 and SH-SY5Y cells, the specific siRNA silencing of *PANK2* affects cell proliferation, induces cellular iron deficiency and increases the expression of the iron exporter ferroportin (Poli et al., 2010). PKAN fibroblasts, maintained in chronic iron supplementation, showed disturbed iron sensor protein iron regulatory protein 1 (IRP1) activity, resulting in deregulation of ferritin and transferrin receptor1 (TfR1), as well as a larger intracellular bioactive labile iron pool (LIP). This effect results in higher reactive oxygen species (ROS) development and leads to increased cellular oxidative status (Campanella et al., 2012).

Mitochondria are the main sites of iron utilisation in the cell (Levi and Rovida, 2009). This organelle employs the metal to sustain the biosynthesis of the iron sulphur cluster (ISC) and heme cofactors, which are prosthetic groups of widespread proteins involved in key biological processes, such as electron transfer, DNA synthesis and repair, metabolic and regulatory processes (Stehling et al., 2014). Thus, mitochondria play a central role in cell life, not only for energy supply but also for cellular iron handling. This important role is highlighted by the fact that defects in mitochondrial iron homeostasis lead to pathological phenotypes and cell death (Levi and Rovida, 2009). Here, we evaluated mitochondrial functionality in terms of iron handling and energetic profile to investigate whether the iron-dependent oxidative status alteration, previously revealed in PKAN patients' fibroblasts (Campanella et al., 2012), also affects the mitochondrial compartment. Furthermore, by taking advantage of the recently developed technology (Amamoto and Arlotta, 2014; Caiazzo et al., 2011) that allows neurons to be directly transdifferentiated from fibroblasts, we generated induced neurons (iNs) from PKAN patients to establish a suitable disease model in which to study the consequences of *PANK2* dysfunction.

Material and methods

Cell culture

We used primary skin fibroblasts from three unaffected subjects (controls 1, 2 and 3, two neonatals and one adult) purchased from ATCC and from three PKAN patients selected from the Movement Disorders Bio-Bank available at the Neurogenetics Unit of the Neurological Institute 'Carlo Besta' (INCB), Milan, Italy. Two PKAN patients (marked F419fsX472(a) and F419fsX472(b), biopsy was made at the age of two and four years old) (Campanella et al., 2012) were brothers who are homozygous for the same frame shift mutation that results in a truncated PANK2 protein (F419fsX472). The third, Y190X (Hartig et al., 2006), was homozygous for a mutation that produced a truncated amino acid chain. The fibroblasts were grown in DMEM (Lonza) supplemented with 10% FBS (Lonza), 100 mg/ml streptomycin, 100 U/ml penicillin and 4 mM L-glutamine (Sigma).

Generation of iNs from human fibroblasts by direct reprogramming

Human fibroblasts from patients and controls were grown in medium for fibroblasts (DMEM, FBS, nonessential amino acids, sodium pyruvate, and penicillin/streptomycin) plated onto Matrigel-coated 24-well plates (5×10^4 cells/well). For the immune-histochemical analysis, some of these cells were plated onto Matrigel-coated glass coverslips. On the second day, the fibroblasts were infected by lentivirus in which cDNAs for transcription factors (Mash1, Nurr1, and Lmx1a) had been cloned (Caiazzo et al., 2011) under the control of a tetracycline-responsive promoter. Sixteen to twenty hours after infection, the cells were switched into fresh fibroblast medium containing doxycycline (2 mg/ml), and after a further 48 h, the medium was replaced with neuronal inducing medium (DMEM F12, 25 μg/ml insulin, 50 μg/ml transferrin, 30 nM sodium selenite, 20 nM progesterone, and 100 nM putrescine and penicillin/streptomycin) containing doxycycline (all from Sigma). The medium was changed every 2–3 days for a further 20 days.

Immunoblotting

Soluble cellular extracts for immunoblotting were obtained by lysing cells in 20 mM Tris–HCl, pH 7.4, 1% Triton X-100, and protease inhibitor cocktail (Roche) followed by centrifugation at 16,000 *g* for 10 min. Fifteen micrograms of total proteins was separated by sodium dodecyl sulphate-polyacrylamide gel electrophoresis (SDS-PAGE), and immunoblotting was performed using specific antibodies: anti-citosolic aconitase (cAco) (Campanella et al., 2012) was used at a dilution of 1:500; anti-mitochondrial aconitase (mAco) (Antibody Verify) was used at a final concentration of 1 μg/ml; the anti-β-actin antibody (Sigma) was used at a dilution of 1:6000; the mouse monoclonal anti-PANK2 (Origene) antibody was used at a dilution of 1:2000; and the mouse monoclonal anti-SDH (70 kDa subunit) (MitoScience) was used at a final concentration of 0.1 μg/ml, followed by peroxidase-labelled secondary antibodies (Sigma-Aldrich). Band intensity was revealed by the ECL-chemiluminescence kit (GE Healthcare). The total protein contents were measured using the BCA protein assay (Thermo Fisher Scientific) calibrated with bovine serum albumin.

Determination of aconitase activity

Aconitase activity was in-gel assayed as described in Tong and Rouault (2006). The patient and control fibroblasts were grown in DMEM, harvested, washed in PBS and lysed in 20 mM Tris–HCl buffer, pH 7.4, 1% Triton X-100, protease inhibitor cocktail, 2 mM citrate, 0.6 mM MnCl2, and 40 mM KCl. Soluble extracts (40 μg) in 25 mM Tris–HCl, pH 8.0, 10% glycerol, bromophenol blue, were loaded on PAGE gels containing 8% acrylamide, 132 mM Tris base, 132 mM borate, and 3.6 mM citrate in the separating gel; and 4% acrylamide, 67 mM Tris base, 67 mM borate, 3.6 mM citrate in the stacking gel. The run was performed at 180 V for 2.5 h at 4 °C. Aconitase activity was determined in the dark at 37 °C by incubating the gel in 100 mM Tris–HCl, pH 8.0, 1 mM NADP, 2.5 mM cis-aconitic acid, 5 mM MgCl2, 1.2 mM MTT, 0.3 mM phenazine methosulfate, and 5 U/ml isocitrate dehydrogenase. The quantification of the signal was performed using the NIH image software ImageJ.

Please cite this article as: Santambrogio, P., et al., Mitochondrial iron and energetic dysfunction distinguish fibroblasts and induced neurons from pantothenate kinase-associated neuro..., Neurobiol. Dis. (2015), http://dx.doi.org/10.1016/j.nbd.2015.02.030

Determination of heme content

Heme content was measured in fibroblasts from patients and controls as previously described (Santambrogio et al., 2011). Briefly, the cells were washed with phosphate-buffered saline and dissolved in 0.25 ml of 98% formic acid and incubated for 15 min. The heme content was evaluated by analysing the clear supernatant at 400 nm, with an extinction coefficient of $1.56 \times 10^5 \times M^{-1} \times cm^{-1}$. The data were normalised to protein content as determined by the BioRad Protein Assay (BioRad).

Oxidised protein detection

Oxidised proteins were detected using the OxyBlot Protein Oxidation Detection Kit (Millipore) following the manufacturer's instructions. Briefly, 10 μg of the soluble cellular extracts was derivatised to 2,4 dinitrophenylhydrazone, and 5 μg was loaded on a 12% SDS-PAGE gel, blotted and incubated with an anti-DPN antibody. The bound activity was revealed by a ECL-chemiluminescence kit (GE Healthcare).

Glutathione measurement

Fibroblasts, treated or not with 1 mM TCEP (tris[2-carboxyethyl]phosphine) for 30 min at 37 °C, were incubated with 20 μM ThiolTracker Violet (Invitrogen) for 30 min at 37 °C, washed with PBS and fixed in 4% paraformaldehyde in PBS for 20 min at room temperature. The images were acquired by Zeiss Axiovert 135 TV fluorescence microscope, and the ThiolTracker Violet signal was quantified by ImageJ software. iNs were incubated with 20 μM ThiolTracker Violet (Invitrogen) for 30 min at 37 °C, washed with PBS and fixed in 4% paraformaldehyde in PBS for 20 min at room temperature. The cells were then permeabilised for 3 min in PBS containing 0.1% Triton X100 and 10% normal goat serum. Next, the cells were incubated with Alexa Fluor 647 mouse anti-human CD56 (N-CAM, BD Biosciences, diluted 1:40) for 1 h at 37 °C, and with 2 μg/ml Hoechst for 2 min. After washing, the cells were analysed by IN Cell Analyzer 1000 system (GE Healthcare). The ThiolTracker Violet fluorescence in N-CAM-positive cells was collected to compare relative glutathione contents.

Determination of LIP

LIP was measured using the iron-sensitive fluorescent probe RPA (rhodamine B-[(1,10-phenanthrolin-5-yl)-aminocarbonyl]benzyl ester) (Squarix Biotechnology). Control of fluorescence probe incorporation was performed with RPAC (rhodamine B-[(phenanthren-9-yl)-aminocarbonyl]-benzylester), an analogue of RPA but without iron binding capacity and subsequent quenching. Briefly, fibroblasts were plated in 96-well plates and incubated with or without 100 μM FAC and 200 μM ascorbic acid (Sigma) for 18 h. The cells were incubated in HBSS supplemented with 10 mM glucose and 2 μM RPA or RPAC for 15 min at 37 °C. After two washes with HBSS, the cells were maintained in HBSS supplemented with 10 mM glucose. Basal fluorescence was measured using a Victor3 Multilabel Counter (Wallac, Perkin Elmer) at 530 nm (excitation) and 590 nm (emission). The quenching of RPA by iron was revealed after the addition of the specific iron chelator PIH (final concentration: 2 mM) for 30 min. The results were normalised for protein content.

Determination of ROS

Fibroblasts were incubated with 30 μM dihydrorhodamine-123 (DHR-123, Molecular Probes) for 15 min at 37 °C and then washed with PBS and maintained in HBSS supplemented with 10 mM glucose. The fluorescence was determined using the Victor3 Multilabel Counter (PerkinElmer) at 485 and 535 nm for excitation and emission, respectively. The cells were incubated in HBSS for 30 min at 37 °C with 0.3 M H_2O_2, and fluorescence was determined as above.

iNs generated from fibroblasts were incubated with Alexa Fluor 647 mouse anti-human CD 56 (anti-N-CAM; BD Biosciences) for 1 h, with 20 μM of 2′,7′-dichlorodihydrofluorescein diacetate (H_2DCFDA; Molecular Probes) for 15 min and with 2 μg/ml of Hoechst 33342 for 2 min. All of these incubations were performed at 37 °C. The cells were washed and analysed using an IN-Cell Analyzer 1000 system (GE Healthcare). The fluorescence of DCF from N-CAM-positive cells was collected to compare the relative ROS contents.

Determination of mitochondrial membrane potential

Fibroblasts were incubated with 4 μg/ml of oligomycin (Sigma) for 1 h at 37 °C and with 2 μg/ml of Hoechst 33342 for 2 min. Then, 20 nM of tetramethylrhodamine methyl ester (TMRM; Molecular Probes) was added, and its incorporation was followed by analysis with the IN-Cell Analyzer 1000 system for 2 h. Next, 4 μg/ml of FCCP (Sigma) was added to depolarise the mitochondrial membrane, and TMRM signal followed for other 10 min.

iNs generated from fibroblasts were incubated with Alexa Fluor 488 mouse anti-human CD 56 (anti-N-CAM; BD Biosciences) for 1 h, with 20 μM of TMRM (Molecular Probes) for 15 min, and with 2 μg/ml of Hoechst 33342 for 2 min. All of these incubations were performed at 37 °C. The cells were washed and analysed by the IN-Cell Analyzer 1000 system (GE Healthcare). The fluorescence of TMRM from N-CAM-positive cells was collected to compare the relative mitochondrial membrane potential.

Analysis of mitochondrial network and Shape Factor

The cells were plated on 35-mm glass-bottom dishes in complete DMEM. After 24 h, Mitotracker Red (Invitrogen) was added at a final concentration of 10 nM for 30 min at 37 °C. The cells were then washed three times with PBS, and a medium with 25 mM HEPES and without Phenol Red was added. Fluorescence was visualised on an Axiovert 200 epifluorescence inverted microscope (Zeiss, Germany) equipped with a 40× fluorite objective using a CARV II Confocal Imager (BD Biosciences). The images were acquired using a CCD camera (Roper Scientific, USA). All of the imaging data were collected and analysed using MetaMorph acquisition/analysis software (Universal Imaging Corp., Downingtown, PA, USA).

The amount of mitochondrial fragmentation was evaluated using the Shape Factor function of the MetaMorph software. Shape Factor evaluates the circular shape of an object and attributes a score near 0 in the case of a flattened object and a score near 1 for a perfect circle. We defined three shape factor groups to classify the different morphologies of the mitochondrial networks: Group I: shape factor 0–0.3 consisted of cells with a filamentous mitochondrial network; Group II: shape factor 0.3–0.6 consisted of cells with filamentous network but with the presence of round-shaped mitochondria; and Group III: shape factor 0.6–1 consisted of cells with high fragmentation with only round-shaped mitochondria. For each cell type, a total of 100 images, collected in four different experiments, were used to calculate the percentage of the different shape factors.

ATP evaluation

Fibroblasts were plated at 8000 cells/well in 96-well plates. The next day, total cellular ATP was measured using the ATPlite kit (PerkinElmer Life Sciences) according to the manufacturer's procedure. This method is based on the mono-oxygenation of luciferin, which is catalysed by luciferase in the presence of Mg^{2+}, ATP, and oxygen, resulting in a luminescent signal that is proportional to the ATP concentration. The plate was read on a Victor plate reader (Perkin Elmer) in luminescence mode. The cell numbers were

Please cite this article as: Santambrogio, P., et al., Mitochondrial iron and energetic dysfunction distinguish fibroblasts and induced neurons from pantothenate kinase-associated neuro..., Neurobiol. Dis. (2015), http://dx.doi.org/10.1016/j.nbd.2015.02.030

evaluated with the CyQUANT kit (Invitrogen). Total ATP was then normalised for cell number.

Statistical analyses

The data, except where otherwise indicated, are reported as the mean +/− SD values or as representative of at least three independent experiments with similar results. Statistically significant differences between controls and patients were determined in all the experiments by one-way ANOVA analyses with Bonferroni's post-test and by Student's *t*-test; *, ** and *** indicated $p < 0.05$, $p < 0.01$ and $p < 0.001$, respectively. A p value <0.05 was considered statistically significant. Both analyses gave similar significance except where specified.

Results

PKAN fibroblasts show altered iron dependent oxidative status

We analysed fibroblasts from three PKAN patients and healthy subjects. One PKAN patient carried a homozygous c.569insA mutation that resulted in a premature stop codon at amino acid position 190 (p. Y190X) (Hartig et al., 2006); the other two patients are brothers and carried a homozygous c.1259delG mutation, producing a frame shift mutation resulting in the substitution of 53 amino acids and the creation of a stop codon (F419fsX472) (Campanella et al., 2012; Zorzi et al., 2011). As shown by western-blot analysis in Fig. 1A, PANK2 is virtually absent in all three patients, whilst a normal level of the protein is present in the controls. We then determined cellular oxidative status and its relationship with iron content in these cells by treating control and PKAN fibroblasts with the iron-chelator deferoxamine (DFO) for 18 h. The content of carbonylated proteins in the DFO-treated and untreated cellular extracts was then evaluated by Oxyblot (Fig. 1B). The results confirmed that untreated PKAN fibroblasts showed increased carbonylated protein levels compared to control cells (Fig. 1B, DFO −). Interestingly, whilst DFO treatment ameliorated the level of carbonylated proteins in PKAN fibroblasts, it was completely ineffective in control fibroblasts (Fig. 1B, DFO +). Moreover, by monitoring ThiolTracker Violet intensity, we observed a significant reduction in levels of both total and reduced glutathione in PKAN fibroblasts compared to controls (Fig. 1C).

PKAN fibroblasts show mitochondrial iron homeostasis dysfunction

To verify whether the defect in PANK2 activity affected mitochondrial iron homeostasis, we tested for the presence of potentially toxic free iron (LIP) in the mitochondrial compartment using the iron sensing mitochondrial target-specific fluorescent probe (rhodamine B-[(1,10-phenanthrolin-5-yl)-aminocarbonyl]benzyl ester, RPA). This probe has been largely used with success in previous works to specifically measure the mitochondrial LIP (Cabantchik, 2014; Ma et al., 2015; Rauen et al., 2007). Rhodamine B-[(phenanthren-9-yl)-aminocarbonyl]-benzylester (RPAC), an analog of RPA but without iron binding capacity and subsequent quenching, was used to monitor the incorporation of the probe driven by mitochondrial-membrane-potential in the control and patients' cells. The cells were incubated with or without 100 mM ferric ammonium citrate (FAC) for 18 h. The RPAC fluorescence was measured and the results indicated that the amount of incorporated probe was similar in control and patients' cells in all the conditions (not shown). Then, RPA fluorescence was measured before and after the addition of the iron chelator PIH (pyridoxal isonicotinoyl hydrazone) (Rauen et al., 2007). The result indicated that the size of the mitochondrial LIP was statistically higher in PKAN fibroblasts than in control cells in both basal growth conditions (Fig. 2A) and with iron supplementation (not shown). As labile iron can promote ROS formation, we measured their generation using the ROS sensitive mitochondrial probe dihydrorhodamine 123 (DHR-123) in basal growth condition and after iron supplementation (Campanella et al., 2009). The fluorescence intensity was significantly higher in PKAN fibroblasts than in controls under basal growth conditions (Fig. 2B) and after iron addition (not shown). In PKAN cells only, this difference further increased after incubation with 0.3 mM H_2O_2 both in basal growth condition (Fig. 2C) and after iron supplementation (not shown). To test the efficiency of ISC biosynthesis, we evaluated the in-gel enzymatic activity of cAco and mAco, two ISC-containing proteins, after separation on non-denaturing PAGE (Fig. 2D, upper panel), a higher sensible method with respect to the one previously used (Campanella et al., 2012). Densitometric analysis of the bands showed a reduced enzymatic activity of both aconitase forms (Fig. 2D, lower panels). However, the amount of aconitase proteins as evaluated by western blotting with specific antibodies was similar between PKAN and control fibroblasts (not shown). Furthermore, we evaluated heme biosynthesis that, other than depending on the ISC-containing ferrochelatase, represents the other major iron-containing product in mitochondria. We measured

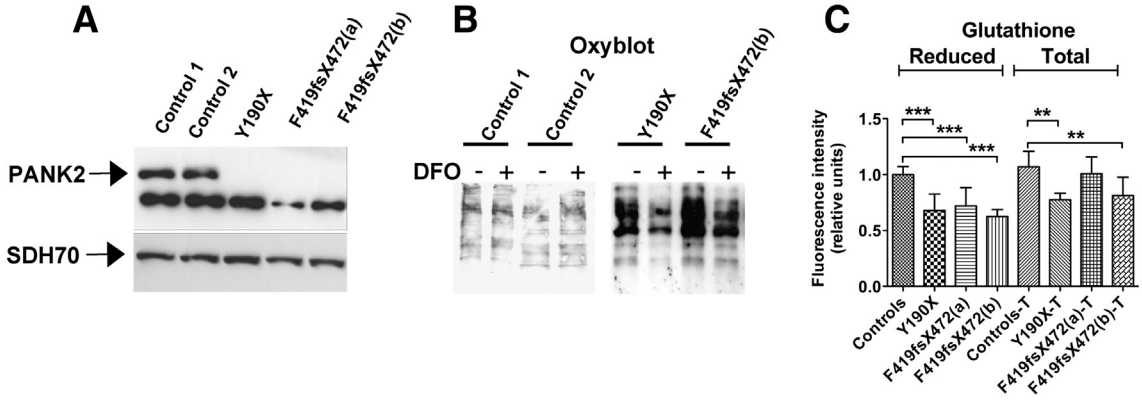

Fig. 1. PKAN fibroblasts show altered oxidative status. (A) The determination of the PANK2 protein content in fibroblast soluble extracts. The arrows point to PANK2 mature peptide (47 kDa) and to SDH70 used as loading control. The other lower band, present in patients and controls, is a non-specific reaction of the antibody. (B) The fibroblasts were treated or not with 100 μM deferoxamine (DFO) for 18 h, and the levels of carbonylated proteins in soluble cell extracts were then analysed by Oxyblot. One representative of three independent experiments is shown. (C) Measurements of total and reduced glutathione content in fibroblasts evaluated using the specific fluorescent probe ThiolTracker Violet. The images were acquired by fluorescence microscopy, and the quantified signal, relative to controls, was plotted as the mean and standard deviation of three independent experiments in triplicate. **$p < 0.01$, ***$p < 0.001$.

Please cite this article as: Santambrogio, P., et al., Mitochondrial iron and energetic dysfunction distinguish fibroblasts and induced neurons from pantothenate kinase-associated neuro..., Neurobiol. Dis. (2015), http://dx.doi.org/10.1016/j.nbd.2015.02.030

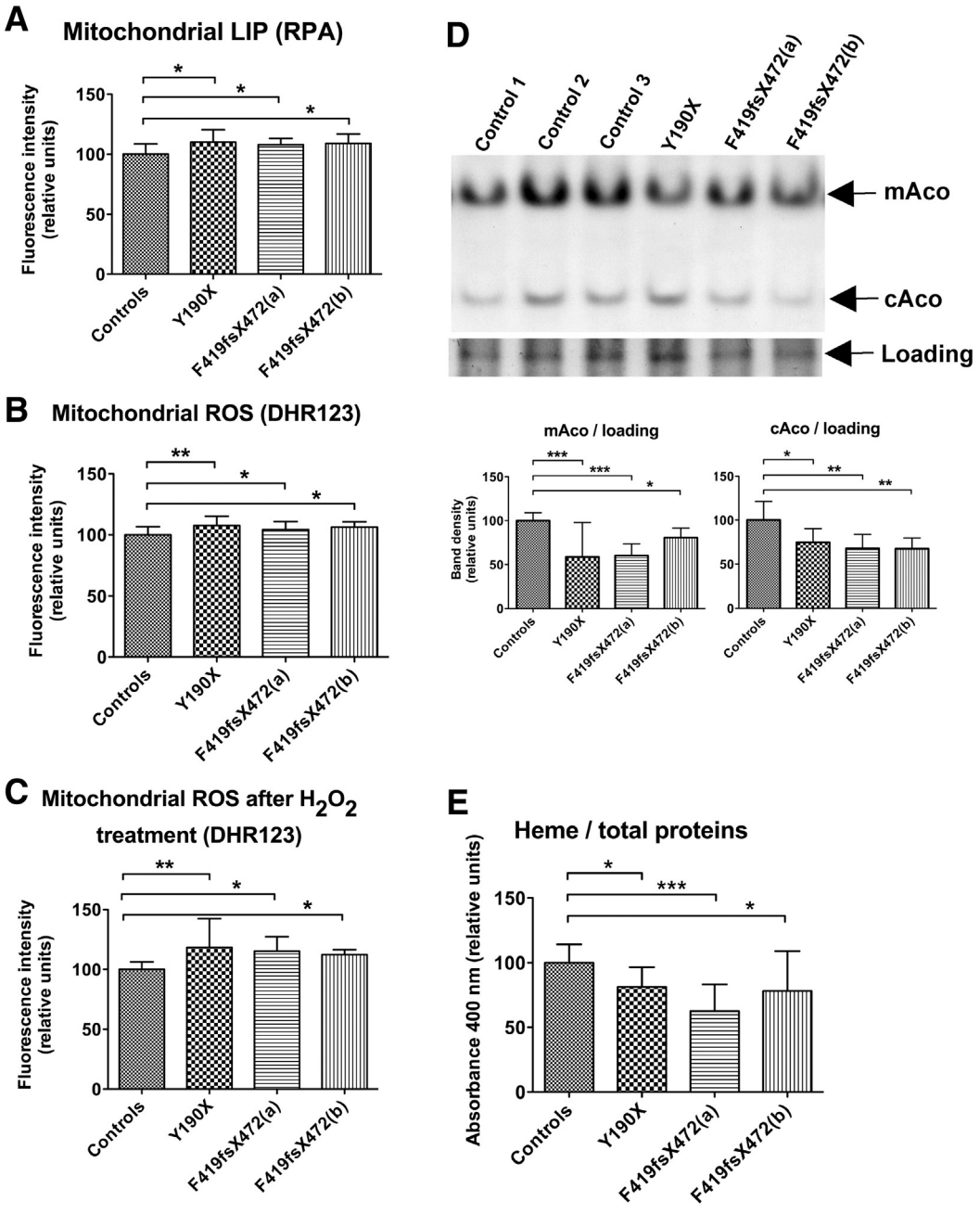

Fig. 2. PKAN fibroblasts show altered mitochondrial iron handling. (A) The evaluation of the mitochondrial LIP in untreated fibroblasts by the specific probe RPA. The mean and SD of three independent experiments made in quadruplicate, and the bars indicate statistically significant differences, * $p < 0.05$. (B and C) The cells were treated or not with 0.3 mM H_2O_2 for 30 min, and the mitochondrial ROS generation was evaluated on untreated B or treated C fibroblasts using the fluorescent probe DHR-123. The mean and SD of three independent experiments made in quadruplicate, *$p < 0.05$, **$p < 0.01$. (D) The enzymatic activity of aconitase was evaluated on soluble cell homogenates that were separated on non-denaturing PAGE gels. The arrows indicate the position of mitochondrial aconitase (mAco), of cytosolic aconitase (cAco) and of the protein band stained with Coomassie blue used for loading control. The histograms show the densitometry of aconitase bands relative to controls, with the mean and SD of three independent experiments, *$p < 0.05$, **$p < 0.01$, ***$p < 0.001$. (E) The evaluation of heme content in untreated fibroblasts by absorbance at 400 nm of the soluble cell lysates. The mean and SD of six independent experiments, *$p < 0.05$, ***$p < 0.001$.

heme content in fibroblasts by monitoring the absorbance of soluble extracts from cells lysed in formic acid at 400 nm. We observed a significant difference in heme content, corresponding to a 25% reduction in PKAN compared to the control fibroblasts (Fig. 2E).

PKAN fibroblasts show energetic mitochondrial dysfunction

We further investigated the ability of mitochondria to maintain the cellular energy requirement. The mitochondrial membrane potential was evaluated with the mitochondria-specific fluorescent probe tetramethylrhodamine methyl ester (TMRM) on fibroblasts in the presence of the ATPase inhibitor oligomycin. The kinetics of TMRM incorporation was followed for 2 h by monitoring the fluorescence of the probe using the IN-Cell Analyzer 1000 system. Starting from 30 min, the mean kinetics of the controls was statistically higher than for PKAN patient fibroblasts (Fig. 3A, *$p < 0.05$). These data indicated that the PKAN fibroblasts incorporated less probe compared to control cells, suggesting lower membrane hyperpolarisation. We investigated mitochondrial morphology after loading cells with Mitotracker Red and examination by fluorescence microscopy. The fibroblasts were scored into different categories on the basis of mitochondrial morphology. Representative images of these classes of mitochondrial morphology are shown in Fig. 3B. A total

Please cite this article as: Santambrogio, P., et al., Mitochondrial iron and energetic dysfunction distinguish fibroblasts and induced neurons from pantothenate kinase-associated neuro..., Neurobiol. Dis. (2015), http://dx.doi.org/10.1016/j.nbd.2015.02.030

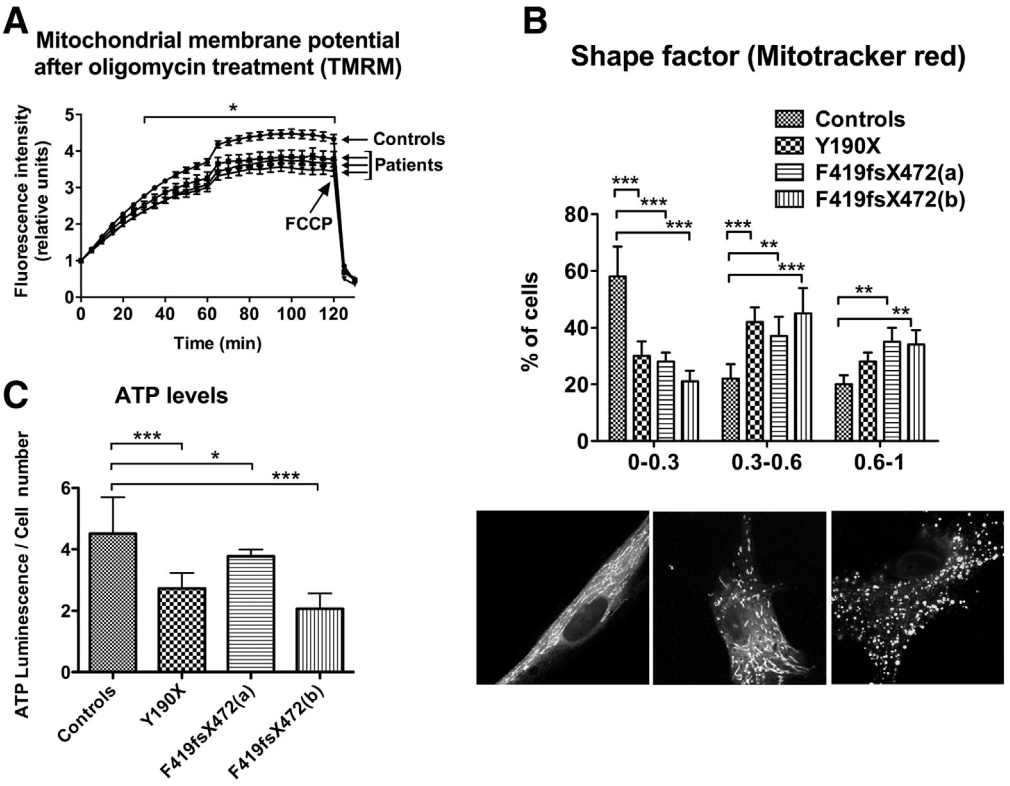

Fig. 3. PKAN fibroblasts show altered mitochondrial functionality. (A) The fibroblasts were incubated with 4 μg/ml of oligomycin for 1 h, and the mitochondrial-specific fluorescent probe TMRM was then added. Its incorporation was followed using the IN-Cell Analyzer 1000 system for 2 h. Plots, normalised on starting points, show the kinetics of TMRM incorporation, with the mean and SEM of three independent experiments, * $p < 0.05$ from 30 min with the exception of patient Y190X that resulted significant only from 60 min by one-way ANOVA analyses with Bonferroni's post-test. The arrow indicates the time of FCCP addition. (B) Fibroblasts were incubated with MitoTracker Red fluorescent probe. The evaluation of the mitochondrial shape factor was performed on images obtained by fluorescence microscopy. The histogram shows the percentage of cells with the indicated shape factor, with the mean and SD of four independent experiments, ** $p < 0.01$, *** $p < 0.001$. (C) Evaluation of ATP content in fibroblasts. Total ATP levels were evaluated by the ATPlite kit. The data are presented as the mean of two controls (reported as a single bar) and three patients, reported separately, with the mean and SD of three independent experiments. * $p < 0.05$, *** $p < 0.001$.

of 100 different images were obtained and quantified for each sample. The amount of mitochondrial fragmentation was evaluated using the Shape Factor function of MetaMorph software. This function evaluates the circular shape of an object and attributes a score near 0 in the case of a flattened object and a score near 1 for a perfect circle. The Shape Factor average of PKAN patients' fibroblasts was closer to 1 than in the control subjects. The mitochondrial network of PKAN patients with loss-of-function mutations was more fragmented than controls, indicating an impaired bioenergetic profile. The difference between these two samples was statistically significant (Fig. 3B upper panel; * $p < 0.05$; ** $p < 0.01$). In line with this observation, we observed a reduction in ATP levels in PKAN fibroblasts compared to control cells (Fig. 3C; * $p < 0.05$; ** $p < 0.01$).

Generation and characterisation of induced neurons from PKAN fibroblasts

Human neurons were generated from patient and control fibroblasts by direct neuronal reprogramming (Caiazzo et al., 2011; Cozzi et al., 2013). Lentiviruses expressing the transcription factor combination Ascl1, Nurr1 and Lmx1a were used to transduce fibroblasts to generate iNs, which were then maintained in a neurobasal medium supplemented with a cocktail of growth factors and inducing molecules (see the Material and methods section). iNs were identified in the reprogrammed cell culture by immunostaining with the specific neuronal marker class III β-tubulin (TuJ1), N-CAM and MAP2, as well as the dopaminergic-specific enzyme tyrosine hydroxylase (TH) (Fig. 4A and data not shown). At least 50% of the TuJ1-positive cells were also positive for TH. We used TuJ1-positive cells to evaluate neuronal reprogramming efficiency, which was approximately 5% and comparable between PKAN and control cells (Fig. 4B). We then used iNs to evaluate several parameters, including the oxidative status and mitochondrial functionality. Due to the low efficiency of direct cellular reprogramming, we developed a method for in vivo analysis at single cell level by selecting the live neurons using the specific neuronal membrane marker N-CAM.

PKAN induced neurons show altered oxidative status

First, we analysed the amount of ROS specifically present in iNs grown in basal conditions. The cells were incubated with the fluorescent ROS-sensitive dichlorofluorescein (DCF), and the images were acquired by the IN-Cell Analyzer 1000 system. The identity of iNs was verified by the expression of the neuronal specific marker N-CAM, and only the N-CAM-positive cells were utilised to calculate the fluorescence of the DCF (Fig. 4C). The quantification of fluorescent intensity specific to iNs indicated that PKAN iNs contained higher ROS levels than control iNs (Fig. 4D). Moreover, an analysis of ThiolTracker Violet treated cells revealed that PKAN iNs contained significant lower reduced glutathione levels compared to control iNs (Fig. 4E).

PKAN induced neurons show alterations in mitochondrial membrane potential

A similar approach was used to evaluate mitochondrial functionality in neuronal cells. We measured mitochondrial membrane potential by quantifying the TMRM signal 15 min after treatment with the probe; the images were collected as above. As previously described, only N-CAM-positive cells were utilised to calculate the TMRM fluorescence (Fig. 4F). The quantification of TMRM intensity showed that PKAN iNs had significantly lower membrane potentials compared to control iNs (Fig. 4G).

Please cite this article as: Santambrogio, P., et al., Mitochondrial iron and energetic dysfunction distinguish fibroblasts and induced neurons from pantothenate kinase-associated neuro..., Neurobiol. Dis. (2015), http://dx.doi.org/10.1016/j.nbd.2015.02.030

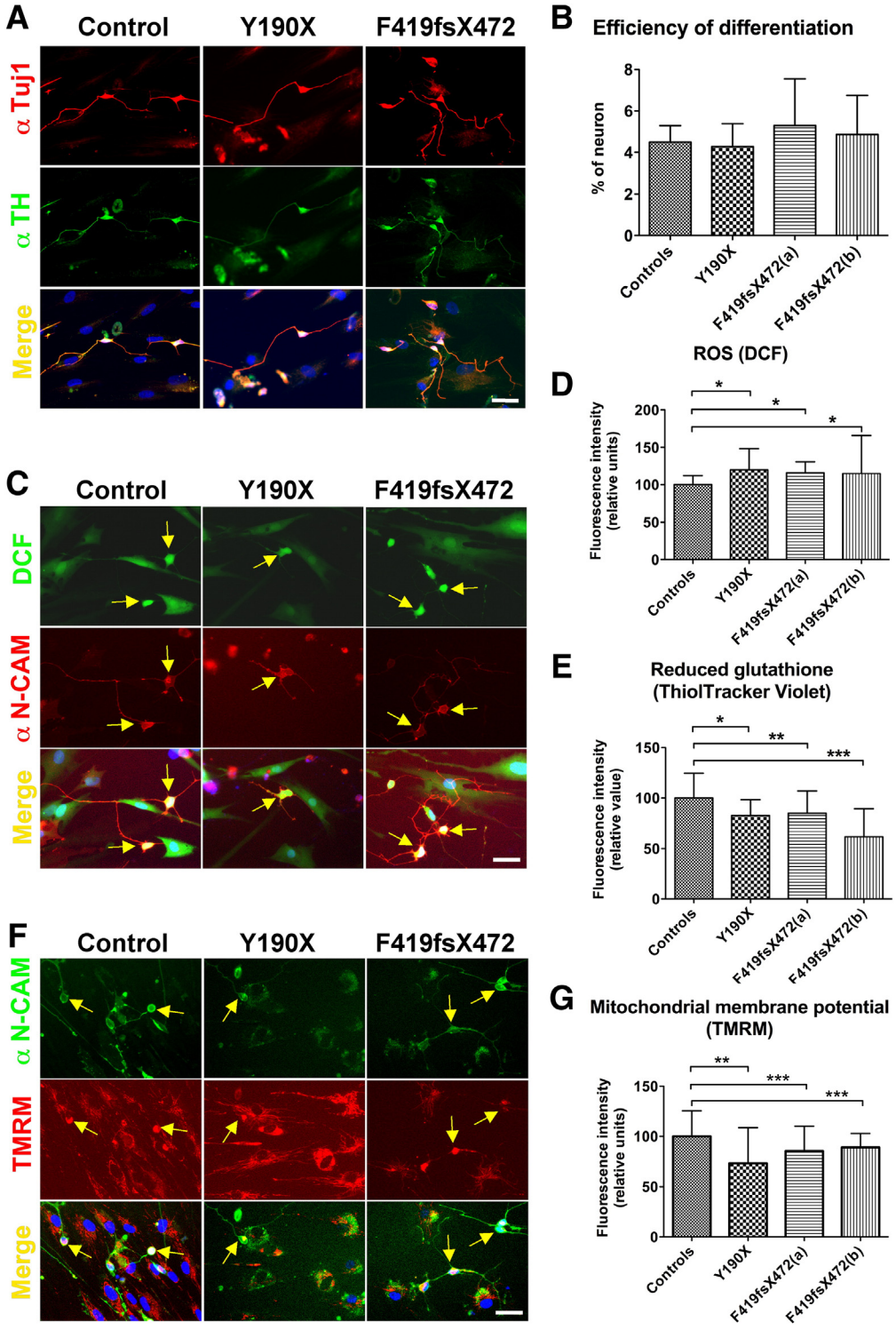

Fig. 4. Characterisation of induced neurons obtained from PKAN fibroblasts by direct reprogramming. (A) The induced neurons were stained for neuronal class III beta tubulin (α-Tuj1, top panels in red) and tyrosine hydroxylase (α-TH, middle panels in green). Hoechst was used to stain cell nuclei (in blue), and the lower panels show the merged images, scale bar = 100 μm. Tuj1, a neuronal marker, was used to calculate the reprogramming efficiency, and the results are plotted in panel B. (C) Live cells stained with the ROS-sensing fluorescent probe DCF (top panels in green) and with the neuron-specific anti-N-CAM antibody (middle panels in red); merged images are shown in the lower panels, with the nuclei stained with Hoechst. The fluorescence was analysed using the IN Cell Analyser 1000 System, scale bar = 100 μm. (D) The DCF fluorescence signal from N-CAM-positive cells (from panel C) were quantified, and the data are shown in the plots as the mean and SD of three independent experiments (at least 50 neurons per type), $^{*}p < 0.05$. (E) The ThiolTracker Violet fluorescence signal from N-CAM-positive cells was quantified (experiments were performed as in panel C, with ThiolTracker in place of DCF), and the data are shown in the plots as the mean and SD of three independent experiments (at least 50 neurons per type), $^{*}p < 0.05$, $^{**}p < 0.01$. (F) Live cells were stained with the mitochondrial membrane potential sensible fluorescent probe TMRM (middle panels in red) and with the neuron-specific α-N-CAM antibody (top panels in green). The merged images are shown in the lower panels, with nuclei stained with Hoechst. The fluorescence was analysed using an IN-cell analyser, scale bar = 100 μm. (G) The TMRM fluorescence signal from N-CAM-positive cells (from panel F) was quantified, and the data are shown in the plots as the mean and SD of three independent experiments (at least 50 neurons per type), $^{**}p < 0.01$, $^{***}p < 0.001$.

Please cite this article as: Santambrogio, P., et al., Mitochondrial iron and energetic dysfunction distinguish fibroblasts and induced neurons from pantothenate kinase-associated neuro..., Neurobiol. Dis. (2015), http://dx.doi.org/10.1016/j.nbd.2015.02.030

Discussion

PKAN is a severe and disabling neurodegenerative disorder, the pathogenic mechanisms of which are largely unknown (Zhou et al., 2001). The low amount of CoA due to the PANK2 enzymatic defect has a devastating impact on many biological processes. CoA is utilised as a cofactor in approximately 4% of all known enzymes; thus, its imbalance inhibits a wide range of enzymatic pathways (Leonardi et al., 2005). This effect was highlighted by the studies of PKAN disease models in flies and mice. These analyses revealed different types of CoA-deficiency related phenotype, such as the following: sterility (Afshar et al., 2001; Kuo et al., 2005); abnormal locomotor function, neurodegeneration, and reduced life span (Bosveld et al., 2008); mitochondrial impairment (Brunetti et al., 2012; Rana et al., 2010); altered cytoskeleton function (Siudeja et al., 2012); protein acetylation (Siudeja et al., 2011); disrupted circadian locomotor patterns and a unique transcriptional signature (Pandey et al., 2013). However, all of these investigations have not clarified the mechanism of one of the major features of the human disease, brain iron accumulation, which has not been reported neither in flies nor in mice (Brunetti et al., 2012; Rana et al., 2010).

To approach this question, we previously examined iron metabolism in PKAN fibroblasts, demonstrating an abnormal behaviour of *PANK2* deficient cells in response to treatment with iron and the consequent alteration of oxidative status (Campanella et al., 2012). In the previous study, we concentrated our attention on cytosolic iron handling. As mitochondrial iron homeostasis and cytosolic iron homeostasis are strictly interrelated, we hypothesised that iron mishandling could also occur in the mitochondria, thereby affecting organelle functionality. For this reason, we extended our analysis to mitochondria to determine whether and how mitochondrial iron alteration could impact on the cell's bioenergetic profile. Interestingly, we detected a larger mitochondrial LIP also under basal conditions, whereas the increase in the size of the cytosolic LIP was appreciable only after chronic iron supplementation (Campanella et al., 2012). Nevertheless, the availability of high levels of mitochondrial iron did not appear to be properly utilised in ISC and heme biosynthesis, thus they resulted defective in PKAN fibroblasts. The reasons why this occurs and how the PANK2 deficiency is involved are still obscure. Very recent data, obtained on isolated mammalian mitochondria, demonstrated that ISC biosynthesis requires, other than iron and sulphur, also GTP, NADH and ATP (Pandey et al., 2015). A very reliable hypothesis could be that the impairment of the Krebs cycle due to CoA deficiency might result in lower production of GTP and NADH, with the consequent partial iron utilisation in ISC biosynthesis.

Moreover, LIP and ROS are tightly controlled in cell and large variations are not expected. In fact, the detected increased size of the LIP resulted in a slight increase in mitochondrial ROS production, which plays a central role in the regulation of ISC enzyme activity and, in particular, in Acos enzyme functions. Both the cAco and mAco contain [4Fe–4S] clusters that are responsible for their catalytic activity, which is regulated by reversible oxidation (Bulteau et al., 2003). The main role of mAco is to control cellular ATP production via the regulation of intermediate flux in the Krebs cycle. cAco has two different functions: in the ISC-containing form, it operates as an enzyme, whereas in the oxidised form, it is involved in the control of iron–protein translation as IRP1 (Lushchak et al., 2014). Thus, the reduction of their activities, caused by their higher oxidation produced by ROS or by diminished production of ISC, has an effect both on ATP production and iron homeostasis, which we demonstrated to be altered in PKAN fibroblasts.

In addition, other mitochondrial features appeared defective in patients' cells, such as the mitochondrial membrane potential and mitochondrial morphology, suggesting a global organelle impairment, which can lead to energetic failure. Interestingly, a mitochondrial morphology alteration was also recently reported in the muscles of a PKAN patient with a defined genetic mutation (Brunetti et al., 2014), indicating that variation of mitochondrial morphology can also be detected in vivo in different patient cell types. An altered mitochondrial membrane potential was also detected in neurons derived from a *Pank2* KO mouse model (Brunetti et al., 2012).

Obviously, we cannot exclude the possibility that the energetic impairment detected in PKAN fibroblasts could also derive from membrane alterations due to CoA deficiency-induced defects in phospholipid synthesis; more detailed studies are needed to clarify this point. In fact, the partial mitochondrial swelling and depolarisation detected in PKAN fibroblasts suggest mitochondrial membrane damage. However, as reported by previous studies on isolated rat liver mitochondria, iron may catalyse the peroxidation of lipids in the mitochondrial inner membrane, which can result in a limited depolarisation (Gall et al., 2012). Mitochondrial membrane depolarisation is a strong stimulus for opening the mitochondrial permeability transition pore (Bernardi et al., 1992; Gogvadze et al., 2003), which is considered one of the causative events of neuronal injury (Crompton, 2004). The opening of the pore may facilitate mitochondrial iron import from the cytosolic compartment, further increasing the size of the mtLIP, not utilised by the intra-mitochondrial biosynthetic pathways, thus exacerbating the injury.

Extensive studies on *Saccharomyces cerevisiae* demonstrated that the cells respond to reduced ISC synthesis with increased cellular iron uptake and intracellular iron re-distribution, resulting in mitochondrial iron accumulation until the metal precipitates as an amorphous mineral (Lill and Muhlenhoff, 2008). These pathologic events have also been described to occur in human disorders, such as Friedreich's ataxia (Koeppen et al., 2007; Vaubel and Isaya, 2013) and Parkinson disease (Horowitz and Greenamyre, 2010a; Mastroberardino et al., 2009) as well as during the physiological ageing process (Isaya, 2014). In fact, in recent times, there has been growing evidence of the role of mitochondrial iron dysfunction in the pathogenesis of common neurodegenerative diseases (Horowitz and Greenamyre, 2010b). Overall, the data indicate that defects in mitochondrial ISC biogenesis seem to represent a common primary mechanism, which triggers abnormal intracellular iron distribution. This effect results in cytosolic iron starvation and mitochondrial iron accumulation, oxidative phosphorylation deficits and oxidative stress (Isaya, 2014; Nunez et al., 2012).

To clarify whether this abnormal iron distribution has a primary or a secondary etiopathological role or is simply an epiphenomenon, more work on different disease models is necessary. In any case, even if iron dysregulation in PKAN may play a secondary role, its accumulation is harmful and can aggravate the damage observed in the basal ganglia, thus possibly justifying the iron chelation treatment proposed in patients (Zorzi et al., 2011). Certain brain regions, such as the globus pallidus and the substantia nigra, have high iron contents, which are necessary for the synthesis of neurotransmitters. These regions are particularly prone to the process of abnormal intracellular iron distribution, which may also contribute to the age-dependent iron accumulation (Isaya, 2014; Urrutia et al., 2013). We approached this question employing direct neuronal cell reprogramming technology (Amamoto and Arlotta, 2014; Caiazzo et al., 2011), which allowed us to obtain human neurons starting from fibroblasts. Although this technique has an overall low efficiency in neuronal generation, we succeeded in obtaining enough neurons from PKAN and healthy subject fibroblasts for an in depth analysis. Our data indicate that it is feasible to generate human neuronal cells, even in cases of genetic alterations that lead to mitochondrial impairment, as in the case of PKAN. In addition, as previously determined in fibroblasts, our results confirm, for the first time in PKAN induced neurons, the presence of an altered oxidative status in basal conditions and the impairment of mitochondrial functions. iN technology represents a very powerful system to investigate disease-relevant pathogenetic mechanisms. However, this technology does not currently allow the generation of striatal neurons, which represent the most affected neuronal population in PKAN. Considering how fast direct neuronal reprogramming technologies have been developing, we predict that an even more appropriate human neuronal model will be soon available to further investigate PKAN pathogenetic mechanisms. Nevertheless, our approach has enabled the identification of altered

Please cite this article as: Santambrogio, P., et al., Mitochondrial iron and energetic dysfunction distinguish fibroblasts and induced neurons from pantothenate kinase-associated neuro..., Neurobiol. Dis. (2015), http://dx.doi.org/10.1016/j.nbd.2015.02.030

biological processes that are relevant in diseased neurons; therefore, the present results are more relevant than the analyses of other cell types. Our results indicate that PANK-iNs might also represent a suitable system for establishing medium-scale drug screenings to identify new candidate therapeutic compounds for this disease.

Conflict of interested statement

None declared.

Acknowledgements

The financial support of Telethon-Italia (Grant no. GGP11088) is gratefully acknowledged (to SL and VT), of AISNAF to SL, of TIRCON project of the European Commission's Seventh Framework Programme (FP7/2007–2013, HEALTH-F2-2011, grant agreement No. 277984) to VT and of the European Research Council (AdERC #340527) to VB are gratefully acknowledged.

The authors wish to thank Dr. Alberto Locca for experimental support, Dr. Des Richardson for providing us the iron chelators, and Dr. Alessandro Campanella for critical reading of the manuscript. Part of this work was carried out in ALEMBIC, an advanced microscopy laboratory established by the San Raffaele Scientific Institute and the Vita-Salute San Raffaele University. The authors would also like to thank the Cell lines and DNA Bank of Paediatric Movement Disorders and Neurodegenerative Diseases of the Telethon Genetic Biobank Network, which is supported by TELETHON Italy (project n. GTB09003) and the Bank for the Diagnosis and Research of Movement Disorders (MDB) of the EuroBiobank.

References

Afshar, K., Gonczy, P., DiNardo, S., Wasserman, S.A., 2001. Fumble encodes a pantothenate kinase homolog required for proper mitosis and meiosis in *Drosophila melanogaster*. Genetics 157, 1267–1276.

Amamoto, R., Arlotta, P., 2014. Development-inspired reprogramming of the mammalian central nervous system. Science 343, 1239882.

Angelini, L., Nardocci, N., Rumi, V., Zorzi, C., Strada, L., Savoiardo, M., 1992. Hallervorden–Spatz disease: clinical and MRI study of 11 cases diagnosed in life. J. Neurol. 239, 417–425.

Bernardi, P., Vassanelli, S., Veronese, P., Colonna, R., Szabo, I., Zoratti, M., 1992. Modulation of the mitochondrial permeability transition pore. Effect of protons and divalent cations. J. Biol. Chem. 267, 2934–2939.

Bosveld, F., Rana, A., van der Wouden, P.E., Lemstra, W., Ritsema, M., Kampinga, H.H., Sibon, O.C., 2008. De novo CoA biosynthesis is required to maintain DNA integrity during development of the Drosophila nervous system. Hum. Mol. Genet. 17, 2058–2069.

Brunetti, D., Dusi, S., Morbin, M., Uggetti, A., Moda, F., D'Amato, I., Giordano, C., et al., 2012. Pantothenate kinase-associated neurodegeneration: altered mitochondria membrane potential and defective respiration in Pank2 knock-out mouse model. Hum. Mol. Genet. 21, 5294–5305.

Brunetti, D., Dusi, S., Giordano, C., Lamperti, C., Morbin, M., Fugnanesi, V., Marchet, S., et al., 2014. Pantethine treatment is effective in recovering the disease phenotype induced by ketogenic diet in a pantothenate kinase-associated neurodegeneration mouse model. Brain 137, 57–68.

Bulteau, A.L., Ikeda-Saito, M., Szweda, L.I., 2003. Redox-dependent modulation of aconitase activity in intact mitochondria. Biochemistry 42, 14846–14855.

Cabantchik, Z.I., 2014. Labile iron in cells and body fluids: physiology, pathology, and pharmacology. Front. Pharmacol. 5, 45.

Caiazzo, M., Dell'Anno, M.T., Dvoretskova, E., Lazarevic, D., Taverna, S., Leo, D., Sotnikova, T.D., et al., 2011. Direct generation of functional dopaminergic neurons from mouse and human fibroblasts. Nature 476, 224–227.

Campanella, A., Rovelli, E., Santambrogio, P., Cozzi, A., Taroni, F., Levi, S., 2009. Mitochondrial ferritin limits oxidative damage regulating mitochondrial iron availability: hypothesis for a protective role in Friedreich ataxia. Hum. Mol. Genet. 18, 1–11.

Campanella, A., Privitera, D., Guaraldo, M., Rovelli, E., Barzaghi, C., Garavaglia, B., et al., 2012. Skin fibroblasts from pantothenate kinase-associated neurodegeneration patients show altered cellular oxidative status and have defective iron-handling properties. Hum. Mol. Genet. 21, 4049–4059.

Cozzi, A., Santambrogio, P., Privitera, D., Broccoli, V., Rotundo, L.I., Garavaglia, B., Benz, R., et al., 2013. Human L-ferritin deficiency is characterized by idiopathic generalized seizures and atypical restless leg syndrome. J. Exp. Med. 210, 1779–1791.

Crompton, M., 2004. Mitochondria and aging: a role for the permeability transition? Aging Cell 3, 3–6.

Gall, J., JJr, Skrha, Buchal, R., Sedlackova, E., Verebova, K., Platenik, J., 2012. Induction of the mitochondrial permeability transition (MPT) by micromolar iron: liberation of calcium is more important than NAD(P)H oxidation. Biochim. Biophys. Acta 1817, 1537–1549.

Garcia, M., Leonardi, R., Zhang, Y.M., Rehg, J.E., Jackowski, S., 2012. Germline deletion of pantothenate kinases 1 and 2 reveals the key roles for CoA in postnatal metabolism. PLoS ONE 7, e40871.

Gogvadze, V., Walter, P.B., Ames, B.N., 2003. The role of Fe^{2+}-induced lipid peroxidation in the initiation of the mitochondrial permeability transition. Arch. Biochem. Biophys. 414, 255–260.

Hartig, M.B., Hortnagel, K., Garavaglia, B., Zorzi, G., Kmiec, T., Klopstock, T., Rostasy, K., et al., 2006. Genotypic and phenotypic spectrum of PANK2 mutations in patients with neurodegeneration with brain iron accumulation. Ann. Neurol. 59, 248–256.

Hayflick, S.J., 2014. Defective pantothenate metabolism and neurodegeneration. Biochem. Soc. Trans. 42, 1063–1068.

Horowitz, M.P., Greenamyre, J.T., 2010a. Gene–environment interactions in Parkinson's disease: the importance of animal modeling. Clin. Pharmacol. Ther. 88, 467–474.

Horowitz, M.P., Greenamyre, J.T., 2010b. Mitochondrial iron metabolism and its role in neurodegeneration. J. Alzheimers Dis. 20 (Suppl. 2), S551–S568.

Isaya, G., 2014. Mitochondrial iron–sulfur cluster dysfunction in neurodegenerative disease. Front. Pharmacol. 5, 29.

Koeppen, A.H., Michael, S.C., Knutson, M.D., Haile, D.J., Qian, J., Levi, S., Santambrogio, P., Garrick, M.D., Lamarche, J.B., 2007. The dentate nucleus in Friedreich's ataxia: the role of iron-responsive proteins. Acta Neuropathol. 114, 163–173.

Kruer, M.C., Hiken, M., Gregory, A., Malandrini, A., Clark, D., Hogarth, P., Grafe, M., Hayflick, S.J., Woltjer, R.L., 2011. Novel histopathologic findings in molecularly-confirmed pantothenate kinase-associated neurodegeneration. Brain 134, 947–958.

Kuo, Y.M., Duncan, J.L., Westaway, S.K., Yang, H., Nune, G., Xu, E.Y., Hayflick, S.J., Gitschier, J., 2005. Deficiency of pantothenate kinase 2 (Pank2) in mice leads to retinal degeneration and azoospermia. Hum. Mol. Genet. 14, 49–57.

Leonardi, R., Zhang, Y.M., Rock, C.O., Jackowski, S., 2005. Coenzyme A: back in action. Prog. Lipid Res. 44, 125–153.

Leonardi, R., Zhang, Y.M., Lykidis, A., Rock, C.O., Jackowski, S., 2007. Localization and regulation of mouse pantothenate kinase 2. FEBS Lett. 581, 4639–4644.

Leoni, V., Strittmatter, L., Zorzi, G., Zibordi, F., Dusi, S., Garavaglia, B., Venco, P., et al., 2012. Metabolic consequences of mitochondrial coenzyme A deficiency in patients with PANK2 mutations. Mol. Genet. Metab. 105, 463–471.

Levi, S., Finazzi, D., 2014. Neurodegeneration with brain iron accumulation: update on pathogenic mechanisms. Front. Pharmacol. 5, 99.

Levi, S., Rovida, E., 2009. The role of iron in mitochondrial function. Biochim. Biophys. Acta 1790, 629–636.

Lill, R., Muhlenhoff, U., 2008. Maturation of iron–sulfur proteins in eukaryotes: mechanisms, connected processes, and diseases. Annu. Rev. Biochem. 77, 669–700.

Lushchak, O.V., Piroddi, M., Galli, F., Lushchak, V.I., 2014. Aconitase post-translational modification as a key in linkage between Krebs cycle, iron homeostasis, redox signaling, and metabolism of reactive oxygen species. Redox Rep. 19, 8–15.

Ma, Y., Abbate, V., Hider, R.C., 2015. Iron-sensitive fluorescent probes: monitorino intracellular iron pools. Metallomics 7 (2), 212–222.

Mastroberardino, P.G., Hoffman, E.K., Horowitz, M.P., Betarbet, R., Taylor, G., Cheng, D., Na, H.M., et al., 2009. A novel transferrin/TfR2-mediated mitochondrial iron transport system is disrupted in Parkinson's disease. Neurobiol. Dis. 34, 417–431.

Nunez, M.T., Urrutia, P., Mena, N., Aguirre, P., Tapia, V., Salazar, J., 2012. Iron toxicity in neurodegeneration. Biometals 25, 761–776.

Pandey, V., Turm, H., Bekenstein, U., Shifman, S., Kadener, S., 2013. A new in vivo model of pantothenate kinase-associated neurodegeneration reveals a surprising role for transcriptional regulation in pathogenesis. Front. Cell. Neurosci. 7, 146. http://dx.doi.org/10.3389/fncel.2013.00146. eCollection 2013.

Pandey, A., Pain, J., Ghosh, A.K., Dancis, A., Pain, D., 2015. Fe–S cluster biogenesis in isolated mammalian mitochondria: coordinated use of persulfide sulfur and iron and requirements for GTP, NADH, and ATP. J. Biol. Chem. 290 (1), 640–657.

Perry, T.L., Norman, M.G., Yong, V.W., Whiting, S., Crichton, J.U., Hansen, S., Kish, S.J., 1985. Hallervorden–Spatz disease: cysteine accumulation and cysteine dioxygenase deficiency in the globus pallidus. Ann. Neurol. 18, 482–489.

Poli, M., Derosas, M., Luscieti, S., Cavadini, P., Campanella, A., Verardi, R., Finazzi, D., Arosio, P., 2010. Pantothenate kinase-2 (Pank2) silencing causes cell growth reduction, cell-specific ferroportin upregulation and iron deregulation. Neurobiol. Dis. 39, 204–210.

Rana, A., Seinen, E., Siudeja, K., Muntendam, R., Srinivasan, B., van der Want, J.J., Hayflick, S., et al., 2010. Pantethine rescues a Drosophila model for pantothenate kinase-associated neurodegeneration. Proc. Natl. Acad. Sci. U. S. A. 107, 6988–6993.

Rauen, U., Springer, A., Weisheit, D., Petrat, F., Korth, H.G., de Groot, H., Sustmann, R., 2007. Assessment of chelatable mitochondrial iron by using mitochondrion-selective fluorescent iron indicators with different iron-binding affinities. Chembiochem 8, 341–352.

Santambrogio, P., Erba, B.G., Campanella, A., Cozzi, A., Causarano, V., Cremonesi, L., Gallì, A., et al., 2011. Over-expression of mitochondrial ferritin affects the JAK2/STAT5 pathway in K562 cells and causes mitochondrial iron accumulation. Haematologica 96, 1424–1432.

Schneider, S.A., Zorzi, G., Nardocci, N., 2013. Pathophysiology and treatment of neurodegeneration with brain iron accumulation in the pediatric population. Curr. Treat. Options Neurol. 15, 652–667.

Siudeja, K., Srinivasan, B., Xu, L., Rana, A., de Jong, J., Nollen, E.A., Jackowski, S., et al., 2011. Impaired coenzyme A metabolism affects histone and tubulin acetylation in Drosophila and human cell models of pantothenate kinase associated neurodegeneration. EMBO Mol. Med. 3, 755–766.

Siudeja, K., Grzeschik, N.A., Rana, A., de Jong, J., Sibon, O.C., 2012. Cofilin/Twinstar phosphorylation levels increase in response to impaired coenzyme a metabolism. PLoS ONE 7, e43145.

Please cite this article as: Santambrogio, P., et al., Mitochondrial iron and energetic dysfunction distinguish fibroblasts and induced neurons from pantothenate kinase-associated neuro..., Neurobiol. Dis. (2015), http://dx.doi.org/10.1016/j.nbd.2015.02.030

Stehling, O., Wilbrecht, C., Lill, R., 2014. Mitochondrial iron–sulfur protein biogenesis and human disease. Biochimie 100, 61–77.
Tong, W.H., Rouault, T.A., 2006. Functions of mitochondrial ISCU and cytosolic ISCU in mammalian iron–sulfur cluster biogenesis and iron homeostasis. Cell Metab. 3, 199–210.
Urrutia, P., Aguirre, P., Esparza, A., Tapia, V., Mena, N.P., Arredondo, M., Gonzalez-Billault, C., Nunez, M.T., 2013. Inflammation alters the expression of DMT1, FPN1 and hepcidin, and it causes iron accumulation in central nervous system cells. J. Neurochem. 126, 541–549.
Vaubel, R.A., Isaya, G., 2013. Iron–sulfur cluster synthesis, iron homeostasis and oxidative stress in Friedreich ataxia. Mol. Cell. Neurosci. 55, 50–61.
Zhou, B., Westaway, S.K., Levinson, B., Johnson, M.A., Gitschier, J., Hayflick, S.J., 2001. A novel pantothenate kinase gene (PANK2) is defective in Hallervorden–Spatz syndrome. Nat. Genet. 28, 345–349.
Zorzi, G., Zibordi, F., Chiapparini, L., Bertini, E., Russo, L., Piga, A., Longo, F., et al., 2011. Iron-related MRI images in patients with pantothenate kinase-associated neurodegeneration (PKAN) treated with deferiprone: results of a phase II pilot trial. Mov. Disord. 26, 1756–1759.

Please cite this article as: Santambrogio, P., et al., Mitochondrial iron and energetic dysfunction distinguish fibroblasts and induced neurons from pantothenate kinase-associated neuro..., Neurobiol. Dis. (2015), http://dx.doi.org/10.1016/j.nbd.2015.02.030

microbial cell

Research Article

www.microbialcell.com

Modeling human Coenzyme A synthase mutation in yeast reveals altered mitochondrial function, lipid content and iron metabolism

Camilla Ceccatelli Berti[1], Cristina Dallabona[1], Mirca Lazzaretti[1], Sabrina Dusi[2], Elena Tosi[1], Valeria Tiranti[2], Paola Goffrini[1,*]

[1] Department of Life Sciences, University of Parma, Parma, Italy.

[2] Unit of Molecular Neurogenetics – Pierfranco and Luisa Mariani Center for the study of Mitochondrial Disorders in Children, IRCCS Foundation Neurological Institute "C. Besta", Milan, Italy.

* Corresponding Author: Paola Goffrini, Department of Life Sciences, University of Parma, Parco Area delle Scienze 11/A; 43123 Parma, Italy; Tel: +39 0521905107; Fax: +39 0521905604; E-mail: paola.goffrini@unipr.it

ABSTRACT Mutations in nuclear genes associated with defective coenzyme A biosynthesis have been identified as responsible for some forms of neurodegeneration with brain iron accumulation (NBIA), namely PKAN and CoPAN. PKAN are defined by mutations in *PANK2*, encoding the pantothenate kinase 2 enzyme, that account for about 50% of cases of NBIA, whereas mutations in CoA synthase *COASY* have been recently reported as the second inborn error of CoA synthesis leading to CoPAN. As reported previously, yeast cells expressing the pathogenic mutation exhibited a temperature-sensitive growth defect in the absence of pantothenate and a reduced CoA content. Additional characterization revealed decreased oxygen consumption, reduced activities of mitochondrial respiratory complexes, higher iron content, increased sensitivity to oxidative stress and reduced amount of lipid droplets, thus partially recapitulating the phenotypes found in patients and establishing yeast as a potential model to clarify the pathogenesis underlying PKAN and CoPAN diseases.

doi: *10.15698/mic2015.04.196*
Received *originally: 05.12.2014;*
in revised form: 16.03.2015,
Accepted *22.03.2015,*
Published *06.04.2015.*

Keywords*: Saccharomyces cerevisiae, yeast model, Coenzyme A, NBIA, COASY, mitochondria, iron accumulation, lipid content.*

Abbreviations:
COASY - Coenzyme A synthase,
CoPAN - COASY protein-associated neurodegeneration,
COX - cytochrome c oxidase,
NCCR - NADH-cytochrome c oxidoreductase,
NBIA - neurodegeneration with brain iron accumulation,
PKAN - pantothenate kinase associated neurodegeneration.

INTRODUCTION

In all living cells Coenzyme A (CoA) is the major carrier of acetyl and acyl groups playing a central role in basic cellular functions such as lipids metabolism, Krebs cycle and aminoacid biosynthesis. CoA biosynthesis proceeds through a highly conserved pathway, involving five enzymatic steps: pantothenic acid (vitamin B5) phosphorylation, cysteine conjugation, decarboxylation, conjugation to an adenosyl group and phosphorylation.

Whereas in mammals the last two steps are catalyzed by Coenzyme A synthase (COASY), a mitochondrial bifunctional enzyme possessing both 4'-phospho-pantetheine adenylyltransferase (PPAT) and dephospho-CoA kinase (DPCK) activities [1, 2], in other organisms, such as yeast, PPAT and DPCK activities reside in two different enzymes, Cab4 and Cab5, the products of the essential genes *CAB4* and *CAB5* [3] whose compartmentalization is not well understood.

Recently, it has been reported that dysfunctions of CoA biosynthetic pathway may play a role in the pathogenesis of neurodegeneration with brain iron accumulation (NBIA), a wide spectrum of clinically and genetically heterogeneous diseases characterized by progressive neurodegeneration and high iron content in specific brain region [4, 5, 6].

This concept is supported by the fact that mutations in *PANK2,* encoding the first enzyme in the CoA synthesis, approximately account for 50% of NBIA cases, classified as PKAN (Pantothenate Kinase Associated Neurodegeneration) [7, 8]. Moreover *COASY* gene has been identified as a novel NBIA-associated gene and these NBIA cases have been termed CoPAN (COASY Protein-Associated Neurodegeneration)[9].

Neurodegenerative diseases are often characterized by mitochondrial dysfunctions, altered lipid metabolism and iron accumulation [10, 11, 12] and several evidences linking PKAN and CoPAN to these metabolic alterations have been reported [8, 13, 14, 15, 16].

The development of cellular and animal models is crucial for advancing our understanding of the pathophysiology of these diseases. In the last decade, the yeast *Saccharomyces cerevisiae* has been used as *in vivo* model system to gain insights into the molecular basis of mitochondrial pathologies and neurodegenerative disorders [17, 18]. Despite their simplicity, yeast cells possess most of the basic cellular machinery including pathways required for energy metabolism and protein homeostasis. Moreover, many of the genes and biological systems that function in yeast iron homeostasis are conserved throughout eukaryotes [19].

To investigate if defective CoA metabolism could underlie a more general disequilibrium of lipid metabolism and mitochondrial dysfunctions and its relationship with brain iron accumulation, we have performed phenotypic and biochemical investigation in a recently developed yeast model expressing the pathogenic missense mutation *COASY*^{R499C} found in NBIA patients [9].

The results obtained in this study showed that yeast mutant defective in CoA biosynthesis recapitulates the most important phenotypes found in patients and validated this system to model CoPAN in order to help elucidating important cellular and biochemical aspects of mitochondrial, lipid and iron homeostasis underpinning this disease.

RESULTS

Cellular localization of yeast Cab5 protein

Proteomics studies [20] and *in silico* analysis using the PSORT and MITOPROT programs [21, 22], which allows the prediction of protein localization, suggest for Cab5 a mitochondrial localization. Moreover human CoA synthase is a mitochondrial enzyme and the human gene is able to complement the *cab5*Δ mutation. To confirm experimentally the mitochondrial localization of Cab5p, a carboxyl-terminal fusion of HA epitope to Cab5 was constructed. The *cab5*Δ lethal phenotype was rescued by the re-expression of the tagged wild type allele, indicating that the addition of HA did not disrupt targeting and function of the Cab5 protein. Equivalent amounts of mitochondrial pellet (M) and supernatant (PMS) fractions from cells expressing HA tagged Cab5 (Cab5-HA) were subjected to SDS-PAGE and Western blotting to identify the indicated protein. The great majority of Cab5-HA co-fractionated with the mitochondrial membrane protein porin, while only a small amount remained in the supernatant with the soluble cytoplasmic protein phosphoglycerate kinase (PGK), indicating that Cab5 behaves as a mitochondrial associated protein (Fig. 1A). We further investigated the mitochondrial localization of Cab5p by performing a protease protection assay of intact mitochondria. Cab5-HA exhibited a significant increase in proteinase K sensitivity treatment in respect to both porin, which is only partially exposed on the surface, and to the inner membrane protein Core1 (Fig. 1B). The mitochondria were then treated with 0.1 M Na_2CO_3, pH 11, and supernatant and pellet fractions were generated by centrifugation. As depicted in Fig. 1C the amount of Cab5 associated with mitochondria was significantly reduced but the amount of porin was not altered. Taken together these results suggest that Cab5 is an extrinsic outer membrane protein.

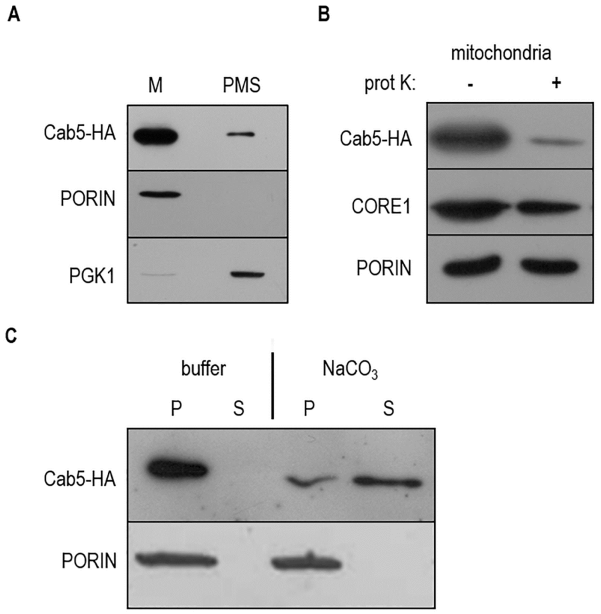

FIGURE 1: Localization of Cab5p. (A) Equal amounts (20 mg) of the mitochondrial fraction (M) and post mitochondrial fraction (PMS) were resolved by SDS-PAGE and analyzed by immunoblotting with HA, PGK1 (cytosolic marker), PORIN (mitochondrial outer membrane marker) antibodies. **(B)** Mitochondria were treated for 60 min at 4°C with proteinase K (prot K) (1 mg/ml). The filter was incubated with anti-HA, anti-CORE1, and anti-PORIN antibodies. Core1 was used as an inner membrane protein control. **(C)** 150 µg of mitochondrial proteins were treated with TEGN buffer or TEGN and 0.1M $NaCO_3$. The insoluble pellet (P) and supernatant (S) fractions were resolved by SDS-PAGE and analyzed by immunoblotting with HA and PORIN antibodies.

Characterization of mitochondrial functions

We have previously demonstrated by HPLC analysis that in the strain expressing the human *COASY*^{R499C} or the yeast *cab5*^{R146C} mutant versions the level of CoA in mitochondria was reduced by 40% compared to wild-type [9]. Given that defective CoA biosynthesis could lead to a variety of metabolic defects we looked for evidence of mitochondrial dysfunction.

In order to reveal a possible respiratory growth defect, serial dilutions of the strains were spotted on mineral medium without pantothenate supplemented with either ethanol or glycerol, at 28°C. As shown in Fig. 2A the OXPHOS growth of the *cab5*Δ/*COASY*^{R499C} mutant was partially affected compared to *COASY* wild type expressing strain. To confirm the growth delay we determined the cell

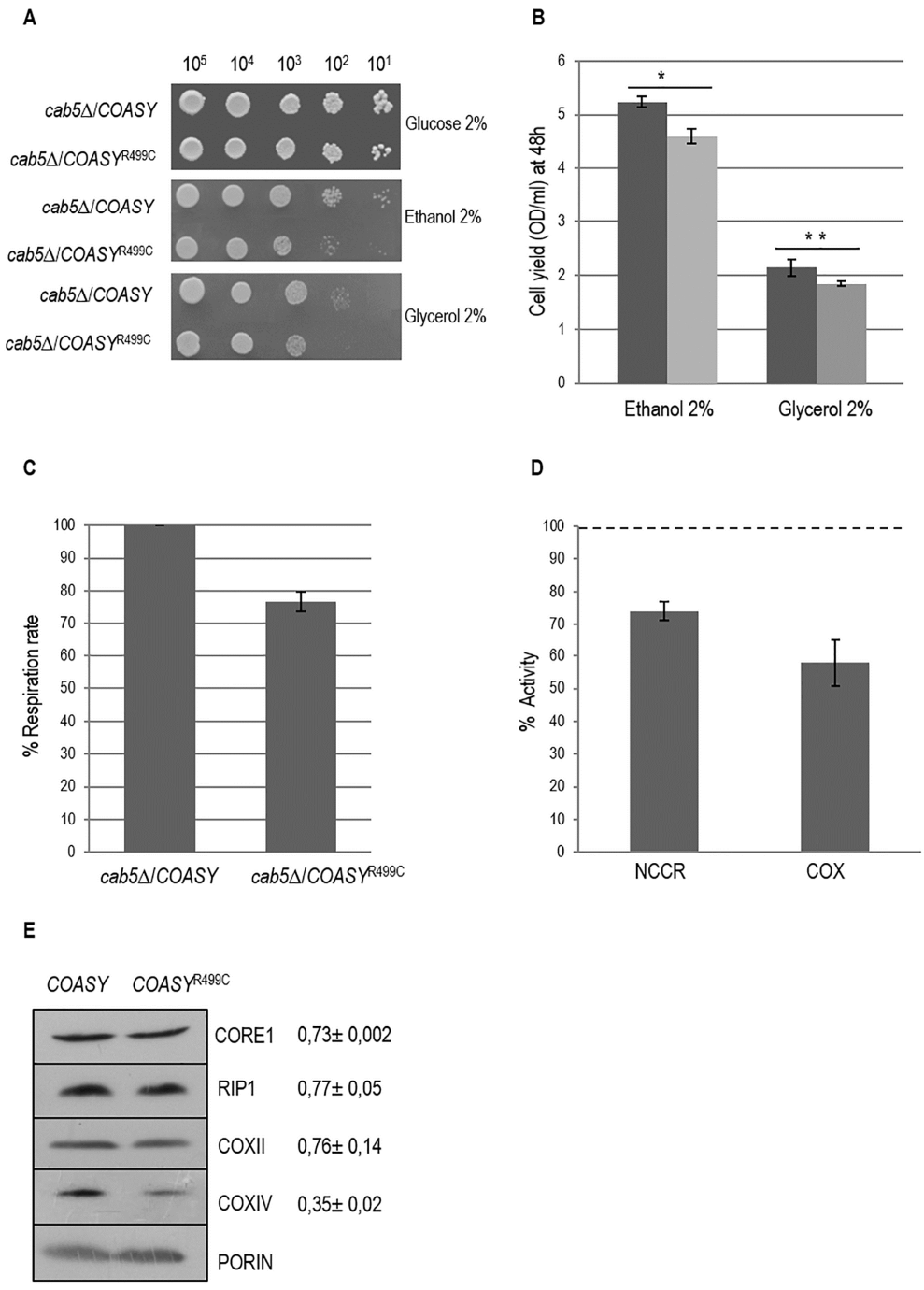

FIGURE 2: Characterization of mitochondrial functions. (A) Oxidative growth phenotype. The strain W303-1B *cab5*Δ was transformed with a pYEX-BX plasmid carrying the wild-type *COASY* or the mutant allele *COASY*^{R499C}. Equal amounts of serial dilutions of cells from exponentially grown cultures (10^5, 10^4, 10^3, 10^2, 10^1) were spotted onto mineral medium (40) plus 2% glucose, 2% ethanol or 2% glycerol without pantothenate. The growth was scored after 5 days of incubation at 28°C. **(B)** Cell yield. Cell yield was calculated by growing cells on liquid medium containing ethanol or glycerol and measuring the optical density at 600 nm after 48h of growth (*COASY* black columns and *COASY*^{R499C} grey columns). Values are mean of three independent experiments. * P < 0.05; **P < 0.01 (unpaired two-tailed t-test). **(C)** Oxygen consumption rates. Respiration was measured in cells grown in mineral medium (40) plus 0.2% glucose and 2% galactose without pantothenate at 28°C. The values observed for the *COASY* mutant strain are reported as percentage of the respiration obtained in cells expressing the wild-type *COASY* gene. **(D)** NADH-cytochrome *c* oxidoreductase (NCCR) and cytochrome *c* oxidase (COX) activities were measured in mitochondria extracted from cells grown exponentially at 28°C in mineral medium (40) plus 0.2% glucose and 2% galactose without pantothenate. The values of the *COASY* mutant are expressed as percentage of the activities obtained in the wild type strain. **(E)** Steady state level of cIII and cIV subunits in cells carrying the wild-type *COASY* and the mutant allele. The filter was incubated with specific antibodies against Core1, Rip1, CoxII, CoxIV and Porin. The signals were normalized according to the control signal (porin) and taken as 1.00 the signal of the *cab5*Δ/*COASY* (wild-type) strain.

yield for each yeast strain grown on ethanol or glycerol. We observed that the OXPHOS growth of the mutant strain was 20% lower as compared to wild type (Fig. 2B).

To further analyze the respiratory deficiency, oxygen consumption and activity of respiratory complexes were measured. Accordingly to the OXPHOS growth phenotype the oxygen consumption rate of the *cab5*Δ/*COASY*^{R499C} was 25% less than that of *cab5*Δ/*COASY* (Fig. 2C). Likewise, the NADH-cytochrome *c* oxidoreductase (NCCR) and cytochrome *c* oxidase (COX) activities were reduced in the mutant strain respectively to 26% and 42% as compared to wild type (Fig. 2D). Accordingly, the steady state levels of complex III and IV subunits are decreased (Fig. 2E). Altogether these results indicate a mitochondrial dysfunction associated to the reduced CoA level.

Mutation in CoA synthase determines an increase of iron content and increased sensitivity to oxidative stress

NBIA disorders, PKAN and CoPAN included, are characterized by iron deposition in the brain but the mechanisms leading to iron overload and its pathophysiological role remain unclear. Since in yeast excessive iron accumulation in the mitochondria led to an increased sensitivity to this ion [23, 24], we first evaluated the inhibition of cellular growth in the *COASY*^{R499C} mutant strain by the addition of $FeSO_4$ to the medium.

As depicted in Fig. 3A, the mutant strain showed a clear growth defect when compared to wild type strain, indirectly indicating a higher iron content.

We then performed a quantitative determination of cellular iron level by a colorimetric assay that relies on the formation of colored iron complexes with BPS after nitric acid digestion of yeast cells and gives results comparable

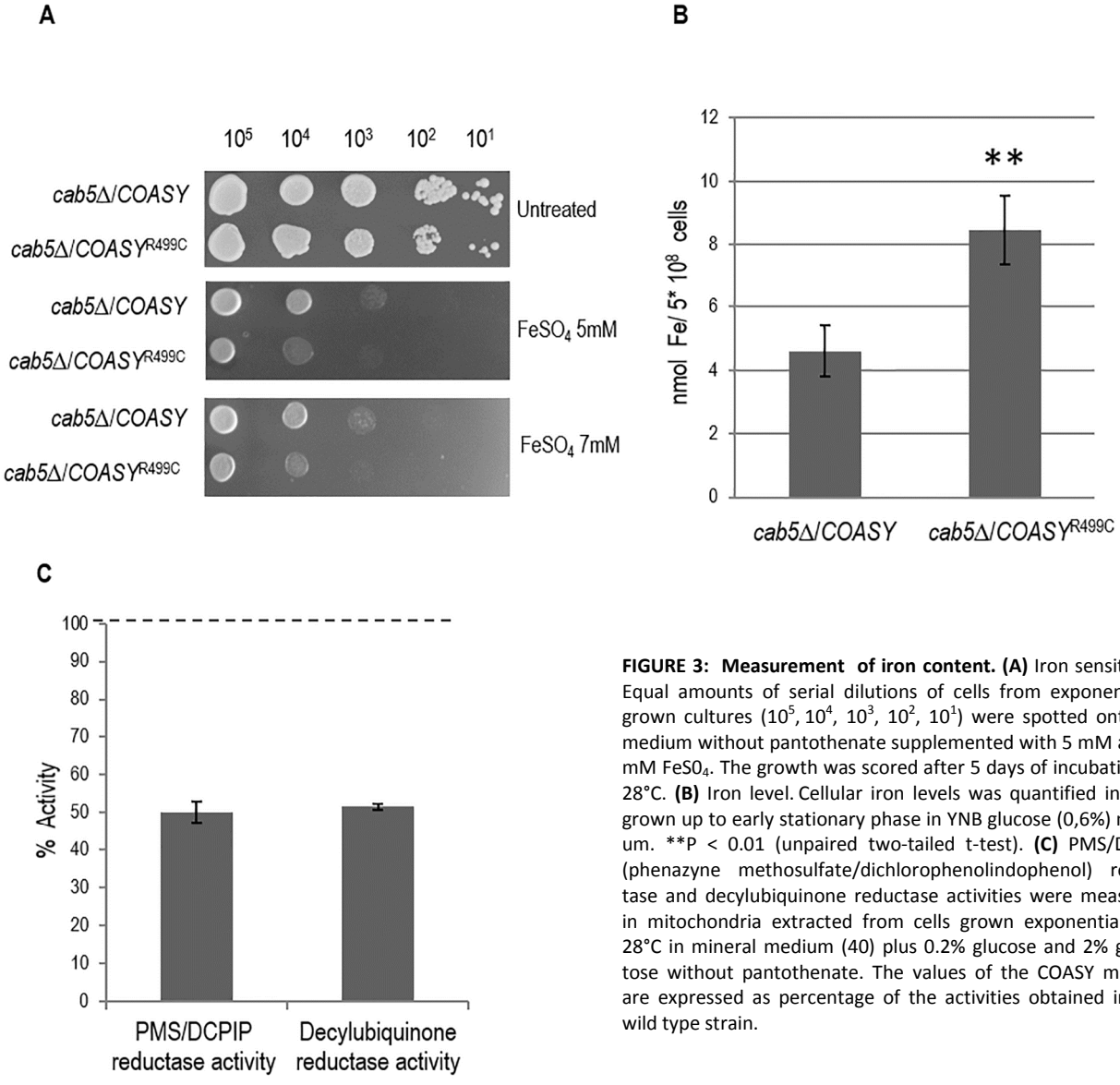

FIGURE 3: Measurement of iron content. (A) Iron sensitivity. Equal amounts of serial dilutions of cells from exponentially grown cultures (10^5, 10^4, 10^3, 10^2, 10^1) were spotted onto 40 medium without pantothenate supplemented with 5 mM and 7 mM $FeSO_4$. The growth was scored after 5 days of incubation at 28°C. **(B)** Iron level. Cellular iron levels was quantified in cells grown up to early stationary phase in YNB glucose (0,6%) medium. **P < 0.01 (unpaired two-tailed t-test). **(C)** PMS/DCPIP (phenazyne methosulfate/dichlorophenolindophenol) reductase and decylubiquinone reductase activities were measured in mitochondria extracted from cells grown exponentially at 28°C in mineral medium (40) plus 0.2% glucose and 2% galactose without pantothenate. The values of the COASY mutant are expressed as percentage of the activities obtained in the wild type strain.

with those with ICP-mass spectrometry [25, 26]. The results obtained showed a two-fold increase in iron content in the *COASY*^{R499C} mutant respect to the parental strain (Fig. 3B).

We then investigated whether the biosynthesis of the Fe-S cluster, a marker of mitochondrial functionality linked to iron metabolism, was affected by COASY deficiency. We determined the activity of succinate dehydrogenase (SDH), a mitochondrial Fe-S cluster enzyme. As shown in Fig. 3C, SDH activity was decreased by about 50%, in the mutant as compared to wild-type strain.

It is known that an excess of iron causes an altered oxidative status [24, 27, 28], another key feature of disease associated to CoA deficiency [14, 29, 30], which may be reflected in hypersensitivity to oxidative stress-induced cell death. To test this hypothesis *COASY*^{R499C} mutant and control strain were exposed to H_2O_2 and cell viability was determined by both spot assay analysis (Fig. 4A) and by counting the formation of colonies (Fig 4B). At the highest H_2O_2 concentration tested (2 mM) wild type cells showed a viability of 10%, while mutant cells showed a viability of 2% (Fig. 4B) demonstrating that a COASY defect leads to oxidative stress susceptibility.

Evaluation of lipid droplets content

Acetyl-CoA is necessary for the production of neutral lipids, which serve as power reserve for the cell and are stored in lipid droplets. Since CoA is involved in the biosynthesis of fatty acids and having demonstrated that the mutant *cab5*Δ/*COASY*^{R499C} shows a 40% reduction of coenzyme A, the content of intracellular lipid droplets in the mutant compared to the wild type was evaluated by fluorescence microscopy and fluorimetric analysis after incubation of the cells with the fluorescent lipophilic dye Nile Red [31]. As shown in Fig. 5A the content of lipid droplets is decreased in the mutant expressing the *COASY*^{R499C}. In order to better quantify this reduction, the fluorescence of cells stained with Nile Red was measured using a fluorescence spectrometer. The measures, performed in triplicate, highlighted a reduction of lipid droplets of 25% in mutant strain compared to wild-type (Fig. 5B).

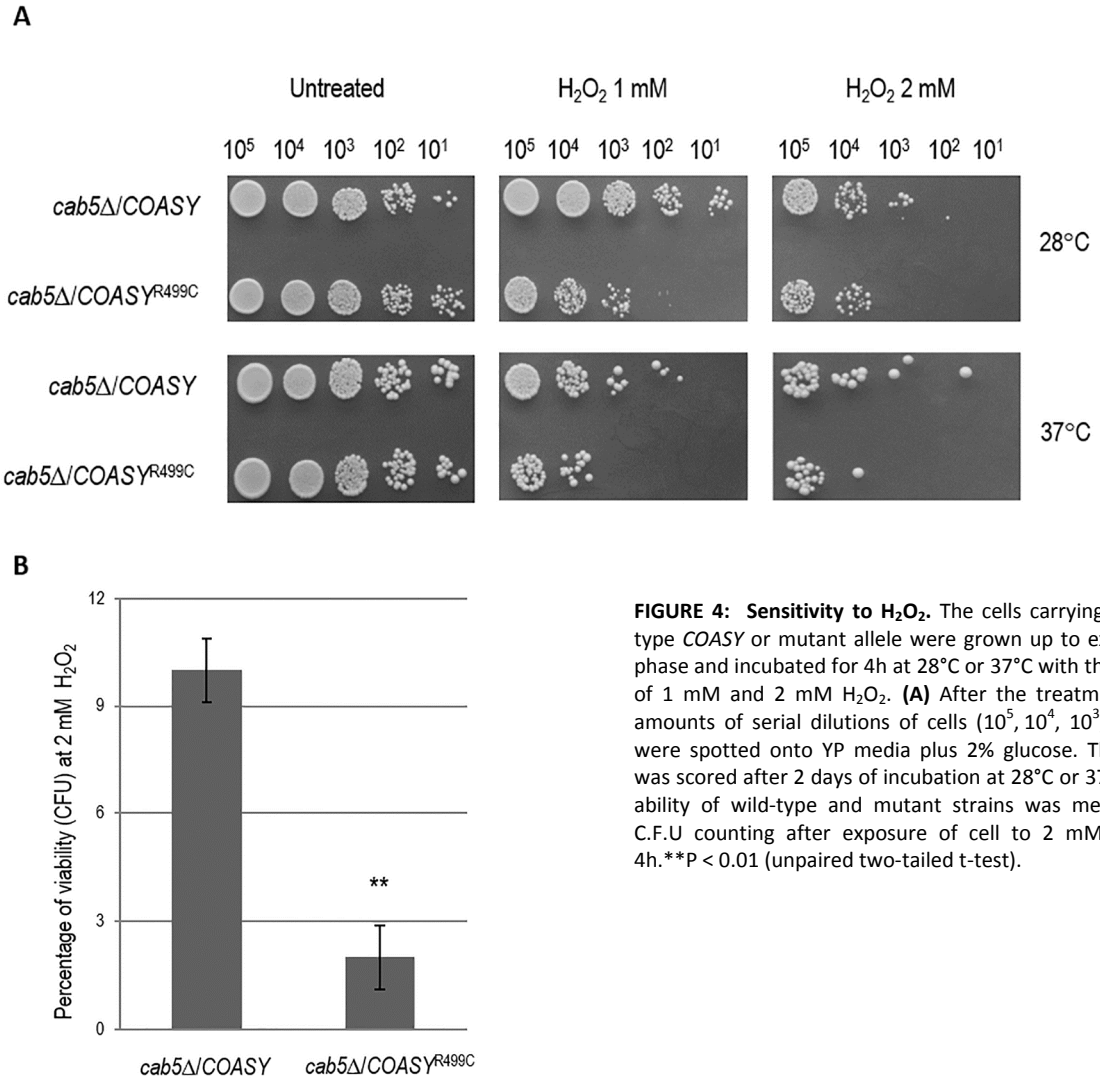

FIGURE 4: Sensitivity to H_2O_2. The cells carrying the wild-type *COASY* or mutant allele were grown up to exponential phase and incubated for 4h at 28°C or 37°C with the addition of 1 mM and 2 mM H_2O_2. **(A)** After the treatment, equal amounts of serial dilutions of cells (10^5, 10^4, 10^3, 10^2, 10^1) were spotted onto YP media plus 2% glucose. The growth was scored after 2 days of incubation at 28°C or 37°C. **(B)** Viability of wild-type and mutant strains was measured by C.F.U counting after exposure of cell to 2 mM H_2O_2 for 4h.**P < 0.01 (unpaired two-tailed t-test).

DISCUSSION

In all living organisms Coenzyme A (CoA) is an essential cofactor in cellular metabolism. CoA biosynthesis follows a highly conserved pathway, involving five enzymatic steps, which utilize pantothenate (vitamin B5), ATP, and cysteine. Mutations in nuclear genes directly involved in CoA biosynthetic pathway have been identified as responsible for some forms of NBIA, namely PKAN and CoPAN. PKAN is caused by mutations in PANK2, encoding the pantothenate kinase 2 enzyme, that account for about 50% of NBIA cases, whereas mutations in CoA synthase COASY have been recently reported as the second inborn error of CoA synthesis leading to CoPAN [9]. In PKAN and CoPAN brain iron accumulation is dramatic but its link with defective CoA synthesis is unknown.

Moreover, many neurodegenerative diseases, PKAN and CoPAN included, are characterized by mitochondrial dysfunctions, oxidative stress, altered lipid metabolism but again the complex relationships linking these factors in the context of disease conditions remain to be elucidated.

Previous attempts to understand the mechanism of PKAN using animal models have met with limited success. A mouse model of PKAN exhibits azoospermia but lacks any neurological phenotype [32]. A *Drosophila* model of PKAN does have a brain phenotype, but this involves the formation of vacuoles, not iron accumulation [33]. The identification and generation of other cellular model may allow a deeper characterization of *COASY* and *PANK2* disease gene products, and the investigation of their pathophysiology *in vivo*. With this aim we developed and characterized a yeast model for CoPAN disease.

Although in yeast, differently from mammalian cells, the last two steps of CoA biosynthesis are catalyzed by two separate enzymes, namely the products of the essential genes *CAB4* and *CAB5*, we have demonstrated that the lethality associated to deletion in *CAB5* could be complemented by human *COASY*. This allowed us to study the human Arg499Cys substitution in yeast and to support the pathogenic role of this mutation associated to a reduced level of CoA [9].

The evaluation of the metabolic consequences of coenzyme A deficiency in yeast revealed mitochondrial dysfunctions; OXPHOS growth was affected and respiration rate significantly decreased. Accordingly, the activity of respiratory chain complexes and steady state levels of mitochondrial respiratory chain subunits were reduced. We also demonstrated that the growth of the mutant strain is not only strongly inhibited in the presence of iron but that the mutant strain showed iron accumulation. This result is consistent with the patient phenotype, with iron overload being a typical sign of PKAN and CoPAN. We have also found that *cab5*Δ/*COASY*^{R499C} mutant was more sensitive to the ROS-inducing agent H_2O_2 indicating an increased oxidative stress that may contribute to the pathogenesis of these diseases. Accordingly, the activity of SDH, a marker of mitochondrial functionality linked to iron metabolism, was reduced in the *COASY* mutant.

Since Acetyl-CoA, one of the most important derivatives of CoA, is also required for the synthesis of fatty acids, we investigated the impact of reduced CoA level by meas-

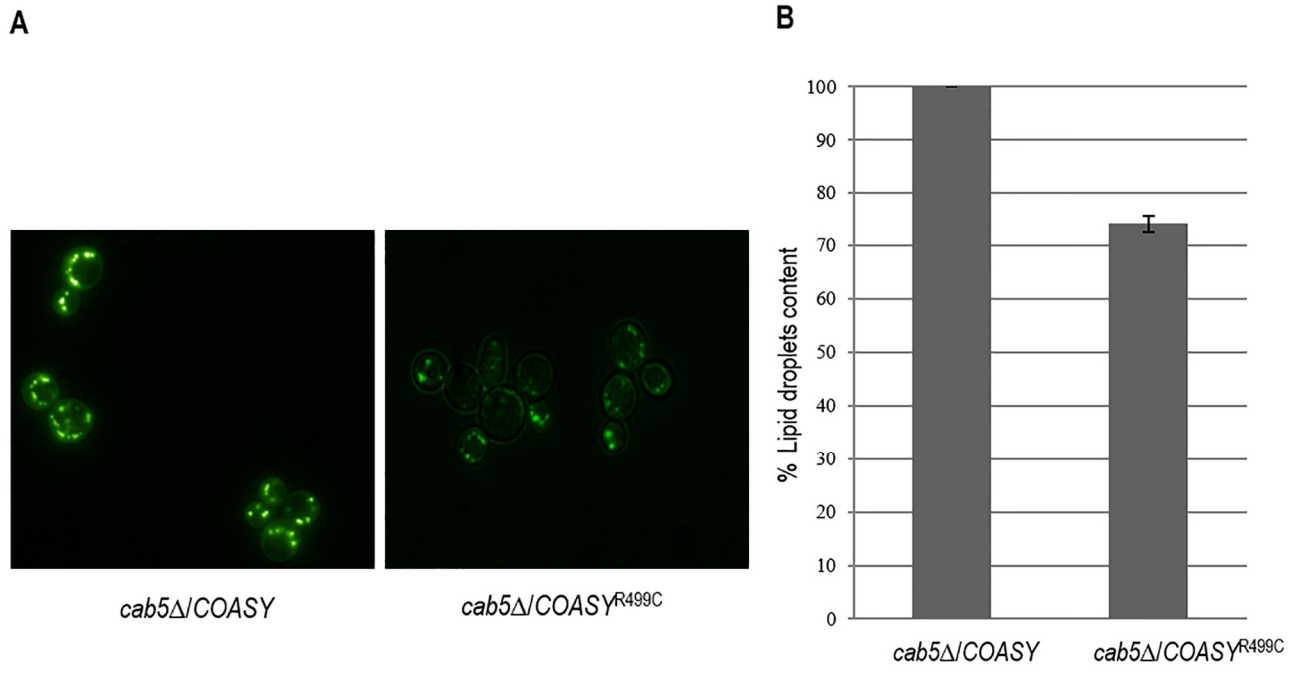

FIGURE 5: Evaluation of lipid droplets content. The intracellular lipid droplets content has been detected by fluorescence microscopy **(A)** and fluorimetric analysis **(B)** after incubation of wild type and mutant cells with the fluorescent lipophilic dye Nile Red (4 μg/ml). The values corresponding to mutant *COASY* are expressed as percentage of the content obtained in the wild type strain.

uring the lipid droplets content in mutant cells by fluorimetric analysis of Nile Red stained cells. Interestingly enough, lipid droplets content was 25% lower in mutant strain as compared to wild-type. The same altered lipid metabolism was also observed in mutant strain for phosphopantothenoylcysteine synthetase (PPCS), another essential enzyme in CoA biosynthetic pathway [34]. These results are in agreement with the hypothesis that low CoA perturbs lipid homeostasis; lipid deregulation was also observed in *Drosophila* CoA mutants and from global metabolic profiling studies in patient-derived fibroblasts [8, 35]. The transcriptional analysis of key genes involved in lipid metabolism would help in elucidating the role of lipid metabolism in the pathology.

Altogether these results established yeast as an appropriate model to study the molecular mechanisms involved in CoA metabolism, and to understand the connection between iron management, mitochondrial function and lipid metabolism in neurodegeneration.

Several pathological phenotypes have been identified in the mutant *COASY* yeast strain thus representing ideal readouts for high throughput screening of chemical libraries as described by Couplan *et al.* [36]. This could allow the identification of new molecules, the first step to set up future therapeutic experimental approaches.

MATERIALS AND METHODS

Yeast strains, media and vectors

Yeast strains used in this study were W303-1B *cab5*Δ (MATα; *cab5*::*KanMx4 ade2-1 leu2-3,112 ura3-1 his3-22,15 trp1-1 can1-100*) carrying pYEX-BX-COASY or pYEX-BX COASY^{R499C} plasmid [9]. For localization studies we used the strain BY4741 (MAT*a*; *his3*Δ*1 leu2*Δ*0 met15*Δ*0 ura3*Δ*0*) transformed with pFL38-Cab5-HA plasmid.

Cells were cultured in mineral medium (40) supplemented with appropriate amino acids and bases for auxotrophy as previously described [37]. To obtain medium lacking pantothenate (40-Pan) a mixture of vitamins without pantothenate was prepared. Yeast cells were transformed by the standard lithium acetate method [38] and cultured in YNB synthetic defined media (For-MediumTM, UK) supplemented with 1 g/l of drop-out powder [39] containing all amino acids and bases, except those required for plasmid selection. Various carbon sources (Carlo Erba Reagents, Italy) were added at the indicated concentration. Media were solidified with 20 g/l agar (For-Medium™). Strains were incubated at 28 or 37°C as indicated.

Plasmid pFL38-Cab5-HA was obtained by PCR overlap technique [40]. In the first set of PCR reactions, the *CAB5* region was obtained using the forward primer CAB5Fw-GGGGGGATCCCCATTGCTTAGAATGGGCGG and the following reverse tag primer CAB5HARv ATCAACCTTATAC**AGCGTAATCTGGAACATCGTATGGGTACGCTGA**AGACTTTTTATTTTG where hemagglutinin (HA) tag sequence is indicated in bold. The second *CAB5* region was obtained using the forward tag primers CAB5HATERFw complementary to CAB5HARv , and the reverse primer CAB5Rv-CCGCGGTACCGAGAACCCATAGAATTCGAC. The final product was obtained using the overlapping PCR fragments as template with CAB5Fw and CAB5Rv as external primers. The product was then digested with *BamH*I and *Kpn*I and cloned in *BamH*I/*Kpn*I digested pFL38 centromeric plasmid [41].

Respiration measurement, biochemical assays and immunoblot analysis of respiratory chain subunits.

Respiratory activity measurement was performed on whole cells at 30°C using a Clark-type oxygen electrode (Oxygraph System, Hansatech Instruments, England) with 1 ml of air-saturated respiration buffer (0.1 M phthalate–KOH, pH 5.0). The reaction started by addition of 20 mg of wet-weight cells [42].

Complex II (SDH), NADH-cytochrome *c* oxidoreductase (NCCR) and complex IV specific activities were measured spectrophotometrically as previously described [42, 43, 44, 45] on a mitochondrial enriched fraction prepared according to Soto *et al*. [46]. Protein concentration was determined by the method of Bradford using the BioRad protein assay following manufacturer's instructions [47]. For SDS-PAGE, 20 µg of mitochondrial proteins were separated on 12% polyacrylamide gels and electroblotted onto a nitrocellulose membrane. The subunits of mitochondrial respiratory complexes were immunovisualized by specific antibodies. The sources of primary antibodies are indicated: anti-Core1 (a kind gift from Prof. Antoni Barrientos), anti-Rip1 (a kind gift from Prof. Alexander Tzagoloff), anti CoxIIp (Abcam Mitoscience), anti-CoxIV (Abcam Mitoscience) and anti-Porin (Abcam Mitoscience). Quantification of protein bands was performed using Multi Analyst software. The signals were normalized according to the control signal (α-Porin) and the signal of the *cab5*Δ/COASY (wild-type) strain was set as 1.00.

Intact mitochondria isolation, subcellular localization experiments and membrane association

Intact mitochondria were isolated from BY4741 strain transformed with a plasmid expressing Cab5-HA under the native *CAB5* promoter after cell wall removal by Zymoliase20T digestion (Nacalai Tesque) and cell disruption with a glass-teflon potter homogenizer [48]. Whole cell extract was centrifuged at 12,000 g for 30 min to yield the mitochondrial pellet (M) and post-mitochondria supernatant (PMS). These fractions were analyzed by immunoblotting with the indicated antibodies (Porin: mitochondrial marker; PGK cytoplasmic marker (Abcam Mitoscience)). The Cab5 protein was immunovisualized using an anti-HA (Roche) specific antibody. Proteinase K protection assay for sub-mitochondrial localization study was performed as previously described [48, 49]. Briefly, 200 µg of mitochondrial proteins were kept in 20 mM HEPES pH 7.4, 0,6 M sorbitol in the presence or absence of proteinase K (1 mg/ml) for 60 minutes on ice. 0,1 M PMSF (phenylmethylsulfonyl fluoride) was added to stop the reaction. The protein pellets were washed once with 20 mM HEPES pH 7.4 plus 0,6 M sorbitol, and suspended in SDS-PAGE sample buffer.

A modified version of the membrane association experiments of Trott and Morano [50] was utilized to determine the resistance of Cab5p to sodium carbonate (pH 11.5) treatment. Equal amounts (150 µg) of the mitochondrial fraction was resuspended in TEGN (20 mM Tris-HCl [pH 7.9], 0.5 mM EDTA, 10% glycerol, 50 mM NaCl) or TEGN and with 0.1 M $NaCO_3$ for 30 min on ice. The samples were subsequently centrifuged at 17,000 g at 4°C to obtain soluble and membrane fractions. The fractions obtained in all type of extraction were separated by

SDS-PAGE and probed with anti-HA and anti-PORIN antibodies.

Measurement of iron content

The iron content was determined by a colorimetric assay, essentially as described before [25, 51]. 5x10^8 cells were washed twice with H_2O, resuspended in 0.5 ml of 3% nitric acid and incubated over night at 95°C. After incubation, samples were centrifuged at 12,000 rpm for 5 min and the supernatant (400 µl) was mixed with 160 µl of 38 mg sodium L-ascorbate ml^{-1} (SIGMA), 320 µl of 1.7 mg BPS ml^{-1} (ACROS ORGANICS), and 126 µl of ammonium acetate (SIGMA) (saturated solution diluted 1:3). Non-specific absorbance was measured at 680 nm and subtracted from the specific absorbance of the iron-BPS complex (535 nm). Iron was quantified by reference to a standard curve using iron sulfate performed as in Tamarit *et al*. [25].

H_2O_2 sensitivity

To determine the sensitivity to oxygen peroxide, cells growing exponentially were exposed to 1 and 2 mM H_2O_2 at 28°C or 37°C for 4 h. Cell viability was determined by spotting equal amounts of serial dilutions of cells (10^5, 10^4, 10^3, 10^2, 10^1) onto YP plates (1% yeast extract, 2% peptone ForMedium™) supplemented with 2% glucose (YPD). Plates were incubated at 28°C or 37°C for two days. To better quantify H_2O_2 sensitivity cell survival was determined by counting the formation of colonies after the treatment.

Lipid droplets content: fluorescence microscopy and fluorimetric analysis

Intracellular lipid droplets were detected using the fluorescent lipophilic dye Nile Red (9-diethylamino-5*H*-benzo[α]phenoxazine-5-one 3 SIGMA-ALDRICH) by fluorescence microscopy and fluorimetric analysis [31, 52, 53]. Wild type and *cab5*Δ/*COASY*^{R499C} strains were grown to mid-log phase in mineral medium (40) containing Yeast Extract (1,5 g/L). To 250 µl of the cultures, adjusted to 1 OD, 10 µl of the stock solution of Nile red [100 µg/ml] were added in order to obtain a final concentration of 4 µg/ml of dye. Fluorescence of the stained cells were obtained with a Leica DM2000 microscope using x 100 magnification and captured using a Leica DFC310FX digital camera with Leica's Imaging Software (Leica Application Suite-LASAF 3.7.0, Leica Microsystem).

To quantify the fluorescence we used the fluorescence spectrometer Tecan SPECTRA Fluor Plus using the software XFLUOR4 V4.51 (excitation at 535 nm and emission at 595 nm). Aliquots of 100 µl of cells stained with Nile red were transferred into 96-well microplates in 4 replicates. For each strain a negative control was performed in which the dye was omitted in order to exclude a possible auto fluorescence of samples. The evaluation of the fluorescence was repeated at 5-minute intervals in a time interval of 20 minutes [53].

ACKNOWLEDGMENTS

The financial support of Telethon GGP11011, Telethon GGP11088 and Fondazione CARIPLO 2011/0526 are gratefully acknowledged. This work was supported by TIRCON project of the European Commission's seventh Framework Programme (FP7/2007-2013, HEALTH-F2-2011, grant agreement no. 277984). We wish to thank Antonietta Cirasolo (University of Parma) for the skillful technical assistance.

CONFLICT OF INTEREST

The authors declare no conflict of interest.

COPYRIGHT

Please cite this article as: Camilla Ceccatelli Berti, Cristina Dallabona, Mirca Lazzaretti, Sabrina Dusi, Elena Tosi, Valeria Tiranti, Paola Goffrini (2015). Modeling human Coenzyme A synthase mutation in yeast reveals altered mitochondrial function, lipid content and iron metabolism. **Microbial Cell** 2(4): 126-135. doi: 10.15698/mic2015.04.196

REFERENCES

1. Zhivoloup A, Nemazanyy I, Babich A, Panasyuk G, Pobigailo N, Vudmaska M, Naidenov V, Kukharenko O, Palchevskii S, Savinska L, Ovcharenko G, Vardier F, Valovka T, Fenton T, Rebholz H, Wang M, Sheperd P, Matsuka G, Filonenko V, and Gout IT **(2002)**. Molecular cloning of CoA Synthase. The missing link in CoA biosynthesis. **The Journal Of Biological Chemistry** 277(25): 22107-22110.

2. Zhyvoloup A, Nemazanyy I, Panasyuk G, Valovka T, Fenton T, Rebholz H, Wang, ML, Foxon R, Lyzogubov V, Usenko V, Kyyamova R, Gorbenko O, Matsuka G, Filonenko V, and Gout IT **(2003).** Subcellular localization and regulation of coenzyme A synthase**. J Biol Chem** 278(50): 50316–50321.

3. Olzhausen J, Schübbe S, and Schüller H **(2009)**. Genetic analysis of coenzyme A biosynthesis in the yeast *Saccharomyces cerevisiae*: identification of a conditional mutation in the pantothenate kinase gene *CAB1*. **Current Genetics** 55(2): 163-173.

4. Gregory A and Hayflick SJ **(2005)**. Neurodegeneration with brain iron accumulation. **Folia Neuropatho** 43(4): 286-96.

5. Brunetti D, Dusi S, Morbin M, Uggetti A, Moda F, D'Amato I, Giordano C, d'Amati G, Cozzi A, Levi S, Hayflick S, And Tiranti V **(2012).** Pantothenate kinase-associated neurodegeneration: altered mitochondria membrane potential and defective respiration in Pank2 knock-out mouse model. **Human Molecular Genetics** 21(24): 5294-5305.

6. Hayflick SJ **(2014)**. Defective pantothenate metabolism and neurodegeneration. **Biochem Soc Tran**s 42(4): 1063-8.

7. Hartig MB, Hörtnagel K, Garavaglia B, Zorzi G, Kmiec T, Klopstock T, Rostasy K, Svetel M, Kostic VS, Schuelke M, Botz E, Weindl A, Novakovic I, Nardocci N, Prokisch H, and Meitinger T **(2006)**. Genotypic and phenotypic spectrum of *PANK2* mutations in patients with neurodegeneration with brain iron accumulation. **Annals Of Neurology** 59(2): 248-256.

8. Leoni V, Strittmatter L, Zorzi G, Zibordi F, Dusi S, Garavaglia B, Venco P, Caccia C, Souza AL, Deik A, Clish CB, Rimoldi M, Ciusani E, Bertini E, Nardocci N, Mooth VK, and Tiranti V **(2012)**. Metabolic consequences of mitochondrial coenzyme A deficiency in patients eith PANK2 mutations. **Molecular Genetics And Metabolism** 105(3): 463–47.

9. Dusi, S, Valletta L, Haach TB, Tsuchiya Y, Venco P, Pasqualato S, Goffrini P, Tigano M, Demchenko N, Weiland T, Schwarzmayr T, Strom TM, Invernizzi F, Garavaglia B, Gregory A, Sanford L, Hamada J, Fontanesi, Bettencourt C, Houldel H, Chiapparini L, Zorzi G, Kurian MA, Nardocci N, Prokisch H, Hayflick S, Gout I, and Tiranti V **(2014)**. Exome sequencing reveals mutation in CoA synthase as a cause of neurodegeneration with brain iron accumulation. **Am J Hum Genet** 94(1): 11-22.

10. Campbell GR, Worrall JT, and Mahad DJ **(2014).** The central role of mitochondria in axonal degeneration in multiple sclerosis. **Mult Scler** 20(14): 1806-1813.

11. Palomo GM and Manfredi G **(2014).** Exploring new pathways of neurodegeneration in ALS: The role of mitochondria quality control. **Brain Res**, doi: 10.1016/j.brainres.2014.09.065.

12. Urrutia PJ, Mena NP, and Núñez MT **(2014).** The interplay between iron accumulation, mitochondrial dysfunction, and inflammation during the execution step of neurodegenerative disorders. **Front Pharmacol** 5:38.

13. Kotzbauer PT, Truax AC, Trojanowski JQ, and Lee VM **(2005)**. Altered neuronal mitochondrial coenzyme A synthesis in neurodegeneration with brain iron accumulation caused by abnormal processing, stability, and catalytic activity of mutant pantothenate kinase 2. **J Neurosci** 25(3): 689-98.

14. Campanella A, Privitera D, Guaraldo M, Rovelli E, Barzaghi C, Garavaglia B, Santambrogio P, Cozzi A, and Levi S **(2012)**. Skin fibroblasts from pantothenate kinase-associated neurodegeneration patients show altered cellular oxidative status and have defective iron-handling properties. **Hum Mol Genet** 21(18): 4049-4059.

15. Colombelli C, Aoun M, and Tiranti V **(2014)**. Defective lipid metabolism in neurodegeneration with brain iron accumulation (NBIA) syndromes: not only a matter of iron. **J Inherit Metab Dis** 38(1): 123-136.

16. Levi S and Finazzi D **(2014)**. Neurodegeneration with brain iron accumulation: update on pathogenic mechanisms. **Front Pharmacol** 5:99.

17. Rinaldi T, Dallabona C, Ferrero I, Frontali L, and Bolotin-Fukuhara M **(2010)**. Mitochondrial diseases and the role of the yeast models. **FEMS Yeast Res** 10(8): 1006-22.

18. Tenreiro S, Munder MC, Alberti S, and Outeiro TF **(2013)**. Harnessing the power of yeast to unravel the molecular basis of neurodegeneration. **J Neurochem** 127(4): 438-52.

19. Bleackley MR and MacGillivray RT **(2011)**. Transition metal homeostasis: from yeast to human disease. **BioMetals** 24(5): 785–809.

20. Reinders J, Zahedi RP, Pfanner N, Meisinger C and Sickmann A **(2006).** Toward the complete yeast mitochondrial proteome: multidimensional separation techniques for mitochondrial proteomics. **J Proteome Res** 5:1543-5.

21. Uberbacher EC, and Mural RJ **(1991)**. Locating protein-coding regions in human DNA sequences by a multiple sensor-neural network approach. **Proc Natl Acad Sci USA** 88 (24): 11261–11265.

22. Claros MG, and Vincens P **(1996).** Computational method to predict mitochondrially imported proteins and their targeting sequences. **Eur J Biochem** 241(3): 779–786.

23. Foury F, and Cazzalini O **(1997)**. Deletion of the yeast homologue of the human gene associated with Friedreich's ataxia elicits iron accumulation in mitochondria. **FEBS Lett** 411(2-3): 373-7.

24. Patil Vinay A, Fox Jennifer L, Vishal M, Gohil Dennis R Winge, and Miriam L Greenberg **(2013)**. Loss of Cardiolipin Leads to Perturbation of Mitochondrial and Cellular Iron Homeostasis. **J Biol Chem** 288: 1696-1705.

25. Tamarit J, Irazusta V, Moreno-Cermeño A, Ros J **(2006)**. Colorimetric assay for the quantitation of iron in yeast. **Anal Biochem** 351(1):149-51.

26. Molik S, Lill R, Mühlenhoff U **(2007).** Methods for studying iron metabolism in yeast mitochondria. **Methods Cell Biol** 80:261-80

27. Schilke B, Voisine C, Beinert H and Craig E **(1999).** Evidence for a conserved system for iron metabolism in the mitochondria of *Saccharomyces cerevisiae*. **Proc Natl Acad Sci U.S.A.** 96(18): 10206–10211.

28. Mühlenhoff U, Richhardt N, Ristow M, Kispal G and Lill R **(2002).** The yeast frataxin homolog Yfh1p plays a specific role in the maturation of cellular Fe/S proteins. **Hum Mol Genet** 11(17): 2025–2036.

29. Wu M, Liu H, Chen W, Fujimoto Y, Liu J **(2009).** Hepatic expression of long-chain acyl-CoA synthetase 3 is upregulated in hyperlipidemic hamsters. **Lipids** 44(11):989-98.

30. Rana A, Seinen E, Siudeja K, Muntendam R, Srinivasan B, Van der Want JJ, Hayflick S, Reijngoud DJ, Kayser O, Sibon OC **(2010).** Pantethine rescues a Drosophila model for pantothenate kinase-associated neurodegeneration. **Proc Natl Acad Sci U S A** 107(15):6988-93.

31. Greenspan P, Mayer EP, and Fowler SD **(1985)**. Nile red: a selective fluorescent stain for intracellular lipid droplets. **J Cell Biol** 100(3): 965-73.

32. Kuo YM, Duncan JL, Westaway SK, Yang H, Nune G, Xu EY, Hayflick SJ and Gitschier J **(2005).** Deficiency of pantothenate kinase 2 (Pank2) in mice leads to retinal degeneration and azoospermia. **Hum Mol Genet** 14(1): 49–57.

33. Yang Y, Wu Z, Kuo YM and Zhou B **(2005).** Dietary rescue of fumblea Drosophila model for pantothenate-kinase-associated neurodegeneration. **J Inherit Metab Dis** 28(6):1055-1064.

34. Nakamura T, Pluskal T, Nakaseko Y, and Yanagida M **(2012)**. Impaired coenzyme A synthesis in fission yeast causes defective mitosis, quiescence-exit failure, histone hypoacetylation and fragile DNA. **Open Biol** 2(9): 120117.

35. Bosveld F, Rana A, van der Wouden PE, Lemstra W, Ritsema M, Kampinga HH, and Sibon OC **(2008).** De novo CoA biosynthesis is required to maintain DNA integrity during development of the Drosophila nervous system. **Hum Mol Genet** 17(13): 2058-69.

36. Couplan E, Aiyar RS, Kucharczyk R, Kabala A, Ezkurdia N, Gagneur J, St Onge RP, Salin B, Soubigou F, Le Cann M, Steinmetz LM, di Rago JP, and Blondel M **(2011**). A yeast-based assay identifies drugs active against human mitochondrial disorders. **Proc Natl Acad Sci U S A** 108(29):11989-94.

37. Magni GE and Von Borstel RC **(1962)**. Different rates of spontaneous mutation during mitosis and meiosis in yeast. **Genetics** 47(8): 1097-1108.

38. Schiestl RH and Gietz RD **(1989)**. High efficiency transformation of intact yeast cells using single stranded nucleic acids as a carrier. **Curr Genet** 16(5-6): 339-4.

39. Kaiser C, Michaelis S, and Mitchell A **(1994)**. Methods in Yeast Genetics. **Cold Spring Harbor Laboratory Press**.

40. Ho SN, Hunt HD, Horton RM, Pullen JK, Pease LR **(1989)**. Site-directed mutagenesis by overlap extension using the polymerase chain reaction. **Gene** 77(1): 51–59.

41. Bonneaud N, Ozier-Kalogeropoulos O, Li GY, Labouesse M, Minvielle-Sebastia L, and Lacroute F **(1991)**. A family of low and high copy replicative, integrative and single-stranded S. cerevisiae/E. coli shuttle vectors. **Yeast** 7(6): 609–615.

42. Goffrini P, Ercolino T, Panizza E, Giache' V, Cavone L, Chiarugi A, Dima V, Ferrero I, and Mannelli M **(2009)**. Functional study in a yeast model of a novel succinate-dehydrogenase subunit B gene germline missense mutation (C191Y) diagnosed in a patient affected by a glomus tumor. **Hum Mol Genet** 18(10): 1860–1868.

43. Fontanesi F, Soto IC, and Barrientos A **(2008)**. Cytochrome c oxidase biogenesis: new levels of regulation. **IUBMB Life** 60(9): 557-68.

44. Barrientos A, , and Díaz F **(2009)**. Evaluation of the mitochondrial respiratory chain and oxidative phosphorylation system using polarography and spectrophotometric enzyme assays. **Curr Protoc Hum Genet** chapter 19:Unit19.3.

45. Jarreta D, Orús J, Barrientos A, Miró O, Roig E, Heras M, Moraes CT, Cardellach F, and Casademont J **(2000)**. Mitochondrial function in heart muscle from patients with idiopathic dilated cardiomyopathy. **Cardiovasc Res** 45(4): 860-865.

46. Soto IC, Fontanesi F, Valledor M, Horn D, Singh R, Barrientos A **(2009)**. Synthesis of cytochrome c oxidase subunit 1 is translationally downregulated in the absence of functional F1F0-ATP synthase. **Biochim Biophys Acta** 1793(11):1776-86.

47. Bradford MM **(1976)**. A rapid and sensitive method for the quantitation of microgram quantities of proteins utilizing the principle of protein dye binding. **Anal. Biochem** 72: 248–254.

48. Glick BS, and Pon LA **(1995)**. Isolation of highly purified mitochondria from Saccharomyces cerevisiae. **Methods Enzymol** 260: 213–223.

49. Diekert K, De Kroon AI, Kispal G, Lill R **(2001)**. Isolation and subfractionation of mitochondria from the yeast Saccharomyces cerevisiae. **Methods Cell Biol** 65: 37-5.

50. Trott A and Morano KA **(2004).** SYM1 is the stress-induced Saccharomyces cerevisiae ortholog of the mammalian kidney disease gene Mpv17 and is required for ethanol metabolism and tolerance during heat shock. **Eukaryot Cell** 3(3):620-31.

51. Almeida T, Marques M, Mojzita D, Amorim MA, Silva RD, Almeida B, Rodrigues P, Ludovico P, Hohmann S, Moradas-Ferreira P, Côrte-Real M, and Costa V **(2008).** Isc1p plays a key role in hydrogen peroxide resistance and chronological lifespan through modulation of iron levels and apoptosis. **Mol Biol Cell** 19(3):865-76.

52. Kimura K, Yamaola M, and Kamisaka Y **(2004)**. Rapid estimation of lipids in oleaginous fungi and yeasts using Nile red fluorescence. **J Microbiol Methods** 56(3): 331-338.

53. Sitepu IR, Ignatia L, Franz AK, Wong DM, Faulina SA, Tsui M, Kanti A, and Boundy-Mills K **(2012)**. An improved high-throughput Nile red fluorescence assay for estimating intracellular lipids in a variety of yeast species. **J Microbiol Methods** 91(2): 321–328.

Section III

Supplementary data

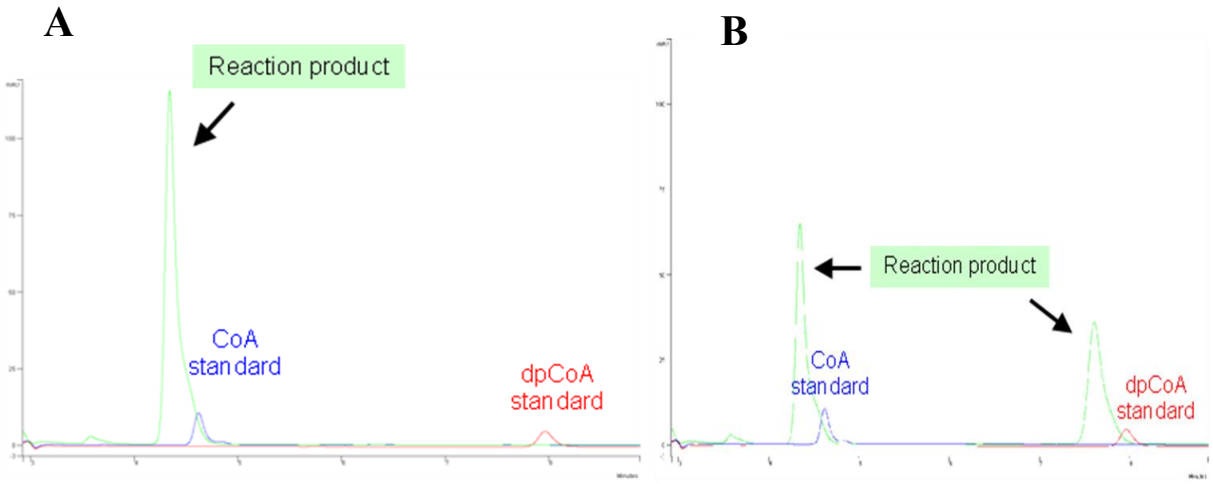

Wild-type COASY + dephospho-CoA

Mutant COASY + dephospho-CoA

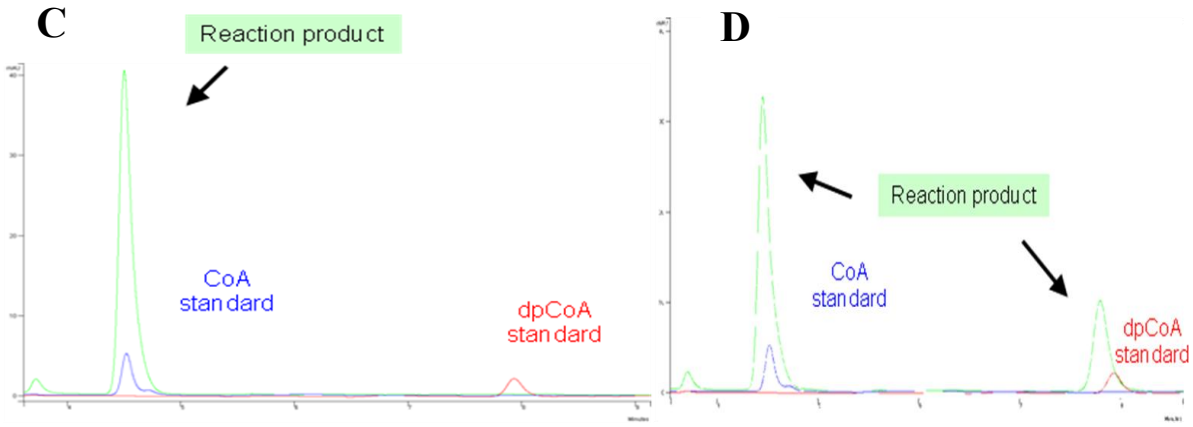

Wild-type COASY + 4-phospho-pantetheine

Mutant COASY + 4-phospho-pantetheine

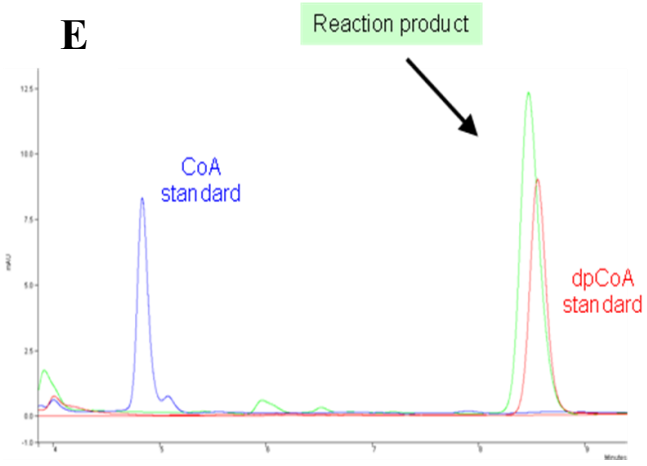

Wild-type PPAT domain + 4-phospho-pantetheine

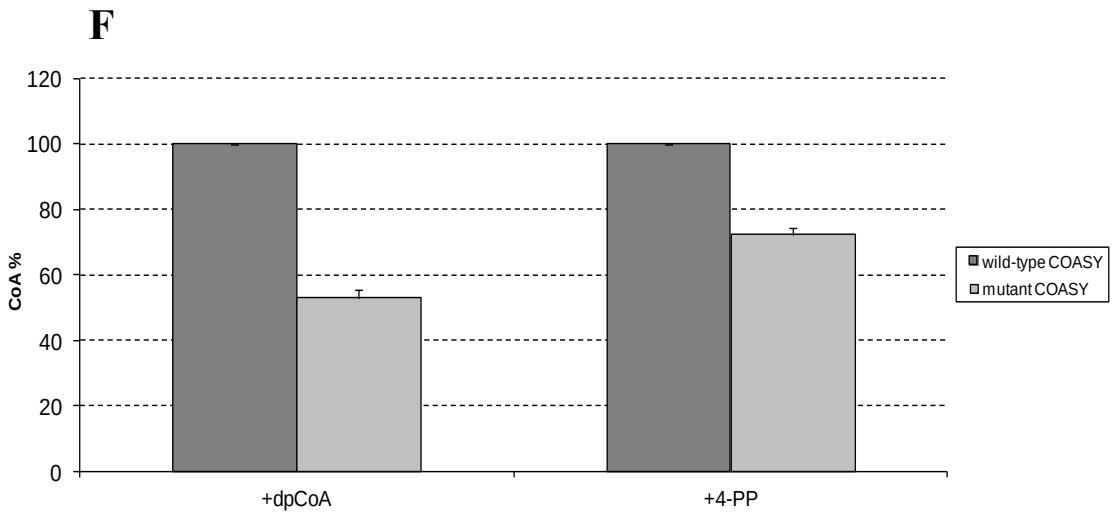

Figure S1. **HPLC Analysis of CoA production by wild-type and mutant human COASY recombinant proteins, and wild-type PPAT domain, obtained in bacteria as His-tag fusion proteins.**

A. Chromatogram showing the peak corresponding to the reaction product (green) obtained from incubation of wild-type COASY recombinant protein with 1mM ATP and 0.1mM dephospho-CoA. The enzyme is able to completely convert dephospho-CoA into CoA.

B. Chromatogram showing the peak corresponding to the reaction product (green) obtained from incubation of mutant COASY recombinant protein with 1mM ATP and 0.1mM dephospho-CoA. The enzyme is able to partially convert dephospho-CoA into CoA.

C. Chromatogram showing the peak corresponding to the reaction product (green) obtained from incubation of wild-type COASY recombinant protein with 1mM ATP and 0.1mM 4-phospho-pantetheine (substrate utilized from PPAT domain to obtain dephospho-CoA and consequently CoA). The enzyme is able to completely convert 4-phospho-pantetheine into CoA.

D. Chromatogram showing the peak corresponding to the reaction product (green) obtained from incubation of mutant COASY recombinant protein with 1mM ATP and 0.1mM 4-phospho-pantetheine. The enzyme is able to partially convert 4-phospho-pantetheine into CoA.

E. Chromatogram showing the peak corresponding to the reaction product (green) obtained from incubation of wild-type PPAT recombinant domain with 1mM ATP and 0.1mM 4-phospho-pantetheine. The enzyme is not able to synthesize CoA, therefore is evident that PPAT does not possess the catalytic synthase activity.

F. Histogram showing the quantification of *in-vitro* CoA production by the recombinant proteins, analyzed by HPLC. Mutant COASY is able to synthesize about 50% of CoA in the presence of 1mM ATP and 0.1mM dephospho-CoA (dpCoA), compared to wild-type protein. Moreover, mutant protein is able to synthesize about 70% of CoA in the presence of 1mM ATP and 0.1mM 4-phospho-pantetheine (4PP).

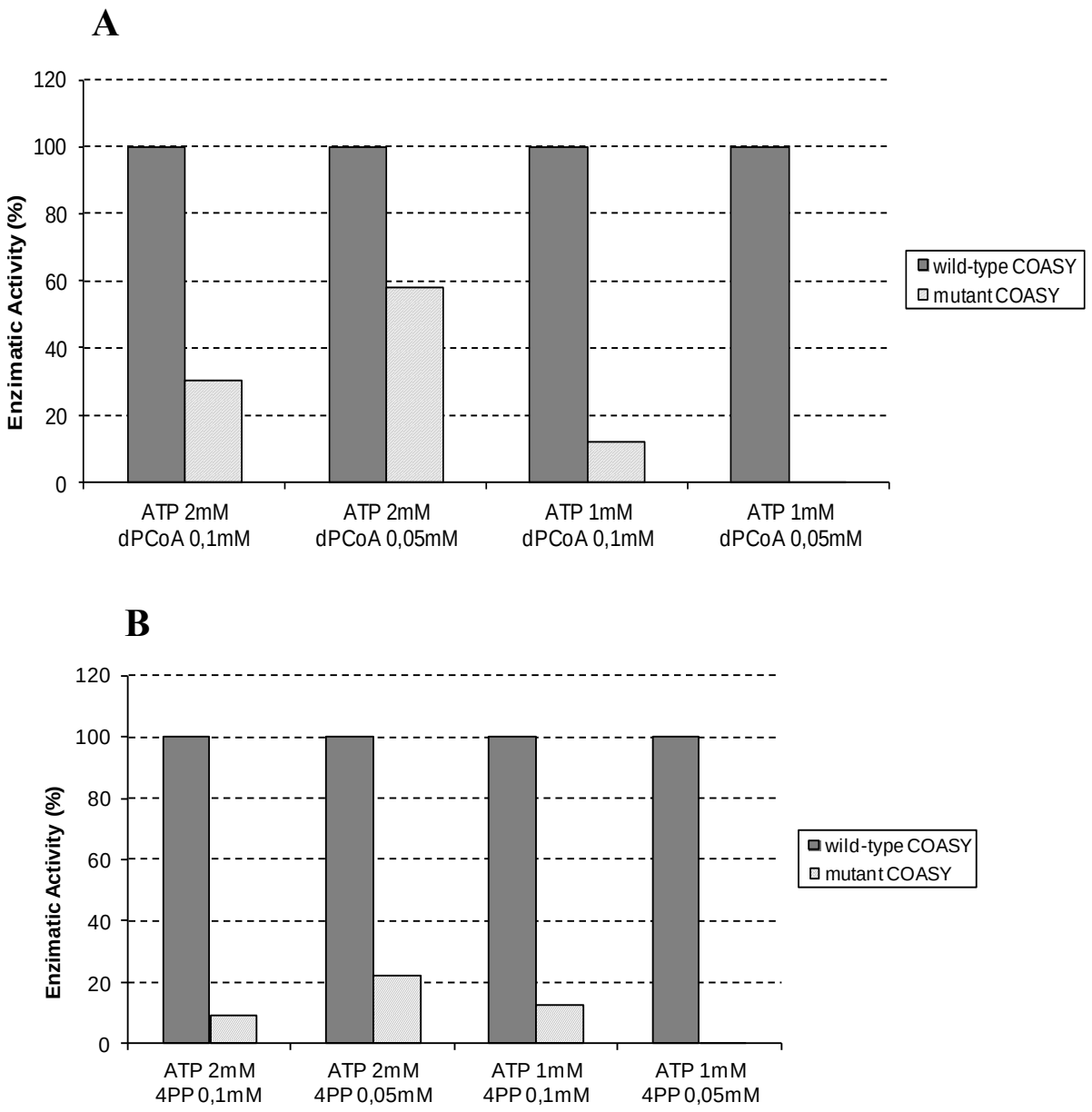

Figure S2. **In-vitro recombinant wild-type and mutant COASY activity measured by biochemical analysis.**

A. Histogram showing the COASY enzymatic activity in the presence of different concentrations of dpCoA and ATP. Mutant COASY shows a reduction of enzymatic activity if compared to wild-type, in all the tested concentration.

B. Histogram showing the COASY enzymatic activity in the presence of different concentrations of 4PP and ATP. Mutant COASY shows a reduction of enzymatic activity if compared to wild-type, in all the tested concentration.

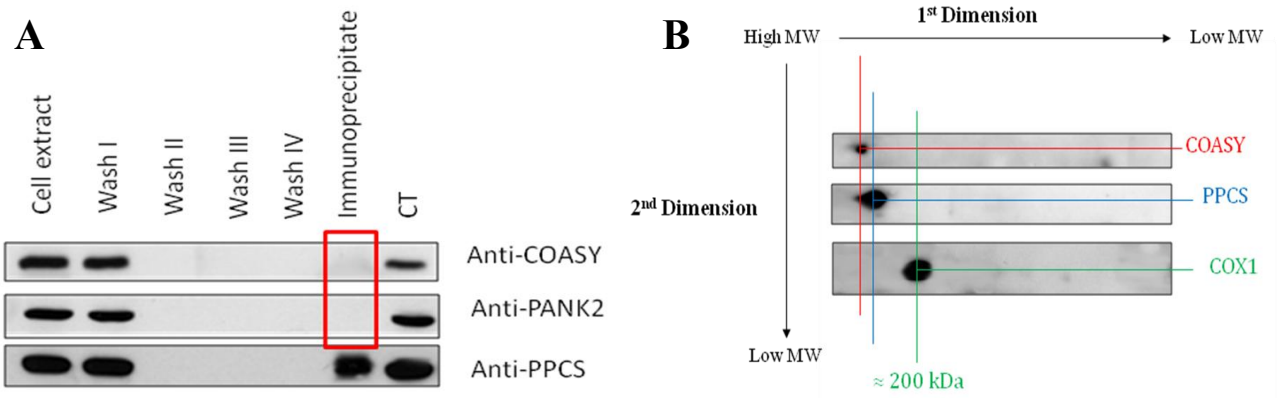

Figure S3. **Cellular analysis to investigate for a protein complex formation of COASY with the other enzymes involved in CoA biosynthesis.**

A. Co-immunoprecipitation analysis on HeLa cell line using phospho-pantothenoyl-cysteine synthetase (PPCS, the second enzyme involved in CoA biosynthesis) like bait. In the anti-COASY and anti-PANK2 panels, in the immunoprecipitate lane bands are absent. It means that COASY and PANK2 do not co-immunoprecipitate with PPCS.

B. 2D-Blue native analysis on HeLa cells. The image shows that COASY and PPCS do not belong to the same protein complex, maybe they belong to different protein complexes greater than 200kDa (size of cytochrome C oxidase, or COX, or complex IV of respiratory chain).